FRAGMENTING THE UNIVERSE
III. THE CONSTRUCTION AND STATISTICS OF 3-D VORONOI TESSELLATIONS

Rien van de Weygaert[1,2]

[1] CITA, 60 St. George St.,Toronto, Ontario, Canada
[2] Sterrewacht Leiden, Leiden, The Netherlands

8U

forms. However, Dirichlet and Voronoi tessellations as applied to random point patterns appear to have arisen independently in various fields of science and technology (df. Meyering 1953; Miles 1970; Stoyan, Kendall & Mecke 1987). For example, in crystallography, one simple model of crystal growth starts with a fixed collection of sites in two- and three-dimensional space, and allows crystals to begin growing from each site, spreading out at a uniform rate in all directions, until all space is filled. The "crystals" then consist of all points nearest to a particular site, and consequently are just the Voronoi regions for the original set of points. Similarly, the statistical analysis of metereological data led to the formulation (around 1910) of Voronoi regions under the name "Thiessen polygons" (Thiessen, 1911). Applications of Voronoi tessellations can therefore be found in fields as diverse as agriculture and forestry (Fischer & Miles 1973), astrophysics (Kiang 1966; Matsuda and Shima 1984; IW; WI; Yoshioka & Ikeuchi 1989; Coles 1990; Van de Weygaert 1991a,b; Ikeuchi & Turner 1991; SubbaRao & Szalay 1992, Williams 1992; Williams, Peacock & Heavens 1992), cell biology (Honda 1983), communication theory (Shannon 1949), crystal growth and aggregates (Meyering 1953; Gilbert 1962), geography (Mardia, Edwards & Puri 1977), geology (Crain 1976; Stoyan & Stoyan 1980), metallography (Boots 1984), physics (Ogawa & Tanemura 1974; Finney 1979) and zoology and ecology (Hamilton 1971). Voronoi tessellations are also used in data analysis of geometrical structures. Finney (1979) used the term 'polyhedral statistics'. Sibson (1980, 1981) described the use of Voronoi tessellations relative to given point patterns as a basis for 'natural neighbour interpolation': interpolating a smooth function for data located at irregularly distributed points. Thiessen (1911) had this in mind when he suggested this tessellation. Due to these diverse applications it has acquired a set of alternative names, such as Dirichlet regions (Dirichlet 1850), Wigner-Seitz cells, and Thiessen figures.

Kiang (1966) was the first to apply Voronoi tessellations to astrophysics, in his study of the mass spectrum obtained in the fragmentation of interstellar clouds. Matsuda & Shima (1984) were the first to propose the use of Voronoi tessellations in cosmology. They pointed out the similarity between two-dimensional Voronoi tessellations and the outcome of numerical clustering simulations in a neutrino-dominated universe by Melott (1983). Independently, Voronoi tessellations were introduced into cosmology by Icke & Van de Weygaert (1987). In their paper (IW) they studied the statistical properties of two-dimensional Voronoi tessellations. After finishing a three-dimensional geometrical Voronoi algorithm, WI found that the Voronoi tessellations also possess some interesting clustering properties, as was confirmed in a Monte-Carlo study by Yoshioka & Ikeuchi (1989). Since then, in particular the observation by Broadhurst *et al.* (1990) of a periodic redshift distribution in a deep, small solid angle, redshift survey (a "pencil beam survey") has caused an increased interest in the use of Voronoi tessellations as a useful description of the clustering of galaxies on large scales (Coles 1990; Van de Weygaert 1991a,b; Ikeuchi & Turner 1991; SubbaRao & Szalay 1992; Williams 1992; Williams *et al.* 1992).

We have constructed two- and three-dimensional Voronoi foams geometrically (IW, WI). In the study of galaxy clustering the advantage of this approach to N-body simulations is that one is not restricted by the resolution or number of particles. Assuming that galaxies populate the walls of the Voronoi cells, the Voronoi model qualitatively reproduces the observed pattern of cells

and sheets in the observed galaxy distribution. A cellular structure can therefore be generated over a part of space beyond the reach of any N-body experiment. This makes the Voronoi model particularly suited for studying the properties of galaxy clustering in cellular structures on very large scales. Although the model cannot say much about the pattern of the galaxy distribution on smaller scales, within the sheets, it can be considered as a useful prescription for the spatial distribution of the sheets themselves. In addition, by experimenting with the distribution of the galaxies within the sheets and the filaments considerable insight into the real galaxy distribution can be obtained.

An alternative use of Voronoi tessellations is as statistical descriptors of the galaxy distribution (cf. the 'polyhedral statistics' of Finney, 1979). The sensitivity of the geometrical characteristics of the Voronoi tessellations to the underlying nucleus distribution (see sect. 4, 5 and 6) makes the Voronoi tessellation, and its dual the Delaunay tessellation, a potentially very useful instrument in the study of the clustering properties of a point process. Although we do not intend to pursue this idea in our work, this approach was taken by Ling (1987) in his thesis. He used the Voronoi tessellation as a tool in studying the higher-order clustering properties of the galaxy distribution. He illustrated the use of the Voronoi tessellation in two dimensions on artificial point processes, the CfA catalogue, and a CDM simulation. He concluded that the statistic is very flexible, allowing a scale-dependent study of the distribution. However, the translation of this statistical information to more familiar statistical descriptors is not straightforward, and might prohibit an extensive use of the Voronoi distribution as a tool in galaxy distribution statistics.

This paper follows the usual outline. In the next section we will present the analytically known characteristic properties of three-dimensional Voronoi tessellations as well as of planar and linear sections through them. Subsequently, section 3 will contain a description of the algorithm to construct geometrically three-dimensional Voronoi tessellations from a random distribution of nuclei. This is followed by a presentation of a Monte Carlo statistical analysis of such tessellations and its constituent cells in section 4. Section 5 contains a presentation of the statistical properties of planar sections through three-dimensional Voronoi tessellations, followed by a similar analysis of linear sections in section 6. Finally, section 7 contains a symmary and discussion of the results.

2. Voronoi and Delaunay tessellations

Formally a Voronoi tessellation can be defined as follows. Assume that we have a distribution of a countable set Φ of nuclei $\{x_i\}$ in $\Re^d$. Let $\vec{x}_1, \vec{x}_2, \vec{x}_3, \ldots$ be the coordinates of the nuclei. Then, the *Voronoi region* Π_i of nucleus i is defined by the following set of points $\vec{x}$ of the space:

$$\Pi_i = \{\vec{x} | d(\vec{x}, \vec{x}_i) < d(\vec{x}, \vec{x}_j) \qquad \text{for all } j \neq i\}, \tag{1}$$

where $d(\vec{x}, \vec{y})$ is the Euclidian distance between $\vec{x}$ and $\vec{y}$. In other words, Π_i is the set of points which is nearer to $\vec{x}_i$ than to $\vec{x}_j$, $\quad j \neq i$. Note that each region Π_i is the intersection of the open half-spaces bounded by the perpendicular bisectors of the segments joining $\vec{x}_i$ with each of the other

$\vec{x}_j$'s. Hence, Voronoi regions are convex polyhedra (3-D) with finite size according to definition (1). Each Π_i is called a *Voronoi polyhedron*. The complete set of $\{\Pi_i\}$ constitute a tessellation of $\Re^d$, the *Voronoi tessellation* $\mathcal{V}(\Phi)$ relative to Φ. In two-dimensional space some authors refer to it as the Dirichlet or Thiessen tessellation. Known formulae for $\mathcal{V}(\Phi)$ are almost entirely confined to the case when Φ is a stationary Poisson process.

A pair of nuclei i and j whose Voronoi polyhedra Π_i and Π_j have a face in common is called a *contiguous pair* and a member of the pair is said to be *contiguous* to the other member. By joining all of the contiguous pairs of nuclei, we obtain a network. In this network, a set of four nuclei (in 2-D it is a set of three nuclei, although the following discussion is three-dimensional the generalization to arbitrary d-dimensional space can be easily made) which are contiguous with one another forms a tetrahedron. The set of tetrahedra constructed in such a manner constitutes a new tessellation, which is called the *Delaunay tessellation*, $\mathcal{D}(\Phi)$ (Delone 1934). These two tessellations, Voronoi and Delaunay, are dual to each other. The tetrahedron in the Delaunay tessellation is called the *Delaunay tetrahedron*. The circumsphere (i.e. its circumscribing sphere) of a Delaunay tetrahedron has two important properties.

I. The circumcenter, i.e. the center of the circumsphere, of a Delaunay tetrahedron is a vertex of the Voronoi tessellation. This immediately follows from the definition of the Voronoi tessellation, wherein the four nuclei which form the Delaunay tetrahedron are equidistant from the vertex concerned (see fig. 3).

II. (Contiguity Condition). The circumsphere of a Delaunay tetrahedron is *empty*, that is, there is no nucleus inside this sphere. This follows from the fact that if a fifth nucleus exists within the sphere, it is nearer to the circumcenter than the four nuclei on the surface of the sphere. Therefore, the center cannot be the common vertex of the Voronoi polyhedra of the four nuclei on the circumsphere surface.

Thus, the Delaunay tessellation can be defined as the tessellation consisting of all the tetrahedra, defined by four nuclei, whose circumsphere does not contain any of the nuclei of the generating set of nuclei. Figure 1 shows the two-dimensional Voronoi tessellation of a point distribution and its dual Delaunay triangulation.

At a vertex of the Voronoi tessellation, generally, four polyhedra meet. If a vertex happens to have five or more polyhedra in common, the vertex is said to be *degenerate*. Degenerate cases occur if the nuclei form a crystalline lattice. An example of a degenerate Voronoi tessellation is the regular square tessellation, arising from a regular square grid of points. While in generic planar Voronoi tesellations only three cells meet at each node, in the regular square tessellation four cells meet at each vertex.

The Voronoi tessellation can be generalized. Miles (1970) defined the *generalized Voronoi tessellation* $\mathcal{V}_n$, which uses for cells the sets of positions sharing the same n nearest neighbours of the generating point pattern ($\mathcal{V}_1 = \mathcal{V}$, the original Voronoi tessellation). Details are given in Miles (1970, 1972) and Miles and Maillardet (1982). The latter paper gives pictures of $\mathcal{V}_n$ for $n = 4$, 16, 64, and 256 relative to a stationary Poisson process.

Another generalization is the *Johnson-Mehl* model (Johnson & Mehl, 1939) which contains a dynamic element. Here 'nuclei' are generated by some birth process, and each nucleus grows so that at time t after its birth it occupies all the previously vacant region within the sphere of radius vt centred on its original point, with v the linear and isotropic velocity of growth (the same for all nuclei). Consequently, if a nucleus is born at a point in the current cell of another nucleus then it vanishes immediately; those that survive form cells that grow radially in each direction with velocity v, till cells of other nuclei are met. In the standard Johnson-Mehl model, the points in $\Re^3 \times [0, \infty)$ giving nucleus birth locations and times form a stationary Poisson process of constant intensity. If all nuclei are born at the same instant then the resulting tessellation is Voronoi. In the general model, however, the cells of the tessellations are not even convex. Formulae for the model are given in Meyering (1953), Gilbert (1962) and Miles (1972).

Still another generalization of Voronoi tessellations, which is probably a better approximation to the cellular distribution of galaxies, are the *weighted Voronoi tessellations* (Boots 1980; Aurenhammer & Edelsbrunner 1984). Here, the distance measure between an arbitrary point in space and a nucleus depends on the nucleus, i.e. the distance is the Euclidian distance weighted by some nucleus-dependent weight function. This will happen when the growth velocity (which is isotropic) differs from nucleus to nucleus (unlike in the "growth interpretation" of the conventional Voronoi tessellation). However, not much work has been done on this generalization, and no analytic results appear to be available.

2.1 Statistical moments of 3-D Voronoi tessellations

Present statistical knowledge about Voronoi tessellations stems from the pioneering works of Meyering (1953), Gilbert (1962), Miles (1970) and Møller (1989). With the exception of some general tessellation properties nearly all analytical work on Voronoi tessellations has concentrated on Voronoi tessellations generated by homogeneous Poissonian point distributions. Even of this case analytical results are quite rare, and are limited to a few distribution functions and statistical moments (expectation values, variances, correlation coefficients). The only completely known distribution function is that of the angles between adjacent edges in two dimensions (IW). To derive that distribution function analytical results on Delaunay triangles obtained by Miles (1970) were used. A few other distribution functions are known in the form of integral formulae, from which all characteristics can be derived by numerical integration. For example, Miles & Maillardet (1982) derived integral formulae for the probabilities p_n of the polygon having exactly n vertices. However, these formulae are very complicated and hence it is very helpful to determine such characteristics by Monte Carlo methods (see sect. 4, 5 and 6).

For the case of general 3-D tessellations (including Voronoi and Delaunay tessellations) Miles (1972) gives some general properties. If N_0 is the number of vertices per polyhedron, N_1 the number of edges per polyhedron and N_2 the number of walls per polyhedron, then Euler's formula tells us that

$$N_0 - N_1 + N_2 = 2. \tag{2}$$

In the case of simple polyhedra, i.e. polyhedra in which each vertex lies in three and only three walls (again, as in the case of Voronoi and Delaunay polyhedra), we then have

$$3N_0 = 2N_1. \tag{3}$$

Other interesting properties (characteristics) of a polyhedron are its volume V, its surface area A_C, and its perimeter S_C. Further characteristics of a tessellation include the area A_W of a wall, the perimeter S_W of a wall, and the length L of an edge.

Following the work of Miles (1972, 1974, 1984), Møller (1989) derived analytical expressions for a large number of first-order moments of d-dimensional Poisson-Voronoi tessellations, as well as of s-dimensional sections through them. From their work an enumeration of analytically calculated first-order moments of a 3-D Poisson-Voronoi tessellation with a nucleus intensity (number density) ρ can be assembled easily. In table 1 we present such a listing of first-order moments, together with the second-order moment of the volume of the cell, as was determined numerically by Gilbert (1962). The second column contains analytical expressions, while the third column contains numerical expressions. We should remark here that the analytical estimates of Møller (1989) do not agree with the outcome of our Monte Carlo calculations presented in section 4 in the case of the first order moments of the the surface area of a cell, the perimeter of a wall and the length of an edge. These moments are marked by a star in table 1. In all three cases the correct values can be inferred from the results of Miles (1972). In the table also the quantity N_2^* is mentioned, which is the number of *full neighbours*. Two contiguous cells with a common polygonal face are *neighbours*. If the line joining their nuclei hits this common face, then they are *full* neighbours. A cell has N_2 neighbours, N_2^* of which are full.

Cosmologically important are the characteristics of lower-dimensional sections, both line ('pencil beams') and plane ('slices') sections, through 2-D and 3-D tessellations (in the case of 2-D tessellations just the line sections), in other words, the stereological properties of tessellations. From the general formulae for s-dimensional sections through d-dimensional Poisson-Voronoi tessellations given by Miles (1984) and Møller (1989) the results on the one-dimensional (linear) and two-dimensional (planar) sections through 3-D tessellations can easily be inferred. For planar sections through a three-dimensional ($d \geq 3$) Poisson-Voronoi tessellation generated by Poissonian distributed nuclei with a number density ρ of nuclei, table 2 gives the moments which have been derived by Miles (1984) and Møller (1989), together with a numerically derived moment by Gilbert (1962). As in the case of table 1, the second column gives the analytical expressions, while the third column gives the numerical expressions (with cell we here mean the 2-D section cut by the section plane through the 3-D cell). For linear sections through such a d-dimensional ($d \geq 2$) Voronoi tessellation the mean length $\langle\lambda\rangle$ of an edge in the linear section is given by

$$\langle\lambda\rangle = E(L) = \frac{d\,\Gamma(d-\frac{1}{2})\,\Gamma\left(\frac{d+1}{2}\right)^2}{(d-1)!\,\rho^{1/d}\,2\,\Gamma\left(\frac{d}{2}+1\right)^{2-(1/d)}\,\Gamma\left(2-\frac{1}{d}\right)}. \tag{4}$$

This result is obtained by using the general line section property of a tessellation that relates the mean edge length $E_1(L)$ in a linear section through an arbitrary tessellation with the average volume and average surface area of a cell (see Miles 1972; Møller 1989),

$$E_1(L) = 4\,\frac{E(V)}{E(A)}, \tag{5}$$

wherein $E(V)$ is the mean cell volume and $E(A)$ the mean cell surface area. Table 3 gives some moments for of the mean edge length $\langle\lambda\rangle$ of a linear section through two-dimensional and three-dimensional Poisson-Voronoi tessellations, which were obtained by using either equation (4) or by numerical integration (Gilbert 1962; Miles 1972; Møller 1989). These quantities are interesting in the context of the pencil beam redshift surveys (see e.g. Van de Weygaert 1991a).

Although any homogeneous stochastic process in $\Re^d$ gives rise to an associated Voronoi tessellation, evidently the only analytically tractable one is the Poissonian case. However, since other, non-Poissonian, nuclei distributions may give rise to cosmologically interesting cell structures, statistical results of the corresponding Voronoi tessellations can be very useful. These can only be derived by using Monte Carlo calculations.

3. Construction of three-dimensional Voronoi tessellations

Although the need for efficient Voronoi tessellation construction algorithms has increased substantially, not many algorithms have been published in detail. The first 2-D algorithm was the one by Green & Sibson (1978). This is an $\mathcal{O}(N^{3/2})$ algorithm, which may be called rather inefficient compared to the theoretical limit of $\mathcal{O}(N)$. Indeed, Aggarwal *et al.* (1987) succeeded in designing an $\mathcal{O}(N)$ algorithm for a planar Voronoi tessellation. Brown (1979) mentioned the possibility of computing tessellations in k dimensions using tranformations of convex hulls in $k+1$ dimensions. However, since general convex hull algorithms are not available this idea has only been implemented for planar tessellations, giving an $\mathcal{O}(N \log N)$ algorithm. Although efficient two-dimensional algorithms seem to be generally available this is not the case for three-dimensional algorithms. Brostow, Dussault & Fox (1978) and Finney (1979) published three-dimensional algorithms with a computational cost proportional to $\mathcal{O}(N^2 \log N)$ and $\mathcal{O}(N^4)$ respectively. Bowyer (1981) and Watson (1981) presented algorithms for ($k = 2, 3, 4, \ldots$) based on the computation of the Delaunay tessellation of the same point process. In fact, Boots (1974) was the first one to point out that the computation of a Voronoi tessellation could be greatly simplified by working with its dual, which has the additional advantage of a cleaner separation between the topological (incidence relation between the vertices, edges, and faces) and geometrical aspects (coordinates, lengths, angles, etc.) of the

problem (Guibas & Stolfi, 1985). The algorithm we used for the computation of two-dimensional Voronoi tessellations (IW) employs the same principle.

Our three-dimensional Voronoi tessellation construction algorithm basically consists of three major steps. These are (1) the prescription of the distribution of nuclei, (2) the specification of the boundary conditions, and (3) the construction for each nucleus of the cover of its Voronoi tile, i.e. all the faces of its Voronoi polyhedron, which encompasses all points that lie closer to that nucleus than to any of the other nuclei. The first step, the specification of the underlying nuclei distribution, will be described in section 4.

In the second step we take toroidal, periodic boundary conditions, so that the central field (box) is surrounded by 26 equivalent boxes. The central field is taken to be a cube in the present statistical study. This simplifies the analysis to some extent without giving up generality of the results. Because every "boundary" field has the same distribution of nuclei, the tessellation in those boundary fields is exactly equal to the tessellation in the central field. Another approach is to take the central field and surround it by empty space. In particular near the boundary of the central field this will yield Voronoi cells that can extend towards infinity since they contain that part of space closer to them than to any other nucleus. The statistical analysis of the geometrical properties would therefore be seriously complicated. Still another approach, which probably leads to the similar statistical results, is to embed the central field in a larger box wherein the nuclei are distributed according to the same statistical point process. In that case, the original box should be considered as a small part cut out of a far larger box. The point distribution outside the central field is therefore not an exact copy of the one in the central field. Since we are mainly interested in cosmological applications, where nearly all N-body simulations are carried out in a box with periodic boundary conditions, and because of the accompanying advantage of the interpretational simplification of the statistical results we decided to take the first possibility of toroidal boundary conditions.

In the third step, the actual construction of the Voronoi tessellation from the specified distribution of nuclei, two broad classes of methods can be distinguished. These are (1) Monte Carlo algorithms and (2) geometric algorithms.

(1) The Monte Carlo methods start with a distribution of a large number of "test particles", e.g. Poissonian distributed points or points distributed on a regular grid, which are moved around in the field with the nuclei in such a way that they end up at, or very near, a *facet* (vertices, edges, faces, etc.) of the tessellation. If one plots their position one gets a clear idea of the structure of the underlying tessellation. One of the earliest examples was the method used by Kiang (1966), who determined the Voronoi tessellation of a random distribution of 80 nuclei by determining the nearest nucleus for each point out of a grid consisting of 6400 points. A comparable method is a recursive method. The original square is subdivided, e.g. in four quarters (although the actual number can be chosen freely for optimal convergence). Then the nearest nucleus is determined of each corner of a small square. If not all four corners belong to the same centre, the same subdivision is applied to the small square. In this way one can delineate the tessellation structure rather fast and efficiently. Still another approach was used in the three-dimensional case by WI, Yoshioka & Ikeuchi (1989)

and Weinberg (1989). The test particles are moved along the line pointing to the nearest nucleus, thereby constantly keeping track of the nearest nucleus. When there is a change of nearest nucleus one knows the test particle is situated (within resolution accuracy) in the face of the Voronoi cell surrounding the first nucleus. This game can be continued by moving the test particle around within the wall, until it hits a third nearest nucleus when it enters an edge, and subsequently by moving it along that edge until a fourth closest nucleus has been found when the particle hits a vertex. These Monte Carlo methods can be generalized without much effort to two dimensional space, and indeed to any d-dimensional space. An advantage of the Monte Carlo method is that it is generally applicable, making it the natural method in the case of more general tessellations, like the Johnson-Mehl subdivision of space (Johnson and Mehl, 1939), in which the nuclei start growing at different times, or weighted Voronoi foams (Boots, 1980), in which the growth velocities differ from nucleus to nucleus. An important disadvantage of the Monte Carlo algorithms is their finite resolution, which makes it difficult to trace all facets of the tessellation. One can e.g. never be sure one has found all vertices, because it is possible two vertices are located at a distance shorter than the resolution of the test particles. Another disadvantage is that one does not have the flexibility to play around with all the elements of the tessellation, e.g because one does not know the exact position of all vertices. This certainly is a disadvantage if one intends to study different point clustering schemes within the cell structure defined by the Voronoi tessellation.

(2) The second class of methods is the one of the geometric methods. Their advantage is that they are exact and flexible, and economic in the case of Voronoi tessellations. However, in the case of more general tessellations this need not be true, even though now there is even a geometric method for the construction of two-dimensional weighted Voronoi tessellations, based on convex hulls in three dimensions (see Aurenhammer & Edelsbrunner 1984). Discussions in the literature have mainly concentrated on geometric algorithms (Green & Sibson 1978; Brostow *et al.* 1978; Finney 1979; Tanemura, Ogawa & Ogita 1983).

3.1 The geometric construction theorems

Our geometric algorithm for constructing three-dimensional Voronoi tessellations computes the Delaunay tetrahedra of the point process, followed by establishing the links between the detected Voronoi vertices. A substantial part of our algorithm is described by Tanemura *et al.* (1983). Our implementation of the algorithm deviates from theirs in several ways. Among other things, we used several programming "pearls" (Bentley 1986), such as multidimensional binary trees, to speed up essential parts of the algorithm.

The main part of the algorithm consists of the procedure for constructing a single Voronoi polyhedron, Π_i. The tessellation is then obtained by the repeated use of this procedure for all of the nuclei $i = 1, \ldots, N$. We denote the set of all Delaunay tetrahedra with nucleus i as a common vertex with T_i. Obtaining T_i is equivalent to obtaining Π_i. Note that T_i constitutes a polyhedron, not necessarily convex, whose vertices are nuclei. It will be referred to as a *contiguity polyhedron* of nucleus i. Let C_i be a set of such vertex nuclei of that polyhedron. Each member of C_i corresponds

to a face of Π_i, the face being the perpendicular bisector of that member of C_i and nucleus i. The face of Π_i which corresponds to a certain nucleus, say j, can be determined by determining the Delaunay tetrahedrons of T_i which have the nuclei i and j as common vertices. Figure 2 is a two-dimensional representation of this three-dimensional structure. The solid black dot represents the Delaunay edge between the nuclei i and j. This edge is pointing out of the page, with the nucleus j above i. The solid polygon is the Voronoi face defined by the nucleus i and j, while the open dots are the other nuclei that together with i and j determine this face. Each dashed triangle represents a Delaunay tetrahedron that has the contiguous pair $\{i, i_\alpha\}$ as one of its 6 edges. The dashed lines between the solid dot and the open dots are faces of these Delaunay tetrahedra seen edge-on, while the dashed lines connecting open dots are true edges. The vertices of Π_i are the circumcentres of the corresponding members of T_i. As can be seen from figure 2, other geometries of Π_i, edges for instance, can also be determined from the connectivity among the elements of T_i. Therefore, the efficiency of the algorithm depends on how quickly we can search T_i and the connections in T_i. Determining the set C_i is greatly simplified if at the start of the calculation of P_i we have an already known set S_i of nuclei surrounding nucleus i that includes C_i, i.e. $C_i \subset S_i$ (note that S_i does not include the nucleus i itself). The task is then to determine the contiguous set of nuclei C_i from the set S_i.

The basis of the geometric construction algorithm is formed by the following four theorems.

THEOREM I.
Let a nucleus i_1 be the nearest to a nucleus i. Then i_1 and i are contiguous to each other.

THEOREM II.
Consider a set of triangles $\{i, i_1, j\}$, $j \in S_i$ and $j \neq i_1$. Among them, suppose a triangle $\{i, i_1, i_2\}$ has the minimum circumradius. Then, the triangle is a face of a certain Delaunay tetrahedron, that is, the three nuclei i, i_1, and i_2 are mutually contiguous.

THEOREM III.
Consider a set of tetrahedra $\{i, i_1, i_2, j\}$, where $j \in S_i$ and $j \neq i_1, i_2$. Among them, suppose a tetrahedron $\{i, i_1, i_2, i_3\}$ has the minimum circumradius. Then, the tetrahedron is a Delaunay tetrahedron, that is, the four nuclei i, i_1, i_2, and i_3 are mutually contiguous.

THEOREM IV.
Let a Delaunay tetrahedron $\{i, i_\alpha, i_\beta, i_\gamma\}$ be an element of T_i. Consider a set of tetrahedra $\{i, i_\alpha, i_\beta, j\}$, where $j \in S_i(\alpha\beta|\gamma)$. Among them, suppose the circumcentre of a tetrahedron $\{i, i_\alpha, i_\beta, i_\delta\}$ has the minimum Z-coordinate value, where the coordinate Z of the circumcentre is defined as its distance to the plane $\{i, i_\alpha, i_\beta\}$ and the sign of the coordinate is chosen so that the coordinate of i_γ is negative. Then, the tetrahedron is a Delaunay tetrahedron, that is, the four nuclei i, i_α, i_β, and i_δ are mutually contiguous.

The first one appears to be obvious, but is in fact not trivial. Most authors assume it to be valid without any proof. These theorems and their proofs were presented by Tanemura *et al.* (1983; also see Van de Weygaert 1991b).

3.2 The geometric construction algorithm step-by-step

Although finding the Delaunay tetrahedra is the basic principle of the construction procedure, it is as important to find the right links among them. Figure 3 illustrates how the geometrical elements of the tessellation, i.e. the cells, walls, edges and vertices, are linked with the generating nuclei. In our case the right links are mainly determined by computing all the walls in the tessellation, and keeping track of the cells to which these walls belong. Since the structure of each wall, a polygon, is completely determined by all the vertices that mark the wall, finding and ordering these vertices provides one with the desired knowledge of the links between the vertices. We order the vertices that delineate the wall in such a way that one can draw the wall by just connecting the vertices in the order given by the list. Therefore, the computation of new Delaunay tetrahedra always takes place within the context of the calculation of a new wall. In fact, the construction procedure works by computing the walls shared between the nucleus i and all the nuclei contiguous to it. One keeps track of all the contiguous nuclei which have been found up till now by putting them in the list C_i. The complete Voronoi polyhedron Π_i has been completed when for every nucleus $j \in C_i$ the wall between j and i has been determined.

The prime difference between our implementation of the construction algorithm and the one outlined by Tanemura *et al.* (1983) is that we determine each Delaunay tetrahedron of the complete tessellation only once, instead of four times. This ocurs at the expense of a rather complicated bookkeeping procedure, since once a Delaunay tetrahedron has been found its information has to be passed on to all four nuclei that are its vertices. The same strategy is followed concerning the walls in the Voronoi tessellation. Each wall in the tessellation is shared by two nuclei. Since we do not wish to repeat this twice we calculate a wall between two nuclei i and j, with $i < j$, only for i. Later on, when we are computing the polyhedron Π_j, we just pass on the knowledge about the wall between j and i to Π_j without calculating it again. We therefore only need to tell that i is a nucleus contiguous to j and that the wall they share is the wall between i and j, which is specified by some number.

The tessellation algorithm starts by ordering the nuclei in the box in a multidimensional binary tree (Bentley 1975; Bentley & Friedman 1978; Van de Weygaert 1987), a generalization of the simple binary tree used for sorting and searching. The multidimensional binary tree, also called $k-d$ tree, is a binary tree in which each node represents a subset of the records in the set and a partitioning of that subset. In the $k-d$ tree the nuclei are sorted in such a way that nuclei which lie close together in parameter space also have a nearby position in the tree. This leads to the great advantage that it allows multidimensional searching tasks, like searching for all nuclei within a specific spherical

region or searching for all M-th nearest neighbours, to be solved in a time proportional to $N \log N$, with N the number of records (nuclei) in the set. For a more detailed description see appendix F. A consequence of our implementation of the tree construction is that all nuclei will be renumbered since they are given a number i according to their position in the tree.

A point of consideration concerning the multidimensional binary tree are the periodic extensions of the central field (26 "clones" surround the central field). We chose the strategy not to include the points of the periodic boundary fields in the tree. When we need to look for nuclei in the boundary fields we just translate the searching centre to the correct relative position and then search through the tree of the central field.

After the multidimensional binary tree has been constructed we proceed by constructing for each of the nuclei $i = 1, \ldots, N$ their surrounding Voronoi polyhedra, Π_i, starting with nucleus $i = 1$ and finishing with nucleus $i = N$. The construction procedure works such that as soon as the polyhedron Π_i has been computed the nucleus i can be discarded from any further considerations. Useful notions in the context of the following discussion are the half-space $H_i(\alpha\beta|\gamma)$ and the subset $S_i(\alpha\beta|\gamma)$. The half-space $H_i(\alpha\beta|\gamma)$ is the one determined by the plane through the points $\{i, i_\alpha, i_\beta\}$ and which does not contain i_γ. The subset of S_i which is inside the half-space $H_i(\alpha\beta|\gamma)$ is then denoted by $S_i(\alpha\beta|\gamma)$.

Taking into account the previous considerations, the procedure for computing the complete Voronoi cell Π_i surrounding a nucleus i essentially consists of the following subroutines:

1. Determine S_i, that is a set of nuclei that includes all nuclei contiguous to i. In order to make the amount of computations as low as possible, we try to make the set S_i as small as possible. Since only afterwards one can determine with certainty whether all contiguous nuclei were in S_i or not, we build in an extra procedure for checking this after computing a new Delaunay tetrahedron (appendix C) or a triangle with minimum circumradius (appendix A). If there is the possibility that there are contiguous nuclei outside S_i we have to undertake a corrective procedure. Because the correction calculations are rather expensive the set S_i has to be reasonably large. We therefore have to reconcile the demands that S_i should not be too large in order to avoid an unnecessary computational effort, while at the same time S_i should not be too small in order to avoid the expensive correction procedure. The most natural choice for S_i is to take the set consisting of the N_s nearest nuclei to i, with N_s a number determining the efficiency of the implementation, taking into account the preceding remarks. We take $N_s = 50$, until there are fewer nuclei left to consider (i.e. $N - i < 50$), in which case we take $N_s = N - i$. After we have found these N_s nearest neighbours we sort them in order of increasing distance to nucleus i. The distance to the N_s^{th} nearest neighbour, $d(i, i_{N_s})$, is defined to be the radius R_i of the set S_i. R_i plays a role when checking whether it is sufficient to merely consider the nuclei in S_i when searching for a triangle with minimum circumradius or for a new Delaunay tetrahedron.

   One consequence of our strategy to calculate each Delaunay tetrahedron only once during the whole computation of the tessellation is that once we have finished the calculation of Π_i we have found all the Delaunay tetrahedra which have i as one of the vertices. Consequently, we do not need to consider nucleus i again when searching for new Delaunay tetrahedra. This implies that nucleus i should not be included in the sets S_j for $j > i$. Because the nuclei are so neatly ordered in a multidimensional binary tree and because we determine the Voronoi polyhedra sequentially, this can be done in an efficient way by continually "pruning" the tree. The searching tasks therefore take less and less effort as a consequence of the tree losing its branches one by one.

2. If none of the vertices of the Voronoi cell of nucleus i has been determined before one starts constructing the polyhedron Π_i, one starts by finding a first vertex of that cell. During the calculation of the first vertex the first three nuclei contiguous to i will be found. The construction of Π_i is subsequently continue by computing the wall between i and the first of the three contiguous nuclei that was found when computing the first Delaunay tetrahedron. During the computation of this wall, new contiguous nuclei will be found. They are added to the list C_i of contiguous nuclei. The computation of the first Delaunay tetrahedron involves the following three steps (keeping in mind theorem 1 through theorem 3):

   I. Find the nucleus i_α which is the nearest to the nucleus i. Theorem 1 tells us that i_α is contiguous to i and is a member of C_i.

   II. Consider a set of triplets $\{i, i_\alpha, j\}$, where $j \in S_i$ and $j \neq i_\alpha$. Find the nucleus $j = i_\beta$ so that the triangle $\{i, i_\alpha, i_\beta\}$ has the minimum circumradius, i.e. the radius of the circumscribing circle of the triangle, in the set of triangles considered above. According to theorem 2 the triangle $\{i, i_\alpha, i_\beta\}$ then constitutes one of the faces of a Delaunay tetrahedron. Subsequently, append i_β to the set C_i, i.e. $i_\beta \cup C_i \rightarrow C_i$. See appendix A for a detailed description of this procedure.

   III. Define the normal $\vec{n}$ to the triangular plane $\{i, i_\alpha, i_\beta\}$ such that the the system $\{(\vec{r}_\alpha - \vec{r}_i), (\vec{r}_\beta - \vec{r}_i), \vec{n}\}$ has a right-handed orientation. Consider a set of quartets $\{i, i_\alpha, i_\beta, j\}$ with $j \in S_i(\alpha, \beta; \vec{n})$ and $j \neq i_\alpha, i_\beta$, whereby $S_i(\alpha, \beta; \vec{n})$ is the subset of S_i situated on the positive side of the plane $\{i, i_\alpha, i_\beta\}$ (positive means in the direction of $\vec{n}$). Find the nucleus $j = i_3$ so that the tetrahedron $\{i, i_\alpha, i_\beta, i_\gamma\}$ has the minimum Z-coordinate value, where the coordinate Z of the circumcentre is defined as the distance to the plane $\{i, i_\alpha, i_\beta\}$, and a positive sign of the coordinate is taken along the direction of $\vec{n}$. According to theorem 4 the tetrahedron $\{i, i_\alpha, i_\beta, i_\gamma\}$ is a Delaunay tetrahedron and a member of T_i. This tetrahedron is called the initial Delaunay tetrahedron. Append i_γ to the set C_i, i.e. $i_\gamma \cup C_i \rightarrow C_i$. Essentially this is the same procedure as detecting a new Delaunay tetrahedron starting from an earlier one except that now one does not determine the distance of the circumcentre P_j of the tetrahedron $\{i, i_\alpha, i_\beta, j\}$ to the previous Voronoi vertex V, circumcentre of the Delaunay tetrahedron $\{i, i_\alpha, i_\beta, i_\gamma\}$, but to the circumcentre Ξ of the triangular plane $\{i, i_\alpha, i_\beta\}$. In appendix B one can find a description of how to calculate the coordinates of Ξ. The whole Delaunay tetrahedron detection procedure is

described in appendix C, whereby one should replace V by Ξ, and (v_1, v_2, v_3) by (ξ_1, ξ_2, ξ_3).

Once the first Delaunay tetrahedron has been found, we can find all the others belonging to T_i using the information of the earlier determined members of T_i. This process is outlined in appendix C.

3. If already some vertices of Voronoi polyhedron Π_i are known, then the procedure starts by processing that information in such a way that the calculation of the walls, edges and vertices of Π_i is facilitated. See appendix E for some details.

4. Construct sequentially the walls between nucleus i and all its contiguous nuclei, which are stored in the set C_i. The construction of the wall between the nucleus i and a contiguous nucleus i_α consists of the sequential detection of all Delaunay tetrahedra which have the contiguous pair $\{i, i_\alpha\}$ in common until they enclose the pair $\{i, i_\alpha\}$ without any gap. One can distinguish two cases here.

   The first case is $i_\alpha < i$, which means the common wall has already been determined when constructing Π_{i_α}. The only thing to do in this case is to specify where the data on that wall can be found, in other words specifying the number of the wall. The second case is $i_\alpha > i$, in which case the structure of the wall still needs to be determined, though a certain number of Delaunay tetrahedrons around the pair $\{i, i_\alpha\}$ will already have been found (at least one, otherwise i_α could not be in the list C_i).

   In the second case, the wall construction consists of two tasks: it has to put the previously found Delaunay tetrahedra in the right order, in the meantime filling in the gaps with newly computed ones. Appendix D contains a more detailed description of the procedure of closing the set of Delaunay tetrahedra around a contiguous pair $\{i, i_\alpha\}$.

   The detection of a new Delaunay tetrahedron starts by noting that it shares any of its four triangular faces $\{i, i_\alpha, i_\beta\}$ with another. Thus, we can obtain a new Delaunay tetrahedron $\{i, i_\alpha, i_\beta, i_\delta\}$ from the knowledge of a previously determined one, $\{i, i_\alpha, i_\beta, i_\gamma\}$, by finding a nucleus i_δ, such that the triangular face $\{i, i_\alpha, i_\beta\}$ together with i_δ forms a Delaunay tetrahedron. The procedure for doing this is described in detail in appendix C.

   Initially the set C_i will be constantly growing, since new contiguous nuclei will be found when new Delaunay tetrahedra are found. Towards the completion of Π_i, however, the number of newly found contiguous nuclei will be low. Finally the set C_i will be exhausted, for each of the contiguous nuclei one has determined the wall shared between them and i. Then the construction of the polyhedron Π_i has been completed.

5. After the computation of all the walls that surround Π_i the contiguous nuclei i_α are sorted in ascending order of the number i_α, together with the corresponding data on the structure of the corresponding walls. The data on Π_i are then written to files, so that they can be used for further analysis.

4. Monte Carlo statistical study of 3-D Voronoi foams

Only a few moments of geometrical properties of Voronoi tessellations are known analytically, almost without exception in the case of Poissonian distributed nuclei. Hence, the necessity to use a Monte Carlo approach in assessing the statistical properties of Voronoi tessellations, especially in the case of non-Poissonian distributed nuclei. In this section we present the results of a Monte Carlo study of the statistics of the geometrical properties of 3-D Voronoi foams themselves and their constituents, the cells, walls and edges.

Since a large systematic study, consisting of the calculation of more than ten realisations of each 1000 Voronoi cells for a large choice of underlying nuclei distributions, was not feasible in the available time and would probably not lead to a better qualitative understanding of the behaviour of the geometrical properties as a function of the underlying nuclei distribution it was decided to limit the study to three different distributions of nuclei: a Poissonian distribution, an anticorrelated (somewhat regular) distribution and a correlated distribution. Of these three distributions several realisations were calculated, followed by the determination of four moments of each of the geometrical properties. Accordingly, in this section the data on these four moments are presented in three tables, one for each different nucleus distribution. Additionally, since moments only contain a limited amount of information about the underlying distribution, histograms of the considered considered geometrical properties are presented, as well as some scatter plots in order to understand the correlation between some of the geometrical properties. As a consequence this section, as well as the next one, consists for a large part of the presentation of figures and tables, which should largely speak for themselves.

Before discussing their statistical properties, we first give an impression of the structure of 3-D Voronoi cells by showing some examples. Unlike the two-dimensional case, it is impossible to show all cells of the tessellation together. Probably the best idea of the complete structure of the 3-D Voronoi tessellation can be obtained from two-dimensional planar sections (slices) through the 3-D Voronoi tessellations, as shown in figure 11 (see next section for a discussion). By showing six cells out of a tessellation of 1000 cells figure 4 gives an impression of the large diversity of shapes of the 3-D Voronoi polyhedrons (the sizes are rescaled by the plotting program, the relative sizes of the plots therefore do not bear out the actual size ratios of the cells). The Voronoi walls on the front of the Voronoi polyhedra are bounded by black lines, the walls on the back by dashed lines. The star in the each plot denotes the position of the generating nucleus. In addition, figure 5 shows a stereoscopic pair of three Voronoi cells that share a common edge. As in figure 4 the stars denote the position of the nuclei. In a stereo viewer, the dashed lines will appear at the rear of the picture. When attempting stereo fusion with crossed eyes, the pictures must be reversed to obtain the correct depth perception.

4.1 The spatial distribution of the nuclei

The point distribution that the we explored in our Monte Carlo study consisted of three classes, (1)

correlated distributions, (2) Poisson (uncorrelated) distribution and (3) anticorrelated distributions. The correlated distributions are called Class C distributions, the Poisson distribution the Class P distribution, and the anticorrelated distributions the Class A distributions.

Since there is an infinity of possible prescriptions for both correlated and anticorrelated distributions, we have to make a specific choice. For both the correlated and anticorrelated distributed nuclei we took prescriptions that conform to the ones used in the literature of stochastic geometry. In all cases 1000 nuclei were distributed in a box of size $100 \times 100 \times 100$. In the case of the anticorrelated nuclei the distribution was parametrized by one parameter: the minimum distance δ between any of the nuclei (including the nuclei in the periodic extensions of the central box). We expresss δ in units of the mean distance $n^{-1/3}$ between the nuclei, n being the number density of the nuclei. In the present study we take $\delta = 0.8$, so that every nucleus has a distance to its nearest neighbour of at least $0.8 \times n^{-1/3}$. In the case of the correlated nuclei an adapted version of the Neymann-Scott process is used. This point process is characterized by three parameters N_0, N_1 and λ, and is constructed as follows. One starts with N_0 Poissonian distributed parent points, around each of these parent points N_1 points are uniformly distributed within a sphere of radius λ, whereby λ is expressed in units of the mean distance between the parent points, $n_0^{-1/3}$ (with n_0 the number density of the parent points). The class of correlated distributions in the present study has $N_0 = 200$ and $N_1 = 5$. Consequently, 1000 points are distributed within a box of size $100 \times 100 \times 100$. The third parameter, λ, has a value of 0.4, so that the nuclei are distributed uniformly within a sphere of radius $0.4 \times n_0^{-1/3}$.

Since it is rather difficult to get a good idea of the distribution of points in a three-dimensional illustration, we show the two-dimensional equivalents of these three-dimensional point processes in figure 6. Instead of 1000 points in a box of size $100 \times 100 \times 100$, 100 points are distributed in a square of size 100×100. The mean distance between the points in both the 2-D and the 3-D case is therefore equal to 10.0. In the case of the anticorrelated distribution the minimum distance between the points is also 0.8 times the mean distance between the points, as in the three-dimensional case. In the case of the correlated distribution, $N_0 = 33$ parent points are taken. Around each parent point $N_1 = 3$ points are distributed uniformly within a circle of radius of 0.4 times the mean distance between the parent points, $n_0^{-1/2} = 17.4$. This parent point mean distance is about equal to one between 200 points in three dimensions.

4.2 Statistical analysis

The analysis of the 3-D foams was split into three parts: the analysis of the characteristic properties of the cells, of the walls, and of some general properties, including the properties of edges. For each of the Voronoi tessellations, each consisting of $K = 1000$ cells, a plethora of quantities was determined.

Of the Voronoi cells the following properties were determined:

a. number of vertices per cell, N_0,

b. number of edges per cell, N_1,

c. number of walls per cell, N_2,

d. volume of the cell, V_{cell},

e. surface area of cell, A_{cell},

f. perimeter of cell, S_{cell},

g. form factor of the cell, F_{cell}.

The surface area A_{cell} of the cell is the sum of the areas of the walls that form the boundary of the cell, while the perimeter of the cell is the sum of the lengths of the edges that define the polyhedral surface. The form factor F_{cell} is a dimensionless quantity that tries to describe, partially, the shape of the cell. One has to realize, though, that for a complete description of the shape of a polyhedron more is needed than just one number. In fact, a picture of the polyhedron probably conveys the most information on the shape. We are in particular interested in the question whether the cell looks regular or more needle-shaped. By "regular" we mean an as good as possible approach to the shape of a sphere. Note that a sphere can be considered as a polyhedron whose surface consists of an infinite number of walls of infinitesimal size. We therefore took a form factor that measures the ratio between the volume and the surface area of the polyhedron

$$F_{cell} \equiv 36\pi \frac{V_{cell}^2}{A_{cell}^3}, \tag{6}$$

with V_{cell} the volume of the polyhedron, and A_{cell} the surface area of the polyhedron. In the case of a sphere the form factor $F_{sph} = 36\pi V_{sph}^2/A_{sph}^3$ has the value 1, which is an absolute upper limit to this parameter. Although one should be careful with assigning too much significance to the form factor defined here, it is certainly a useful measuree. Notice that due to the definition of the form factor the size of the cell drops out, so that the form factor is in principle a size-independent quantity. The correlation between the shape and the size of a cell in a tessellation, however, is an interesting issue that will be addressed in the subsequent statistical analysis.

Of the Voronoi walls the following quantities of were determined:

a. number of vertices per wall, N_0^w,

b. area of wall, A_{wall},

c. perimeter of wall, S_{wall},

d. form factor of wall, F_{wall},

e. distance nucleus-wall, D_{nw},

f. volume nucleus-wall, V_{nw}.

The perimeter S_{wall} of a wall is the sum of the lengths of the edges that define the wall, a polygon. As in the case of a 3-D polyhedron the form factor F_{wall} of a wall is an indicator for the shape of the wall, following the same philosophy. In this case the form factor is the ratio between the area of the wall and its perimeter, defined in a dimensionless way,

$$F_{wall} \equiv 4\pi \frac{A_{wall}}{S^2_{wall}}, \tag{7}$$

with A_{wall} the surface area of the wall. The upper limit to F_{wall} is the form factor F_{circ} of a circle, $F_{circ} = 4\pi\, A_{circ}/S^2_{circ} = 1$. The quantity "Distance nucleus-wall" is the distance of the nucleus of the cell to which the wall belongs and the perpendicular projection of this nucleus on this wall. It is therefore half the distance between the nucleus and the neighbour nucleus which share this Voronoi wall (see e.g. Fig. 3b). The measure "Volume nucleus-wall" is the volume of the "pyramid" with the nucleus as top and the wall as base, which is the product of the area of the wall and the distance of the nucleus to the wall ("Distance nucleus-wall"). We consider this quantity because it can be considered as the volume of the "influence region" of the wall in the case of the naive picture of matter flowing radially away from the nucleus towards the wall, so that all matter in this pyramid will end up in this wall. This quantity is therefore a measure for the amount of matter ending up in this wall. Likewise, the "Distance nucleus-wall" is a measure of the surface density of the wall.

In addition to the geometrical properties of the cells and the walls some more properties of the Voronoi foam were considered. Since they concern a wide range of characteristics of the foam, we list them together

a. number density of vertices, J_0,

b. number density of edges, J_1,

c. number density of walls, J_2,

d. length of edge, L,

e. angle between edges that cross, α_{ee},

f. angle between walls that cross, α_{ww}.

The number density of vertices is defined as the number of vertices per unit volume. Since the unit of volume is chosen in such a way that one unit volume contains exactly one nucleus the number density is the ratio of the number of vertices in the tessellation to the number of nuclei generating the tessellation. The number density of edges and the number density of walls are defined in a similar way. Also considered are the length of every edge and the angle between any two edges that have a common vertex. The latter qunatity is the angle subtended by two edges as they cross at the vertex. Remember that four edges meet at a vertex so that each vertex corresponds to six angles. In addition, the the angle between any two walls that have a common edge is determined. Since three walls meet at one edge each edge corresponds to three such angles.

Each quantity mentioned above produces a set $\{A_i\}, i = 1, \ldots, L$. Hereby the total number of points L in the set is proportional to the number K of cells in the tessellation, while it also depends on the specific property under consideration. From the resulting sets $\{A_i\}$ four statistical characteristics of the distribution functions of corresponding quantity A are estimated, namely

i. the mean of each set $\{A_i\}$, $\bar{A}$,

ii. the standard deviation, $\sigma(A)$,

iii. the skewness, $\gamma_1(A)$,

iv. the kurtosis, $\gamma_2(A)$.

As usual the last three quantities are defined by

$$\sigma^2 \equiv E[(X-\mu)^2], \qquad \gamma_1 \equiv \mu_3/\sigma^3, \qquad \gamma_2 \equiv (\mu_4/\sigma^4) - 3. \tag{8}$$

Hereby μ is the expectation value (mean) of the variate X, and μ_k its *kth central moment*,

$$\mu_k = E[(X-\mu)^k]. \tag{9}$$

For a normal distribution $\gamma_1 = \gamma_2 = 0$. From its definition we can see that the skewness provides information on the asymmetry of the distribution function around the mean μ, $\gamma_1 > 0$ implying a slower decrease of the curve on the positive side. The kurtosis is a measure of the "peakedness" of the distribution function. If $\gamma_2 > 0$ a distribution is implied that is more peaked than the normal distribution. However, since most distributions differ a lot from the shape of the normal distribution, the significance of the kurtosis should not be taken too literally.

Estimates of the average and the standard deviation are obtained from the sets $\{A_i\}$ ($i = 1, \ldots, L$) by

$$\bar{A} = \sum_{i=1}^{L} \frac{A_i}{L}, \qquad \sigma(A) = \left\{ \frac{(A_i - \bar{A})^2}{(L-1)} \right\}^{1/2}, \tag{10}$$

while the skewness and kurtosis are estimated from

$$\gamma_1(A) = \frac{1}{\sigma(A)^3} \sum_{i=1}^{L} \frac{(A_i - \bar{A})^3}{L}, \qquad \gamma_2(A) = \frac{1}{\sigma(A)^4} \sum_{i=1}^{L} \frac{(A_i - \bar{A})^4}{L}. \tag{11}$$

The values of the mean, standard deviation, skewness and kurtosis of the various quantities are presented in several tables. In addition to the determination of these four characteristics of the distribution functions also histograms are plotted. In this way a good qualitative idea of the underlying distribution functions can be obtained. These histograms are presented in several figures. They contain the data on one complete foam of 1000 cells. Except for the histograms concerning integer and discrete quantities the plots are constructed by binning the data such that each interval contains the same number of points. The bin width is equal to the difference between the largest and the smallest value of any point contained in it. The height of the histogram at each bin is equal to the relative frequency and is determined from

$$f_i = \frac{n_i}{L\, b_i}, \tag{12}$$

with n_i the number of points in the ith bin, L the total number of points contained in thee set, and b_i the width of the ith bin. If the number of points per bin is chosen carefully this procedure gives proper resolution and a constant scatter per bin. In the case of the histograms concerning integer

and discrete quantities, like the number of vertices per cell and number of walls per cell, each bin just represents the normalized count of points with that (discrete and integer) value. Normalized in this sense means that the area of the histogram is 1.0.

Two final notes concern the uncertainty in the estimated quantities and the units in which the quantities are expressed. Estimates of the uncertainties in the various statistical quantities are obtained by generating $M = 4$ different realizations of nuclei distributions. This is done for the correlated and the anticorrelated nucleus distribution, as well as for the Poisson nucleus distribution. Since the only relevant distance in the tessellations is the mean distance between the generating nuclei, $\lambda = n^{-1/3}$ (n the number density of nuclei), all the quantities involving a dimension are expressed in units of the mean distance. All lengths are therefore divided by a factor λ, all areas by a factor λ^2, and all volumes by a factor λ^3.

4.3 Qualitative behaviour of the derived quantities

Before we start with the properties of the cells, walls, and edges we wish to discuss briefly the number density of these objects as well as of vertices. As stated before we mean with number density the ratio of the number of objects in the tessellation to the number of nuclei generating that tessellation. In the first four rows of table 4a, 4b and 4c one finds the number density of vertices, edges, walls, and cells (which by definition is always one since a cell is generated by exactly one nucleus). Although there are some differences between these number densities in the case of anticorrelated, Poissonian, and correlated nuclei distributions respectively, these differences are relatively small. Consequently, number densities are not very indicative of the underlying nucleus distribution.

In figure 7 through figure 10 histograms of the distribution functions of the various tessellation properties are shown. Each figure consists of three parts, (a), (b) and (c). The (a) figures contain the distribution functions of the properties of a Voronoi tessellation generated by Poissonian distributed nuclei, while (b) contains the corresponding distribution functions for anticorrelated nuclei, and (c) for correlated nuclei. One should keep in mind that while the abscissa axis has always the same scale, the ordinate axis automatically scales with the height of the distribution function.

Figures 7a, b, and c contain the histograms of the 1) volume of a Voronoi cell, 2) surface area of a Voronoi cell, 3) perimeter of a cell, 4) form factor of a cell, 5) number of walls per cell, and 6) number of vertices per cell. Since the corresponding histograms in (a), (b) and (c) differ considerably in shape these general Voronoi cell properties are relatively sensitive to the underlying nucleus distribution. One clearly sees the broadening in comparison to the Poissonian case of the histograms in the correlated case, and the narrowing of the histograms in the anticorrelated case. This behaviour is to be expected since a more correlated nucleus distribution will lead to a larger diversity of cells (in both shape and size). On the other side, an anticorrelated distribution will lead to a more crystalline cell structure so that the cells will more and more resemble each other in both size and shape. A very striking histogram is the one on the number of vertices per cell, where one clearly sees that only even values of that (integer) quantity occur. This can be explained by

invoking the Euler relation, equation (2). Since a Voronoi polyhedron has three edges emerging from every vertex on its surface, and each edge is bounded by two vertices, the relation between the number of edges of the polyhderon, N_1, and the number of vertices per polyhedron, N_0, is given by $N_1 = \frac{3}{2}N_0$. Inserting this relation into the Euler relation (eq. 8) we infer that

$$N_0 = 2(N_2 - 2). \tag{13}$$

Since the integer $N_2 - 1$ is multiplied by 2, N_0 will always be an even integer. This is what is observed in figure 7.

An interesting issue is the correlation between the various properties whose histograms are shown in figure 7. Probably the most informative way of doing this is by means of scatter plots, in which for each cell one property of the cell is plotted against the other. Hereby it is useful to look at the relationship between quantities whose possible dependence cannot be due to a common dependence on the size of the cell, as is the case with e.g. the volume and the surface are of a cell. At least one of the quantities to be compared should therefore be independent of the size of the cell. Figure 8 shows four scatter plots of quantities whose correlation is not a priori clear, namely

1. volume V_{cell} against form factor F_{cell},
2. volume V_{cell} against the number of walls N_2,
3. volume V_{cell} against the number of vertices N_0,
4. form factor F_{cell} against number of walls N_2.

The difference in scatter between the different nuclei distributions is quite clear. In the anticorrelated case the points in all four scatter plots are concentrated in a relatively small area. This area increases in size as the underlying nucleus distribution becomes more correlated. Especially the plot of the volume against the form factor is interesting. It shows that the volumes and the shapes of the cells in the tessellation in the anticorrelated case occupy a small range of values. On the other hand, the correlated case shows an enormous diversity with a relatively weak correlation between the volume of the cell and the the shape of the cell. In the case of the Poissonian and anticorrelated nuclei distributions larger cells evidently tend to have a higher form factor. Larger cells therefore tend to have a more spherical shape. Similar conclusions can be drawn from the scatter plots of the volume against the number of walls and the volume against the number of vertices. In all these cases a systematic trend of more vertices and walls as the cells get larger can easily be discerned. On the other hand, the correlation between the shape and the number of walls is not that strong. There is a slight tendency of more regular cells to have a higher number of walls. This tendency is quite strong in the correlated case, but in the Poissonian and in the anticorrelated case it is weak.

In Tables 4a through 4c, the fourth till the tenth row contains the average, standard deviation, skewness and kurtosis of seven cell properties together with an error estimate determined from four different realisations. From these tables it is evident that the expectation values of the various cell properties are not very sensitive to the underlying nucleus distribution. On the other hand, the standard deviation varies considerably as a function of the nucleus distribution. Likewise, the skewness and the kurtosis show considerable variation, although less strong.

Continuing with the properties of the walls we turn to figure 9. This figure presents the histograms of 1) the area of a Voronoi wall, 2) the perimeter of a Voronoi wall, 3) the distance nucleus-wall, 4) the volume nucleus-wall, 5) the form factor of the wall, and 6) the number of vertices per wall. It is quite remarkable that the difference between the histograms of the Poissonian (a), anticorrelated (b) and correlated (c) case is not that large. This implies that the properties of Voronoi walls are less sensitive to the underlying nucleus distribution than the properties of the complete Voronoi cells that were discussed above. The largest difference is the one between the anticorrelated case on the one hand, and the Poissonian and correlated case on the other. Especially noticeable is the relatively strong resemblance between the distributions of the area of the walls. The most sensitive quantities are the "distance nucleus-wall" and the "volume nucleus-wall". Notice the conspicuous bimodal distribution of the "volume nucleus-wall" in the anticorrelated case, as well as the cutoff in the distribution of the distance nucleus-wall. The latter is due to the fact that no two nuclei are closer than 0.8 times the mean distance between two nuclei. The difference in shape between the walls of the anticorrelated case on the one hand and the correlated and Poissonian case on the other, is also quite conspicuous. However, it is striking that the shape distribution in the correlated and the Poissonian case are nearly the same.

Also remarkable is that both the distribution function of the area of a wall as well as that of the volume nucleus-wall in all three cases diverges when that quantity approaches zero. This behaviour is partially reflected in the non-zero value of the perimeter distribution function when the perimeter approaches zero. This is true for all three nuclei distributions. This is totally unlike the behaviour of the distribution functions of the cell properties as shown in the histograms in Fig. 7a, b, and c. The implication of this behaviour is that the tessellation contains a lot of very small walls (small area, small perimeter and small volume nucleus-wall), while it does not contain a lot of small cells.

In table 4a through 4c the 12th till the 17th row tabulate the average, standard deviation, the skewness and the kurtosis of the six wall quantities. Interesting is that in this case not only the mean is rather insensitive to the nucleus distribution, but that also the standard deviation is relatively insensitive. Exceptions are the standard deviation of the "distance nucleus-wall" and the "volume nucleus-wall". This could already be concluded by looking at the histograms of these quantities. On the other hand, it is interesting to notice that the skewness of the corresponding quantities does show far more variation. It may therefore be concluded that the distribution functions of wall properties start to show reasonable differences in the third-order moment. This is unlike the cell properties, which already show considerable differences in the second-order moment.

Finally, we turn towards some other important properties of the Voronoi tessellation, namely the length of the edges in the tessellation, and the angle between any two walls that share an edge, as well as the angle between any two edges that share a vertex. In the case of the histogram on the length of the edges in Fig. 10a, 10b and 10c a significant difference between the anticorrelated case and the correlated and Poissonian case can easily be discerned. As in the case of the walls the histograms of the length of the edges are biased towards small edge lengths. Interesting is that the distribution function in the anticorrelated case is nearly flat for small edges. Studying the

corresponding row in table 4a through 4b one sees that just as in the case of the wall properties one needs to look at the skewness of the distributions to see large differences between the different cases. Larger differences can be seen in the case of the angles, both between walls and edges. This is in agreement with the conclusion of IW (1987) that angles between edges in a 2-D Voronoi tessellation are the most sensitive quantity to the underlying nucleus distribution. Fig. 10a through 10c clearly show the large difference between the histograms of the angle between edges. The distribution function in the anticorrelated case is evidently narrower than the Poissonian case, while the correlated case has a broader distribution function. This behaviour should be reflected clearly in the kurtosis, as is confirmed by the corresponding row of table 4a through 4c. Although not as clear this behaviour can also be seen in the case of the angles between the walls. The last two rows in table 4a through 4c also show that the standard deviation of both the angle between the edges and the angle between the walls is very sensitive to the underlying nucleus distribution. They therefore form an ideal instrument for determining the nucleus distribution, in particular because they are dimensionless quantities.

The general conclusion from this subsection is that the properties of the cells in a Voronoi tessellation, as well as the angles between edges and between walls, are quite good indicators of the distribution of the generating nuclei. On the other hand, the properties of the walls are far less sensitive. Although perhaps a dangerous extrapolation, these results may imply that in general for cell structures the walls are not very good indicators of the underlying generating process, while the cells themselves are. Thus, if the galaxy distribution resembles a cellular structure — of which a Voronoi tessellation is just a specific model — this means that the walls (or pancakes) in the galaxy distribution are not as useful in studying the underlying spectrum of fluctuations as e.g. the voids in the galaxy distribution.

5. Planar sections through 3-D Voronoi tessellations

One of the most interesting fields in stochastic geometry is stereology. The objective of stereology is to infer information about the geometrical properties of multi-dimensional structure when information is only available in some lower-dimensional form via planar sections, such as slices through mineral material, projections of thick slices, foils or sheets studied by light or electron microscopy, or linear probes, such as might arise in biopsy. The step from spatial structures to their sections involves a great loss of information and so stereological methods commonly yield only 'global' information of a statistical character. A further consequence of this loss of information is that many of the applications require the solution of *ill-posed* mathematical problems: numerical problems in which small deviations due to measurement error can lead to large discrepancies in the final solution.

Applications of stereology arise in the study of geometrical structure of inclusions or pores in opaque bodies such as metals, minerals, synthetic materials, or biological tissues; in these cases the available information must come from linear probes or planar sections. Projection methods are

applied in X-ray analysis and in computerized tomography. In a cosmological context stereology also promises to be an important instrument since the deepest galaxy redshift surveys, from which we hope to learn more about the largest structures in the Universe, are confined either to two dimensions ("slices") or to one dimension ("pencil beam surveys"). From these surveys we hope to infer information about the actual three-dimensional structure of the galaxy distribution.

The first question for statistical work in stereology is how randomness enters the problem, or, stated in another way, what is meant with random. This question was systematically discussed in the now classic paper by Miles (1978). Principally, there are two main answers which are related to the notions of "design approach" and "model approach". In the design approach it is assumed that the structure under study is deterministic while the sampling is random. In the case of planar sections, for example, a usual assumption is that the section planes behave like members of a Poisson plane process. By using independent and uniform objects the design approach is very close to classical ideas of geometrical probability; its main tool is integral geometry. The design approach is the one often taken for biological and medical problems: the objects, such as human organs, are typically unique and inhomogeneous. In the model approach the structure studied is random. Often it is assumed that it is a sample of a stationary and isotropic process. Typically, the section plane is assumed to be the (x, y)-plane. This approach is natural for many situations in materials science. Important mathematical tools of the model approach are marked point processes, random measures and random sets. The resulting formulae are generally similar for both approaches, differing only in the statistical theory and underlying interpretation.

Historically Delesse (1847) and Rosiwal (1898) were probably the first to work in the spirit of stereology. They recognized that under certain assumptions the volume fraction of a component in a body equals the area or linear fraction in a planar or linear section. Wicksell (1925,1926) solved the problem of inferring the size distribution for systems of spheres given planar sections, leading to an Abel integral equation. However, because of its nature of an ill-posed problem it causes great numerical difficulties. The great importance of the subject has been reflected in a vast and flourishing literature. A good, but compact, overview of the subject is given in the book by Stoyan, Kendall and Mecke (1987). The random section approach is described in detail in the papers of Miles and Davy (1977), Miles (1978), and Jensen (1984). The two main textbooks in the field are the one by Weibel (1980) and the one by Serra (1982).

In this section we are naturally interested in the stereology of "dense random packings" of objects, specifically tessellations of polyhedra. While the case of the stereology of spheres is still somewhat analytically tractable, the case of polyhedral objects is very complicated. This will be appreciated immediately if one considers that the shape of an intersection figure varies considerably depending on the plane of intersection. For example for a cube the intersection profiles can be polygons with three, four, five, or six sides. A general stereological theory for tessellations does not exist. However, for the specific case of the Voronoi tessellation there is a stereological theory, i.e. stereological mean value formulae exist in the case of a stationary Poisson process, that make it possible to estimate the spatial cell centre density from planar sections. Analytically known stereological formulae of sections through both 2-D and 3-D Poisson Voronoi tessellations were

already presented in section 2, with table 2 containing some known moments of linear sections and table 3 containing known moments of planar sections. In this respect it may be interesting to realize that a planar section through a 3-D Voronoi tessellation is itself not a 2-D Voronoi tessellation. This observation was realized and proved by Van de Weygaert (1991b). For further knowledge about the stereology of Voronoi tessellations one has to resort to Monte Carlo methods, both for most of the stereological properties of Poisson-Voronoi tessellations as well as for nearly all the properties of sections through Voronoi tessellations generated by non-Poissonian nuclei distributions. We studied the stereological properties of Voronoi tessellations using the Monte Carlo simulations described in section 4.

5.1 The determination of planar sections

Planar sections are studied in this section, linear ones in the next one. In particular interesting is the relationship between either the planar section or the linear section on one side and the "parent" 3-D Voronoi tessellation on the other side. These results may give some insight in what the "slice" and "pencil beam" galaxy redshift surveys can tell about the spatial galaxy distribution if it is indeed cellular, as implied by the observations carried out during the past decade.

Planar sections that are calculated as follows. The 3-D tessellation of 1000 cells is taken as the starting point. Since we are following the "model approach", the section planes are taken parallel to the (x, y) plane. The section planes can therefore be characterized by one parameter: its z-value. Given the section plane, we determine of every polyhedral cell in the 3-D tessellation whether the section plane cuts through it. This can be done relatively easily, by checking the list of the vertices belonging to that cell. If any of these vertices is on the other side of the plane than the nucleus of the cell we know that the cell has been cut in two parts by the section plane. If the cell is not cut we can proceed with checking the following cell. If it is, we have to determine the resulting two-dimensional polygon. This is done by applying the following procedure to every wall of the Voronoi polyhedron. During the Voronoi tessellation construction procedure (section 3) the vertices characterizing each Voronoi wall are sorted in geometrical order. Each pair of consecutive vertices defines an edge, each edge forming a part of the wall boundary. Of each edge we determine whether it has a crossing point with the section plane. This is the case when the two vertices at its tips are on opposite sides of the section plane. The crossing point of such an edge with the section plane is one of the vertices of the section polygon that forms the section of the 3-D Voronoi cell with the section plane. Notice that when a 3-D Voronoi wall is cut by the section plane it will have two edges that cross the section plane, so that it will give two section vertices. Repeating this for all the walls of the Voronoi polyhedron results in a list of section vertices. After ordering them these define the structure of the section polygon. Carrying out this process for all the cells in the 3-D Voronoi foam will then lead to the complete structure of the planar section. Because the 3-D Voronoi foam in our calculation is periodic, every planar section of that foam is also periodic.

Figure 11a, b, and c each show 6 section planes through each of the studied Voronoi foams. The number below each square is the z-value of the section plane. The 6 section planes are taken

at steps of $\Delta z = 5$. Since the mean distance between the nuclei in the 3-D foam is 10.0, this means that the same cells can appear in several section planes. The section tessellations are therefore not independent. The "regularity" of the sectional tessellation is evidently related to the correlation of the underlying nucleus distribution. The most regular tessellation corresponds to the anticorrelated case, the most irregular tessellation to the correlated case. These planar sections also give a good idea of the corresponding 3-D Voronoi tessellation of 1000 cells, in particular when one shows several different section planes through the same 3-D tessellation.

5.2 Quantities derived from the Monte Carlo simulations

For both the correlated, the Poissonian and anticorrelated nuclei distributions 20 planar sections are calculated through the corresponding Voronoi foams of 1000 cells. The data on these 20 planar sections are further analyzed statistically. Since the 20 planar sections are taken from just one realization, no objective errorestimates based on different realisations of the same statistical process can be made.

In the case of these two-dimensional tessellations there are two entities whose geometrical properties can be analyzed statistically: the cells and the edges. Accordingly, the analysis of the 2-D foams was splitted into two parts, the analysis of the characteristic properties of the cells and of some general properties, including the properties of the edges.

The following properties of the sectional 2-D cells were determined:

a. the area of the cell, A^s_{cell},

b. the perimeter of the cell, S^s_{cell},

c. the form factor of the cell, F^s_{cell},

d. the number of vertices per cell, N^s_0.

The perimeter of the cell is just the sum of the lengths of the edges surrounding the polygon, while the form factor F of the sectional cell is defined as for the 3-D Voronoi wall in equation (6).

In addition to the geometrical properties of the cells some more properties of the sectional tessellation were considered. Since they concern a wide range of characteristics of the 2-D tessellation, we list them together:

a. number density of cells, J^s_2,

b. number density of vertices, J^s_0,

c. number density of edges, J^s_1,

d. length of edge, L^s,

e. angle between edges that cross, α^s_{ee},

f. angle between walls-section plane, α^s_{ww}.

The number density of 2-D cells is defined as the number of 2-D sectional cells per unit area. Since the dimensions are normalized such that one has exactly one nucleus per unit volume, so that the

total volume of the box with K nuclei is K, the section plane has size $K^{2/3}$ in the case the K nuclei are distributed in a box. Consequently, the number density of 2-D cells is simply the ratio of the number of 2-D cells in the section plane to the number of nuclei in the tessellation to the power 2/3. The definitions of the number density of the vertices and the number density of the edges are similar. The "angle between edges" of the 2-D sectional tessellation is the angle between any two edges that have a common vertex. In a planar tessellation three edges meet at one vertex, so that one vertex gives three angles. The "angle between walls-section plane" is the angle that the section plane makes with any of the walls of the tessellation that are cut by the section plane.

The subsequent statistical analysis of all the quantities is exactly similar as the one described in the former section.

5.3 Qualitative behaviour of the derived quantities

We first briefly discuss the number density of the cells, edges and vertices in the planar section. In the first three rows of table 5a, 5b, and 5c. From the 20 different section planes through each foam estimates of the standard deviation, skewness and kurtosis of the number densities are obtained. Evidently, the expectation values of these quantities do not vary a lot as function of the underlying distribution of nuclei. On the other hand, the standard deviation appears to be very sensitive, whereby the difference between the correlated case on the one hand, and the anticorrelated and the Poissonian case on the other is quite significant. This is quite striking because in most other properties the Poissonian case resembles the correlated one more than it does the anticorrelated case. Also the skewness of the correlated case is rather dissimilar from the other two cases, while on the other side the kurtosis is more different for the anticorrelated case.

The histograms of the area of a sectional cell, perimeter of a sectional cell, form factor of a sectional cell, and number of vertices per cell are shown in figure 12. Striking is the behaviour of the area of the sectional cells. Its distribution function seems to diverge for very small areas in the case of the correlated, Poissonian, and anticorrelated case. This is unlike the distribution of volumes of the 3-D Voronoi cells, and implies that planar sections have a relatively high percentage of very small cells. In addition the area distribution function shows a bimodal behaviour in the case of Poissonian and anticorrelated nuclei. This bimodal character consists of a peak at small areas and a far broader peak at larger values of the cell area. Finally it falls gradually off to zero towards very large areas. In the correlated case this bimodality is absent, and the area distribution function consists merely of a monotonous decline towards large areas. The small cells clearly dominate in that case. The planar sections in figure 11 clearly illustrate this behaviour. Also the perimeter of the cells shows a clearly different behaviour in the correlated, Poissonian, and anticorrelated case. While the perimeter distribution function is fairly broad in the correlated case, it is rather narrow in the anticorrelated case. The Poissonian case is more or less an intermediate case. Interesting is that the distribution function does not drop off towards zero when the perimeter approaches zero. The effect is smaller though than in the case of the 3-D Voronoi walls in the 3-D "parent"

tessellation (compare with fig. 9). There appears to be a reasonable qualitative resemblance of the distribution functions of the section cells to those of the 3-D Voronoi walls (not cells). In particular the distribution of the form factor and the number of vertices, and in a weaker sense of the perimeter are good examples. The exception is the distribution function of the area of the cells, which shows a bimodal behaviour in the case of the section cells that is totally absent in the distribution of the 3-D walls. Since this is totally unlike the distribution function of the volume of the Voronoi cells in figure 7 (see former section), we can already conclude that it is not trivial to extract information on the 3-D volume distribution from the area distribution of the planar section cells. Table 5a through 5c show that the mean and standard deviation of the number of vertices per wall, the area of a cell, the perimeter of a cell, and the form factor of a cell are rather insensitive to the underlying distribution of nuclei. Significant differences show up in the skewness and the kurtosis of these quantities. The section cells have a systematically higher form factor than the Voronoi walls in the corresponding Voronoi foams. This implies that the section cells have a somewhat more regular shape than the Voronoi walls.

Figure 13 shows histograms of three other properties, the lengths of the edges, the angle between edges and the angle between the section plane and the sectioned Voronoi walls. The distribution function of the section edge lengths shows the same qualitative behaviour as the distribution function of the lengths of the edges in the corresponding 3-D Voronoi foam (see fig. 10). A detailed comparison shows that there are some minor differences. The foam edge distribution, for example, has a larger fraction of smaller edges, while the decline of the distribution function towards larger edge lenghts is slower than in the case of the section edges. In the anticorrelated case the section edge length distribution function displays a plateau at small edges. This could also be observed in the distribution function of the 3-D edge lengths in the corresponding Voronoi foam. The plateau for the section edges is even flatter and extends over a larger range than for the 3-D foam edges. As in the case of the cell properties the average and the standard deviation do not vary much as a function of the underlying nucleus distribution, while the skewness and the kurtosis do. This is clearly born out by the corresponding row in table 5.

The angle between any two crossing section edges shows a behaviour that is remarkably similar to the one of the angle distribution function in the case of two-dimensional Voronoi tessellations (see IW). As expected the distribution function for the correlated case is broader than in the Poissonian case, while it is sharper in the anticorrelated case. This is reflected in the estimates of the kurtosis in the 5th column, 9th row of Table 5a, 5b and 5c respectively. From the same tables it can also be inferred that the standard deviation is reasonably sensitive to the nucleus distribution. Remarkable behaviour is displayed by the distribution function of the angles between the walls and the section planes. The distribution functions In the correlated, Poissonian and anticorrelated cases are all approximately the same, as can be seen from both the histograms and the last row of tables 5a, 5b, and 5c. Average, standard deviation, skewness and kurtosis agree with each other. This behaviour can be understood from the fact that the Voronoi walls apparently have an isotropic distribution in 3-D space. By this we mean that the normal vectors of these walls display an isotropic angular distribution, independent of the nucleus distribution. From this we can also explain the shape of

the distribution function of the angle between the walls and the section plane. Walls that are nearly perpendicular to the slice plane have a far higher chance of being hit than walls that hit at a very small angle. The frequency of the perpendicularly crossing planes amongst the sectioned planes is therefore also very high. The detailed behaviour, however, is not yet explained by this. Naively a "$\sin\alpha$" behaviour would be expected, whereby α is the angle between the wall and the section plane. Clearly, the frequency of lower angles is much less than that. Presumably a more detailed explanation involving geometrical factors is needed to explain the complete behaviour.

To investigate more extensively the point which was made earlier that it is not trivial to extract the 3-D volume distribution from the area distribution of the 2-D section cells, figure 13 also shows scatter plots of the area of the 2-D section cells against the volume of the parent cell. In both the correlated and the Poissonian case a lot of scatter is seen, although there are some systematic trends. Such a systematic trend is the fact that larger areas correspond to larger cells. On the other hand, small areas can correspond to both large and small volumes. In the anticorrelated case this is even more apparent. In that case all the points in the scatter diagram are concentrated in a narrow band nearly parallel to the area-axis. Only for large areas it starts to bend towards larger volumes. It would therefore be nearly impossible in this case to infer anything about the 3-D cell volume distribution, with the possible exception of the largest volumes.

6. Linear sections through 3-D Voronoi tessellations

The linear section through the 3-D tessellation is made by a 'chord' (line), characterized by some starting point and direction. The starting point of the chord can have any position inside the simulation box. The results presented in this section are based on calculations with random positions of the starting point and an isotropically distributed direction. The lenght of the chord is equal to the length of the edge of the box in all cases.

The "linear section procedure" starts with the determination of the nucleus which is closest to the starting point of the chord. By definition, the starting point will be situated in the Voronoi cell of that nucleus. Subsequently, the wall through which the chord pierces before entering the next Voronoi cell is determined. This procedure is repeated by calculating through which wall on the other side of the new Voronoi cell the chord pierces. At first one divides the set of neighbour nuclei, i.e. the ones with whom the present cell shares a wall, into two subsets. This division is based on the intersection of the bisecting plane defined by the current nucleus and the neighbouring nucleus with the line along the chord. If this intersection point lies in the direction opposite to the chord's the neighbour belongs to the subset which is discarded from further consideration. This is the case when the the angle of the chord direction with the connecting line between the neighbour and the current nucleus is larger than 90°. The other subset consists of the neighbours that give intersection points in the direction of the chord. Of the latter subset the intersection point with the smallest distance to the starting point of the chord is selected. The corresponding bisecting plane is the first plane to be crossed by the section chord. In fact, the intersection point is situated in the

corresponding Voronoi wall. The Voronoi wall is the part of the bisecting plane that is part of the boundary of the Voronoi cell. This is obvious, since the crossing point cannot be closer to any other nucleus unless it would have hit another bisecting plane first. The Voronoi cell of the neighbour nucleus with whom the present nucleus shares this bisecting plane is the next cell that is entered by the chord. This procedure is repeated until a crossing point is found that is at a larger distance from the starting point of the chord than the specified length of the chord. The information on the linear section is stored in the form of an ordered list of distances to the starting point of the chord, a list of the angles between the walls which are crossed by the chord and the chord itself, and finally a list of angles between walls on opposite sides of each edge of the linear section.

6.1 Quantities determined in the Monte Carlo simulations

The quantities which are determined for the linear sections are,

a. the section edge length, λ,

b. the section edge length dispersion, $\sigma(\lambda)$,

c. the angle wall - line of sight, α^l_{wl},

d. the angle between adjacent walls that cross, α^l_{ww}.

The section edge length is the length of any edge in the linear section. This is the distance between two consecutive crossing points on the section chord. The "angle wall-line of sight" is the angle between any of the walls that is crossed by the section chord and the chord itself. The "angle between adjacent walls" is the angle between two walls corresponding to two consecutive crossing points. In other words, this is the angle between two walls on opposite sides of a section edge. These quantities are all determined with a view towards the practical application to narrow-angle deep galaxy redshift surveys ("pencil beam surveys") and their possible significance for the existence of cellular structures. The first quantity one is interested in in that case is the distribution of the distances between two crossings through cell walls, i.e. section edge lengths. Nearly as interesting, however, are the angles under which the Voronoi cell walls are hit ("angle wall-line of sight"). In addition, the correlation with the edge length is potentially interesting because of the question whether large edge lengths correspond to other angles than small edges. Likewise, the angles between walls on opposite sides of the edges are interesting because they provide information on how often two walls are aligned. All these quantities have been determined by taking 2500 different, randomly chosen, chords or "lines of sight" through a Voronoi foam of 1000 cells and calculating the corresponding linear sections.

The remaining quantity, the edge length dispersion, has been determined with the recent claims of quasi-periodicity in deep redshift surveys in mind. Periodicity implies that along a line of sight the spacing between all two crossings on that line of sight is approximately equal. Accordingly, of 10000 lines of sight the sections have been determined. Each of these lines give some 12-18 section edges. For each line of sight the standard deviation is determined from that resulting sample of some 12-18 edge lengths. This produces 10000 "edge length dispersions". This number is sufficient

for a good statistical analysis in the form of e.g. a histogram. The probability of having a very small edge length dispersion can be easily inferred from the 10000 data. This is essentially the probability of "periodicity" along a line of sight. We should keep in mind, however, that this is a purely geometrical approach, and that the details of the problem might also depend on the small scale clustering involved.

6.2 Qualitative behaviour of the derived quantities

Quantitative results of the linear section Monte Carlo study are presented in table 6 (a, b and c). This table presents the average, standard deviation, skewness and kurtosis of the considered quantities. Figure 14 (a,b and c) contains histograms of the same quantities while figure 15 presents scatter diagrams between some of the considered quantities. As usual (a) corresponds to the Poissonian nucleus distribution, (b) to the anticorrelated nucleus distribution and (c) to the correlated nucleus distribution.

The histogram of the edge length distribution in figure 14a, b, and c show that the distribution function varies considerably as a function of the underlying nucleus distribution. The histogram in the Poissonian case agrees very well with the curve that Ikeuchi and Turner (1991) derived by numerical integration of an analytically derived differential equation. Such an equation can only be derived for the Poissonian case. It is striking that the distribution function peaks at some finite, relatively large edge length in both the Poissonian and anticorrelated case. The peak is far broader and has a lower amplitude in the correlated case. This seems to point to a systematic behaviour of a peak getting sharper from correlated towards anticorrelated nuclei distributions. In addition, the edge length corresponding to the peak shifts towards higher value when the nucleus distribution becomes more anticorrelated. The decline towards zero towards large edge lengths is also steeper for more anticorrelated nucleus distributions. Interesting is alos that the distribution function is non-zero for small edge lengths. Consequently, there will be a lot of short edges that seriously decrease the chance on periodicity. That the probability of true periodicity in all three cases is truly small is evident from the histograms of the edge length dispersion. The dispersion distribution function peaks at a finite edge length value while it is zero for the small values that correspond to periodicity. The conclusion that periodicity is intrinsically absent in the 3-D Voronoi foams, i.e. in a geometric sense, seems to be inescapable. Table 6 shows that the distribution function of the edge length dispersion differs mainly in the skewness and the kurtosis, while the mean and the standard deviation are quite similar. The same behaviour is displayed by the general edge length distribution. The angle between the wall and the line of sight has practically the same distribution in the case of correlated, Poissonian and anticorrelated nuclei distributions, as can be seen from the histograms and table 6. The fact that the distribution function at 90° is virtually zero implies that the chance of a face-on hit by the line of sight is rather small. Clear differences between the different cases of nuclei distributions, however, show up in the alignment of the walls at opposite ends of the edge, quantified by the angle between adjacent walls. All three histograms peak in the neighbourhood of 75°. However, the peak-angle is shifting towards smaller values as the nuclei

distribution gets more correlated. This also leads to a change in the nature of the asymmetry from more small angles to more large angles as one goes from the anticorrelated to the correlated nucleus distribution. This is clearly quantified by the corresponding kurtosis in table 6.

In Fig. 15a, b and c four scatter plots are shown, containing the following quantities:

a. section edge-length against next section edge-length,

b. section edge-length against volume of cell that is being sectioned,

c. section edge-length against the angle wall-line of sight,

d. section edge-length against angle between adjacent walls,

The first scatter plot, edge length against next edge length tells whether two adjacent edge lengths are correlated, i.e. whether the presence of a large edge length says anything about the next edge length. This is an important property to check since the statistical analysis of for example the probability of periodicity through a Voronoi foam is considerably simplified if such a correlation does not exist. In that case the standard deviation of the edge length distribution is enough to make reliable estimates of the chance of a regular behaviour along a linear section consisting of M edges. This was done by Coles (1990), although he did not check whether there were actually correlations between adjacent edge lengths. The corresponding scatter diagrams in Fig. 15a, b and c seem to confirm that there are indeed no correlations. In itself this may be considered rather surprising, since it implies that if one has a large edge length in a linear section this does not yield information on the length of the next edge.

As in the case of the planar sections it is interesting and important to know what information the linear section edge length distribution contains about the distribution of the volumes of the complete 3-D cells. The second scatter plot of section edge length against volume of the parent cell shows the same qualitative behaviour as in the case of the planar sections. The scatter is even larger than in that case. It will therefore be very hard to infer a reasonable amount of information on the volume distribution of the 3-D cells from the distribution of the edge lengths. In the case of the correlated and Poissonian nuclei distribution more systematic behaviour can be discerned. Large edge lengths are only produced by large cells, as the scatter plot bends away towards larger volumes for large edge lengths. Only a very weak indication for such behaviour is seen in the anticorrelated case. Most points are concentrated in a thick horizontal band that shows some signs of a systematic bending towards large volumes when the edge lengths become large. It will therefore be even more difficult in the anticorrelated case to infer the 3-D cell volume distribution.

Real systematic behaviour is displayed by the two scatter plots of the angles against the section edge length. In the case of the angle between the wall and the line of sight against the section edge length all three cases show that larger edge lengths imply a more face-on hit by the line of sight. This effect gets stronger when the nuclei get more anticorrelated. This may not be so surprising because large edge lengths will nearly always be the consequence of the line of sight passing through the center of a cell. In that case the line of sight is expected to hit a wall more or less face-on upon entering a cell. Really striking is the scatter plot of the section edge length against the angle between adjacent walls. A clear band runs form large angles to small angles as we go from small

edgees towards large edges. This effect gets clearly stronger when the nuclei distribution is more anticorrelated. This implies that the walls at the ends of large edges are almost aligned. This must be due to the same effect as described above, namely that the line of sight hits these walls face-on when it passes through the centre of the cell. The walls at the opposite side of the cell are then aligned with each other. On the other hand, the small edges result for a substantial part from the line of sight passing through the outer parts of a Voronoi cell. In these outer parts the ingoing and outgoing wall have a high probability of touching each other. From the section 4 we know that the angle between the walls in a 3-D foam has an average value of 120° and is highly biased towards large angles. These large angles are therefore expected to occur at small section edge lengths.

6.3 Planar and linear sections: some conclusions

From the above results we conclude that a good and efficient way to study some properties of the underlying distribution is to study sections. However, one has to be very careful in the interpretation of the results of these sections when trying to infer quantitative information on the corresponding three-dimensional structure. Some of the results and conclusions in the discussions in this section are therefore of importance in the interpretation of the "slice" and "pencil-beam" galaxy redshift surveys and in answering the question of the possible existence of a cellular structure in the distribution of galaxies. The general contention should be that qualitative conclusions may be okay but that one should be very careful with quantitative conclusions. For instance, inferring the distribution function of the volumes of voids in the galaxy distribution from slice redshift surveys is not feasible.

We emphasize that the Voronoi foams are cell structures. Therefore thye represent some ordering in 3-D space. However, they do not show any sign of regularity, as was seen in the histogram of the linear section dispersion. It is important to keep this in mind when we use a Monte Carlo model within the context of the Voronoi tessellation for explaining the observed quasi-periodicity in pencil beam redshift surveys (Broadhurst *et al.* 1990; Van de Weygaert 1991a,b). It is certainly not 'what you put in you get out'.

7. Summary and Discussion

Observations over a period of more than a decade have shown that the galaxy distribution on large scales resembles a cellular structure, with voids playing a prominent role. A lot of work has been invested already in trying to understand the formation of this kind of structures by the growth of small density fluctuations in an almost homogeneous Universe under the influence of gravity. Models based on a hierarchical buildup of structure in the Universe seem to be particulary succesfull in explaining the structure from galaxy scales up to scales of groups and clusters. A lot is known about clustering in these hierarchical scenarios, since it involves tractable mathematical

problems. They seem to fail, however, to explain cell-like or foam-like arrangement of matter, consisting of voids, filaments and walls. Not yet a lot of effort has been invested into a theoretical understanding of clustering within cell structures. The main problem is that a solid mathematical background on this subject is lacking. This is the reason for studying in detail the mathematical and computational foundations of a statistical geometrical model that can be considered as one of the best defined paradigms for a non-regular (non-crystalline) cellular structure, the Voronoi tessellation. Although one can expect it to have many useful applications in astrophysics, until recently this mathematical concept was not widely known. The beauty of the Voronoi tessellation is that although it is based on a simple definition it leads to a structure of great richness that as yet is still largely unexplored.

In its cosmological context the Voronoi tessellation can be considered as the skeleton of a galaxy distribution. Such a skeleton would result from an idealized model of structure formation in the Universe dominated by the expansion of underdense regions in the matter distribution. Because there are no other disturbing effects involved such an idealization provides a lot of insight into the statistical properties of a cellular distribution of galaxies. In this way a better understanding of the systematics of cellular clustering can be obtained. This will be very useful when interpreting more complicated and realistic models of clustering. Since the observations teach us that such models should always contain a cellular galaxy distribution on large scales we know that this is important. The details, though, will certainly differ from the simple Voronoi model.

The main emphasis of this paper has been on a systematic Monte Carlo study of the geometrical properties of Voronoi tessellations as a function of the generating nucleus distribution. In addition to providing us with insight into the information on the underlying physical processes contained in a cellular galaxy distribution, a further reason for this work was the fact that in the relevant mathematics literature not much is known about general Voronoi tessellations. The statistical results presented here can therefore also be considered as a relevant contribution to their understanding.

Directly interesting in the cosmological context is the stereological study of the Voronoi tessellations. This stereological study teaches us what we can learn about three-dimensional cellular structures from lower dimensional observations, such as planar and linear sections. Since the galaxy distribution is often studied by means of redshift surveys confined to "slices" or "pencil beams" this has immediate practical consequences. We found that once can indeed infer interesting qualitative results on the real 3-D distribution from lower-dimensional sections, but that one should be very skeptical about any quantitative results.

Acknowledgements.

During the finishing stage of this paper I received the sad news of the passing of Prof. J.H. Oort. Here I would like to express my gratitude for the many discussions and his constant interest and enthusiasm, in particular during the early stages of this work; a greater support and encouragement is hardly imaginable.

I am most indebted to Vincent Icke, this work being the product of our year-long very instructive collaboration. I am grateful to him and to P.T. de Zeeuw for their assistance, comments and suggestions which were so essential in making this paper readable. It is also a pleasure to thank B. Jones for his encouragement, enthusiasm, advice and useful ideas. Very encouraging were the discussions with and remarks of Eleni Chatzichristou. Finally, I would like to thank D. Kendall for his interest in and advice about stochastic geometry, and J.D. Barrow for making available a copy of N. Ling's thesis.

Appendix A. Finding a triangle with minimum circumradius

Given a nucleus i and its closest neighbour, the nucleus i_α, a third nucleus i_β has to be found such that the radius of the circumscribing circle of the triangle $\{i, i_\alpha, i_\beta\}$ is minimal. The most straightforward way is to determine for each nucleus $j \in S_i$ the centre of the circumscribing circle, followed by the determination of the radius of the circle. The point leading to the smallest radius is then the third nucleus i_β. However, we followed a less direct, but computationally advantageous, method.

In figure A1 we have drawn a triangle $\{i, i_\alpha, i_\beta\}$ with its circumscribing circle. The positions of i, i_α, and i_β are $\vec{r}_i$, $\vec{r}_\alpha$ and $\vec{r}_\beta$ respectively. The problem has three relevant parameters. The first one is d, the distance between i and i_α, which is fixed. The other two are θ, the angle between $(\vec{r}_\alpha - \vec{r}_\beta)$ and $(\vec{r}_i - \vec{r}_\beta)$ and r, the distance between the centre of the circumscribing circle and i. The relation between these 3 parameters is given by

$$r = \frac{d}{2\sin\theta}, \tag{A1}$$

so that the minimum of r corresponds to a maximum of $\sin\theta$. That the angle θ has to be as large as possible is already apparent from figure A1. Notice that θ has an upper limit of $\pi/3$,

$$d = d(i, i_\alpha) \quad \text{is minimal} \quad \Rightarrow \quad d(i, i_\beta) \geq d \quad \Rightarrow \quad \theta \leq \frac{\pi}{3}. \tag{A2}$$

In the range of θ, $0 \leq \theta \leq \pi/3$, $\cos\theta$ is a monotonically decreasing function. Finding i_β therefore means finding the nucleus which minimizes $\cos\theta$. In practice, $\cos\theta$ is determined from the vectors $\vec{r}_i$, $\vec{r}_\alpha$, and $\vec{r}_\beta$,

$$\cos\theta = \frac{(\vec{r}_i - \vec{r}_\beta)\cdot(\vec{r}_\alpha - \vec{r}_\beta)}{|\vec{r}_i - \vec{r}_\beta|\,|\vec{r}_\alpha - \vec{r}_\beta|}. \tag{A3}$$

The nucleus $j \in S_i$ that yields the smallest $\cos\theta$, using equation (A3), is therefore the nucleus i_β which together with i and i_α forms a triangle with minimum radius r_{min}.

After having determined the nuclei $j \in S_i$ for the smallest $\cos\theta$, it has to be checked whether there might be nuclei outside of S_i that could give a lower circumradius. The condition for this not being the case is that $2\,r_{min} \leq R_i$, with R_i the radius of the set S_i. When this condition is indeed

met there cannot be any nucleus outside S_i yielding a lower circumradius. When this is not the case the search has to be continued ourside S_i. This is done by checking all nuclei around i within a radius r_{min} from i. This search is speeded up considerably by the use of the multidimensional binary tree data structure (Appendix F).

Appendix B. Determining the circumcentre of a triangle

Given a triangle defined by the three nuclei $\{i, i_\alpha, i_\beta\}$, the centre Ξ of the circumscribing circle is determined as follows (see fig. A1).

The positions of the nuclei i, i_α, and i_β are $\vec{r}_i$, $\vec{r}_\alpha$ and $\vec{r}_\beta$, while $\vec{\xi}$ is the position of the centre Ξ. If the angle between the vectors $(\vec{r}_i - \vec{r}_\beta)$ and $(\vec{r}_\alpha - \vec{r}_\beta)$ is θ, the angle between the vectors $(\vec{r}_i - \vec{\xi})$ and $(\vec{r}_\alpha - \vec{\xi})$ is equal to 2θ. Because $\{i, \Xi, i_\alpha\}$ is an isosceles triangle one can easily infer that $\vec{\xi}$ is given by

$$\vec{\xi} = \frac{\vec{r}_i + \vec{r}_\alpha}{2} + r\cos\theta\,\vec{n}_c\,, \tag{B1}$$

with r the radius of the circumscribing circle, and $\vec{n}_c$ the unity vector perpendicular to the vector $(\vec{r}_\alpha - \vec{r}_i)$. This vector is directed such that $\{(\vec{r}_\alpha - \vec{r}_i), \vec{n}_c\}$ forms a right-handed system. It can be written as $\vec{n}_c = \vec{m}_c/\sin\theta$, where $\vec{m}_c$ and $\sin\theta$ are given by

$$\vec{m}_c \equiv \vec{R}_{\alpha i} \times (\vec{R}_{\beta\alpha} \times \vec{R}_{\beta i}); \qquad \sin\theta = |\vec{R}_{\beta\alpha} \times \vec{R}_{\beta i}|\,, \tag{B2}$$

with the vectors $\vec{R}_{\alpha i}$, $\vec{R}_{\beta i}$, and $\vec{R}_{\beta\alpha}$ defined by

$$\vec{R}_{\alpha i} \equiv \frac{\vec{r}_\alpha - \vec{r}_i}{|\vec{r}_\alpha - \vec{r}_i|}\,, \qquad \vec{R}_{\beta i} \equiv \frac{\vec{r}_\beta - \vec{r}_i}{|\vec{r}_\beta - \vec{r}_i|}\,, \qquad \vec{R}_{\beta\alpha} \equiv \frac{\vec{r}_\beta - \vec{r}_\alpha}{|\vec{r}_\beta - \vec{r}_\alpha|}\,. \tag{B3}$$

Inserting $\vec{m}_c = \sin\theta\,\vec{n}_c$ and equations (A1) into equation (B1) leads to the following expression for Ξ,

$$\vec{\xi} = \frac{\vec{r}_i + \vec{r}_\alpha}{2} + \frac{d\cos\theta}{2(1-\cos^2\theta)}\,\vec{m}_c\,. \tag{B4}$$

Since d, $\cos\theta$, $\vec{r}_i$ and $\vec{r}_\alpha$ are already known from the determination of the triangle $\{i, i_\alpha, i_\beta\}$ with minimum circumradius r (appendix A) we only need to evaluate $\vec{m}_c$ to obtain the coordinates (ξ_1, ξ_2, ξ_3) of Ξ. Computationally this is done most efficient from the expression

$$\vec{m}_c = \vec{R}_{\alpha i} \times (\vec{R}_{\beta\alpha} \times \vec{R}_{\beta i}) = \vec{R}_{\beta\alpha}(\vec{R}_{\alpha i} \cdot \vec{R}_{\beta i}) - \vec{R}_{\beta i}(\vec{R}_{\alpha i} \cdot \vec{R}_{\beta\alpha})\,. \tag{B5}$$

Appendix C. Detecting a new Delaunay Tetrahedron

Given a Delaunay tetrahedron $\{i, i_\alpha, i_\beta, i_\gamma\}$ a new Delaunay tetrahedron $\{i, i_\alpha, i_\beta, i_\delta\}$ is obtained as follows.

Note that the nuclei i_γ and i_δ are located on opposite sides of the plane $\{i, i_\alpha, i_\beta\}$. If that were not the case i_δ would either have been located within the circumsphere of $\{i, i_\alpha, i_\beta, i_\gamma\}$ or i_γ within the circumsphere of $\{i, i_\alpha, i_\beta, i_\delta\}$. The first case is impossible since $\{i, i_\alpha, i_\beta, i_\gamma\}$ is a Delaunay tetrahedron, while the second case would imply that $\{i, i_\alpha, i_\beta, i_\delta\}$ cannot be a Delaunay tetrahedron. Therefore i_δ is located in the set $S_i(\alpha\beta|\gamma)$.

For each nucleus $j \in S_i(\alpha\beta|\gamma)$ we determine the sphere circumscribing j and the triplet $\{i, i_\alpha, i_\beta\}$. Define the Z-axis to be the axis passing through the circumcentre of the triangle $\{i, i_\alpha, i_\beta\}$, perpendicular to its plane and with the positive direction on the side of $H_i(\alpha\beta|\gamma)$. Notice that since all tetrahedra $\{i, i_\alpha, i_\beta, j\}$ as well as the tetrahedron $\{i, i_\alpha, i_\beta, i_\gamma\}$ share the triangular face $\{i, i_\alpha, i_\beta\}$ their circumcentres lie on the Z-axis. According to Theorem IV, the fourth vertex nucleus i_δ yields the smallest Z coordinate value of the sphere centre (not of the nucleus j itself !) among the nuclei of $S_i(\alpha\beta|\gamma)$. Figure C2 illustrates this circumstance. The coordinates (p_1, p_2, p_3) of the circumcentre P of the new Delaunay tetrahedron $\{i, i_\alpha, i_\beta, i_\delta\}$ are given by the vector equation

$$\vec{P} = \begin{pmatrix} v_1 \\ v_2 \\ v_3 \end{pmatrix} + Z \cdot \begin{pmatrix} n_1 \\ n_2 \\ n_3 \end{pmatrix}; \qquad Z = \frac{d(P,V)}{|\vec{n}|} = d(P,V)\,, \tag{C1}$$

as both P and V are situated on the Z-axis. Note that V, with coordinates (v_1, v_2, v_3), is the Voronoi vertex defined by the tetrahedron $\{i, i_\alpha, i_\beta, i_\gamma\}$. In fact, the circumcentres P and V are the Voronoi vertices defining the edge $P - V$, one of the edges surrounding the polygon wall defined by the contiguous pair $\{i, i_\alpha\}$. The vector $\vec{n}$ is the normal to the plane $\{i, i_\alpha, i_\beta\}$, with a counterclockwise direction,

$$\vec{n} = \frac{(\vec{r}_\alpha - \vec{r}_i) \times (\vec{r}_\beta - \vec{r}_i)}{|(\vec{r}_\alpha - \vec{r}_i) \times (\vec{r}_\beta - \vec{r}_i)|}\,, \tag{C2}$$

where $\vec{r}_i$, $\vec{r}_\alpha$, and $\vec{r}_\beta$ are the positions of the nuclei i, i_α and i_β. For reasons of computational efficiency we defined V to have $Z = 0$. The coordinates of P can be found from the Voronoi vertex requirement,

$$d(P, i_\delta) = d(P, i) \qquad (\,= d(P, i_\alpha) = d(P, i_\beta))\,. \tag{C3}$$

After some algebraic manipulation this leads to the following expression

$$Z = \frac{1}{2}\;\frac{\{(x_i - 2v_1) + x_\delta\}(x_i - x_\delta) + \{(y_i - 2v_2) + y_\delta\}(y_i - y_\delta) + \{(z_i - 2v_3) + z_\delta\}(z_i - z_\delta)}{n_1(x_i - x_\delta) + n_2(y_i - y_\delta) + n_3(z_i - z_\delta)}\,, \tag{C4}$$

where (x_i, y_i, z_i) and $(x_\delta, y_\delta, z_\delta)$ are the coordinates of the nuclei i and i_δ respectively. The procedure of detecting a new Delaunay tetrahedron therefore consists of determining Z for each point $j \in$

$S_i(\alpha\beta|\gamma)$ from equation (C4), inserting the coordinates (x_j, y_j, z_j) of j for $(x_\delta, y_\delta, z_\delta)$, and taking the one with the lowest value. That j is the nucleus i_δ which together with i, i_α and i_β forms a Delaunay tetrahedron.

Before calculating Z for a nucleus $j \in S_i$ it is determined whether it belongs to $S_i(\alpha\beta|\gamma)$. The condition for a nucleus $\vec{r}_j$ to belong to $S_i(\alpha\beta|\gamma)$ is that

$$\vec{n} \cdot (\vec{r}_j - \vec{r}_i) > 0 . \tag{C5}$$

Since the inner product is the denominator of expression (C4) it is first checked whether (C5) holds, after which the calculation of Z according to (C4) is continued. If $2r_D > R_i$, with r_D the circumradius of the tetrahedron $\{i, i_\alpha, i_\beta, i_\delta\}$ and R_i the radius of the set S_i, there might be nuclei outside S_i that lie within the circumsphere of $\{i, i_\alpha, i_\beta, i_\delta\}$. In that case Z is determined for all nuclei not belonging to S_i and situated within the sphere around i and radius r_D. Before doing so, however, by means of (C5) it is checked whether such a nucleus j belongs to $H_i(\alpha\beta|\gamma)$. After having followed this procedure the detection of the new Delaunay tetrahedron has been completed.

Appendix D. Completion of a wall around a Contiguous Pair $\{i, i_\alpha\}$

An essential part of the Voronoi cell construction is the computation of the wall shared by the contiguous pair $\{i, i_\alpha\}$. The structure of the polygonal Voronoi walls is completely specified by the geometrically ordered list of vertices that delineate the wall. Geometrical order in this context is the sequence of vertices as they are connected when drawing the boundary of the polygon. An important task is therefore to establish these links between the vertices.

The vertices in the Voronoi wall defined by the nuclei i and i_α are the circumcentres of all the Delaunay tetrahedra that have the edge $\{i, i_\alpha\}$ as one of their 6 edges. Figure D1 is a two-dimensional representation of this three-dimensional arrangement of Delaunay tetrahedra. The edge $\{i, i_\alpha\}$ is represented by a black dot. It points out of the page, with nucleus i_α situated on top of nucleus i. Each triangle represents a Delaunay tetrahedron with the pair $\{i, i_\alpha\}$ as common edge. The identity of each of these Delaunay tetrahedra is therefore determined by the other two nuclei, e.g. i_β and i_γ. While the lines that connect to the black central dot represent a Voronoi wall seen edge-on, the lines connecting the outer nuclei are true Voronoi edges. Figure D1 represents a typical situation at the start of the determination of the structure of the Voronoi wall defined by the pair $\{i, i_\alpha\}$. Only a fraction of the relevant Delaunay tetrahedra have been determined, so that the pair $\{i, i_\alpha\}$ is not yet completely enclosed. The Delaunay tetrahedra that are already known were determined either during the construction of another Voronoi polyhedron or during the construction of any of the other Voronoi walls of Π_i.

When starting the construction of the polyhedron Π_i the information on the previously determined Delaunay tetrahedra that have the nucleus i as one of their vertices is processed. The information on such a Delaunay tetrahedron is passed on to the lists W_j of the Voronoi walls shared

by i and any of the other three contiguous nuclei j that are its vertices. Specifically, when a Delaunay tetrahedron has as vertices the nuclei i, i_α, i_β and i_γ, the relevant data on this Delaunay tetrahedron are passed on to the list W_{i_α} for the wall between i and i_α, W_{i_β} for the wall between i and i_β and W_{i_γ} for the wall between i and i_γ. The information that W_{i_α} gets consists of three data. These are its circumcentre V, which is a vertex of Π_i, and the two other nuclei besides i and i_α, i_β and i_γ. The same, with the obvious adjustments, is done for W_{i_β} and W_{i_γ}. The order of i_β and i_γ in W_{i_α} is an essential ingredient, that is further specified in Appendix E. During the construction of Π_i the wall lists W_j of any of the contiguous nuclei j for which the structure of the corresponding wall has yet to be determined are updated when a newly calculated Delaunay tetrahedron has j as one of its vertices. Completed walls will not receive any new data. By definition all their vertices are known, so that the corresponding Delaunay tetrahedra will not be calculated again.

At the beginning of the determination of the structure of the wall between the nuclei i and i_α the position of the Delaunay tetrahedra in the list W_{i_α} is rather arbitrary. This position is determined by the chronological order in which the tetrahedra were calculated, not by their geometrical sequence inside the wall. Consequently, the wall construction procedure consists of a geometrical ordering of the tetrahedra in W_{i_α} and the filling in of the gaps between them (see fig. D1), i.e. the calculation of new Delaunay tetrahedra following the description in appendix C. The first step is to take the first Delaunay tetrahedron in W_{i_α}, whose circumcentre is the first vertex of the wall. Subsequently, we move around the edge $\{i, i_\alpha\}$ until we return at this first Delaunay tetrahedron. For example, when the first Delaunay tetrahedron is $\{i, i_\alpha, i_\beta, i_\gamma\}$, the second step consists of the search for the tetrahedron that shares the triangular face $\{i, i_\alpha, i_\beta\}$ with the first tetrahedron. First, we look for such a tetrahedron in W_{i_α}. When it indeed contains such a Delaunay tetrahedron its circumcentre is the second vertex of the wall. When such a tetrahedron does not yet exist a new Delaunay tetrahedron is determined. Information on such a newly computed Delaunay tetrahedron $\{i, i_\alpha, i_\beta, i_\delta\}$ is passed on to the lists W_{i_β} and W_{i_δ} as well as to the nuclei i_α, i_β and i_δ. This information will therefore be used during the determination of Π_i, when constructing the walls shared between i and i_β and between i and i_δ, and during the determination of the Voronoi cells Π_{i_α}, Π_{i_β} and Π_{i_δ}. This process is repeated until we have to find a Delaunay tetrahedron with a triangular face $\{i, i_\alpha, i_\gamma\}$. Because that is the first Delaunay tetrahedron, the construction of the wall shared by the nuclei i and i_α has been completed.

Appendix E. The permutation ordering of the vertices of a Delaunay tetrahedron

In order to let the program run efficiently it is necessary to order the four vertices of every Delaunay tetrahedron in a fixed way. Specifically we this means than when one takes any of the six edges of the tetrahedron, defined by two of the four vertices, one always knows which of the other two nuclei will come first when turning counterclockwise around the edge (see fig. E1).

The solution to this problem is rather easy. Assume that the Delaunay tetrahedron was computed during the construction of the Voronoi polyhedron around i_α, during the determination of

the wall shared with nucleus i_β. In addition, assume that the third and fourth nucleus of the Delaunay tetrahedron are i_γ and i_δ respectively. When rotating counterclockwise around the edge $\{i_\alpha, i_\beta\}$ the nucleus i_γ is met before the nucleus i_δ. The vertices of this Delaunay tetrahedron are therefore ordered as $\{i_\alpha, i_\beta, i_\gamma, i_\delta\}$. Every positive permutation of this list yields a correct geometrical ordering. Table E1 shows how these permutations work out. The number in the vertical list is the one of the first nucleus, the one of which we are constructing its Voronoi cell. The number in the horizontal list is the one of the second nucleus, the one that together with the first nucleus defines the wall being constructed. The table then gives, between brackets, the third and, after the comma, the fourth nucleus. For example, if δ and γ are first and second nucleus respectively, the table tells that β and α are third and fourth nucleus respectively. This permutation order is implemented as a look-up table in the construction program.

Appendix F. The multidimensional binary tree

An important issue in the Voronoi tessellation construction is the efficient search for points in three-dimensional space. One of the main problems in this multidimensional searching is the need for a data structure in which points that lie closely together in multidimensional space are also situated at a nearby position in the data structure. We achieve this by means of the *optimized multidimensional binary tree* of Friedmann, Bentley and Finkel (1977).

In this datastructure the databaseis stored in a binary tree in which each node represents a subset of the records in the complete set and a geometric partitioning of that subset. The *root* of the tree represents the entire set. Each nonterminal node has two *successor nodes*. Those sucessor nodes represent the two subsets defined by the partitioning. The terminal nodes represent mutually exclusive small subsets of the data records, which collectively form a partition of the record space. These terminal nodes are called *buckets*. Figure F1 illustrates the multidimensional binary tree by means two-dimensional subdivisions and the corresponding tree representation.

The structure and efficiency of the tree is determined by three factors. The first one is the choice of the *discriminating key* at each level in the tree, which can range from 1 to k as in k dimensions each record is represented by k keys. The second one is the *partition value* of the discriminating key. All records in the subset with key values less than or equal to the partition value belong to the left successor node, while those with a larger value belong to the right successor node. Given the domain of a node, the partition determines the geometric boundaries of the subsets corresponding to its successor nodes. Note that the geometric boundaries of a node define a cell in multidimensional space, and that the volume of such a cell is smaller for subsets defined by nodes deeper in the tree. The third factor is the size of a bucket, i.e. the maximum number of records in each terminal node. We followed the choice that Friedmann *et al.* (1977) used for their optimized k-d tree:

1. The *partition value*. The partition is located at the *median* of the marginal distribution of (the discriminator) key values, irrespective of which key is chosen for the discriminator.

2. The *discriminating key value*. Choose at every nonterminal node the key with the largest spread in values as the discriminator. The spread S is defined as,

$$S = \frac{1}{M}\sum_{l=1}^{M} |x_k(l) - \bar{x}_k|, \tag{F1}$$

with M the number of points in the subsample, $x_k(l)$ the k key value of point i in the subsample, and $\bar{x}_k$ the mean k value of the M points in the subsample.

3. The *bucket size* is chosen to be 2, based on an efficiency study by Van de Weygaert (1987).

In this way the multidimensional binary tree is as symmetrical as possible, and consequently its efficiency for searching tasks optimal. The construction process can be summarized as the recursive partitioning of a subset according to the prescriptions given above till you have a subset with less records than the bucket size. In our Voronoi construction algorithm we use a modified version of this $k-d$ tree. While starting with a complete tree, it is systematically pruned during the Voronoi tessellation construction. Whenever the Voronoi cell around a nucleus has been determined the nucleus is taken out of the tree. Since the Voronoi tessellation construction procedure is sequential, and because every node in the tree represents a certain range of points (e.g. $i = M, \ldots, N$) this can be done rather efficiently. As soon as the Voronoi cell of nucleus N has been constructed, the branches at all levels of the tree that represent nuclei with a number lower than N can be pruned.

The searching algorithm using the multidimensional binary tree is most easily described as a recursive procedure. The following description is for nearest neighbour searching. Adjustments for other searching tasks can be made relatively easy. An illustration of searching within a certain range is provided in figure F1. A first step is the definition of a query record. In the case of the search for the nearest neighbours to some point the query record consists of the coordinates of that point, while in the case of the search for all the points within a sphere it is the centre of the sphere.

The argument to the recursive procedure is the node under investigation. The first call passes the root of the tree as this argument. If the node under investigation is terminal *(bucket)*, all the records in the bucket should be examined. If the node under investigation is not terminal, the recursive procedure is called for the node representing the same side of the partition as the query record. In the case of closest neighbour searching a list of the M ($M = 1, 2, 3, \ldots$) closest records so far encountered and their distance to the query record is maintained as a priority queue during the search. Whenever a record is examined and found to be closer than the most distant member of this list, the list is updated.

When control returns to a specific node after having descended the tree, a test is made to determine if it is necessary to consider the records on the other side of the partition, the one opposite to the query record. It is necessary to consider the corresponding subset only if the geometric boundaries delimiting those records overlap the ball (sphere in 3-D) centered at the query record with radius equal to the distance to the Mth closest record so far encountered. This is referred to as the "*bounds-overlap-ball*" test. If the bounds-overlap-ball test fails, none of the records on the opposite side of the partition can be among the M records closest to the query

record. If the bounds do overlap the ball, then the records of that subtree must be considered and the procedure is called recursively for the node representing that subset. A "*ball-within-bounds*" test is made before ascending the tree to a higher level, in order to determine if it is necessary to continue the search. This test determines whether the ball is entirely within the geometric domain of the node. If so, the current list of M nearest neighbours is correct for the entire file and no more records need be examined.

In the case of ball searching, i.e. searching for all points in the sample that lie within a ball (sphere) around a point, the algorithm used is nearly the same as the one just described, with the centre of the ball serving as query record. There are two differences. The first one is that instead of maintaining a list of the M closest neighbours found sofar a list is maintained of all the points inside the ball found sofar. Because no priority queue is needed the distances of these points to the query record need not be kept. Secondly, there is a difference concerning the "bounds-overlap-ball" test. Because the radius of the search ball remains constant during the search, instead of gradually decreasing as in the nearest neighbour searches, we only need to apply this test once for each considered node. Once we know that there is an overlap, we know that the points in the subfile of the node have to be examined, possibly partly if it is a nonterminal node. Because in the case of nearest neighbour searching the search ball decreases in size during the search through the subset, the ball may not be overlapping the domain of the node anymore upon return at the node.

TABLE 1. Moments of 3-D Poisson-Voronoi tessellation

Number density of vertices	$J_0 = \frac{24}{35}\pi^2\rho$	$J_0 = 6.768\rho$
Number density of edges	$J_1 = \frac{48}{35}\pi^2\rho$	$J_1 = 13.535\rho$
Number density of walls	$J_2 = \left(\frac{24}{35}\pi^2 + 1\right)\rho$	$J_2 = 7.768\rho$
Number density of cells	$J_3 = \rho$	
Number of vertices per cell	$E(N_0) = \frac{96}{35}\pi^2$	$E(N_0) = 27.07$
Number of edges per cell	$E(N_1) = \frac{144}{35}\pi^2$	$E(N_1) = 40.61$
Number of walls per cell	$E(N_2) = \frac{48}{35}\pi^2 + 2$	$E(N_2) = 15.54$
		$E(N_2^*) = 8$
Number of vertices per wall	$E_2(N_0) = \frac{144\pi^2}{24\pi^2 + 35}$	$E_2(N_0) = 5.228$
Number of edges per wall	$E_2(N_1) = \frac{144\pi^2}{24\pi^2 + 35}$	$E_2(N_0) = 5.228$
Volume of cell	$E(V) = \frac{1}{\rho}$	
		$E(V^2) = \frac{1.180}{\rho^2}$
Surface area of cell	$E(A_C) = \left\{\frac{256\pi}{3\rho^2}\right\}^{1/3}\Gamma(5/3)^*$	$E(A_C) = 5.821\rho^{-2/3}$
Perimeter of cell	$E(S_C) = \frac{(4\pi)^{5/3}\Gamma(1/3)}{5(9\rho)^{1/3}}$	$E(S_C) = 17.496\rho^{-1/3}$
Area of wall	$E(A_W) = \frac{35 \times 2^{8/3}\pi^{1/3}\Gamma(2/3)}{(9\rho)^{2/3}(24\pi^2 + 35)}$	$E(A_W) = 0.3747\rho^{-2/3}$
Perimeter of wall	$E(S_W) = \frac{7 \times 2^{10/3}\pi^{5/3}\Gamma(1/3)}{(9\rho)^{1/3}(24\pi^2 + 35)}^*$	$E(S_W) = 2.252\rho^{-1/3}$
Length of edge	$E(L) = \frac{7\Gamma(1/3)}{9(36\pi\rho)^{1/3}}^*$	$E(L) = 0.4309\rho^{-1/3}$

* (formula agrees with Miles, 1972; disagrees with Møller, 1989)

NOTES TO TABLE 1: Moments of characteristics of 3-D Voronoi tessellations generated by Poissonian distributed nuclei with number density ρ. The 2nd column contains the analytically known moments, all first-order moments. The 3rd column contains numerical values, including the second-order moment of the volume V of a Voronoi cell. From Møller (1989), Miles (1972), and Gilbert (1962).

TABLE 2. Moments of 2-D sections through 3-D Poisson-Voronoi tessellation

Number density of vertices	$J_0 = \frac{2\,\Gamma(1/3)(16\pi^5\rho^2/9)^{1/3}}{15}$	$J_0 = 2.9159\,\rho^{2/3}$
Number density of edges	$J_1 = \frac{3}{2}J_0$	$J_1 = 4.3739\,\rho^{2/3}$
Number density of cells	$J_2 = \frac{1}{2}J_0$	$J_2 = 1.4580\,\rho^{2/3}$
Number of vertices per cell	$E(N_0) = 6$	
Number of edges per cell	$E(N_1) = 6$	
Area of cell	$E(A) = \frac{15}{\Gamma(1/3)(16\pi^5\rho^2/9)^{1/3}}$	$E(A) = 0.6859\,\rho^{-2/3}$
		$E(A^2) = 0.698\,\rho^{-4/3}$
Perimeter of cell	$E(S) = \frac{30\,\Gamma(2/3)}{(36\pi\rho)^{1/3}\,\Gamma(1/3)}$	$E(S) = 3.1356\,\rho^{-1/3}$
Length of edge	$E(L) = \frac{5\,\Gamma(2/3)}{(36\pi\rho)^{1/3}\,\Gamma(1/3)}$	$E(L) = 0.5226\,\rho^{-1/3}$

NOTES TO TABLE 2: Moments of characteristics of the two-dimensional section, which is a 2-D tessellation of convex polygons, through a three-dimensional Voronoi tessellation generated by Poissonian distributed nuclei with spatial number density ρ. The 2nd column contains analytical expressions, the 3rd column numerical ones. From Møller (1989) and Miles (1972).

TABLE 3. Moments of the edge length of a linear section through a Poisson-Voronoi tessellation

$d = 2$	length of edge	$\langle\lambda\rangle = \frac{\pi}{4\sqrt{\rho}}$	$\langle\lambda\rangle = 0.7854\,\rho^{-1/2}$
$d = 3$	length of edge	$\langle\lambda\rangle = \frac{(81/32\pi\rho)^{1/3}}{\Gamma(2/3)}$	$\langle\lambda\rangle = 0.6872\,\rho^{-1/3}$
			$\langle\lambda^2\rangle = 0.632\,\rho^{-2/3}$
			$\langle\lambda^3\rangle = 0.668\,\rho^{-1}$
			$\langle\lambda^4\rangle = 0.774\,\rho^{-4/3}$

NOTES TO TABLE 3: Moments of the length λ of an edge in a linear section through a Voronoi tessellation generated by Poissonian distributed nuclei with number density ρ. The top row contains the expression for a two- dimensional Voronoi tessellation, while the lower rows correspond to three-dimensional Voronoi tessellations. The 2nd column contains analytically known expressions, the 3rd column gives the numerical values, including several numerically calculated higher order moments. From Møller (1989) and Miles (1972).

TABLE 4a. 3-D Voronoi Tessellation properties; Poissonian distributed nuclei

Quantity x	$\bar{x}$	$\sigma(x)$	$\gamma_1(x)$	$\gamma_2(x)$
Number density of vertices	6.747 ± 0.014			
Number density of edges	13.493 ± 0.028			
Number density of walls	7.747 ± 0.014			
Number density of cells	1.000 ± 0.000			
Number of vertices per cell	26.986 ± 0.055	6.61 ± 0.18	0.346 ± 0.029	-0.029 ± 0.030
Number of edges per cell	40.479 ± 0.083	9.92 ± 0.27	0.346 ± 0.029	-0.029 ± 0.030
Number of walls per cell	15.493 ± 0.028	3.305 ± 0.091	0.346 ± 0.029	-0.029 ± 0.030
Volume of cell	1.000 ± 0.000	0.418 ± 0.009	0.73 ± 0.11	0.70 ± 0.39
Surface area of cell	5.801 ± 0.018	1.461 ± 0.043	0.28 ± 0.11	-0.01 ± 0.17
Perimeter of cell	17.443 ± 0.054	3.655 ± 0.094	0.305 ± 0.035	0.00 ± 0.13
Form factor of cell	0.540 ± 0.006	0.082 ± 0.003	-0.565 ± 0.032	0.36 ± 0.11
Number of vertices per wall	5.2255 ± 0.0014	1.564 ± 0.016	0.582 ± 0.016	0.058 ± 0.024
Area of wall	0.3744 ± 0.0015	0.3722 ± 0.0037	1.266 ± 0.047	1.40 ± 0.19
Perimeter of wall	2.2518 ± 0.0092	1.2009 ± 0.0050	0.089 ± 0.022	-0.796 ± 0.029
Form factor of wall	0.6389 ± 0.0005	0.1635 ± 0.0011	-0.855 ± 0.035	0.40 ± 0.13
Distance nucleus-wall	0.6402 ± 0.0017	0.2092 ± 0.0051	-0.024 ± 0.022	-0.333 ± 0.074
Volume nucleus-wall	0.0645 ± 0.0001	0.0579 ± 0.0009	1.177 ± 0.097	1.52 ± 0.47
Length of edge	0.4309 ± 0.0018	0.3216 ± 0.0023	0.829 ± 0.020	0.209 ± 0.044
Angle between edges	$111^\circ.107 \pm 0.018$	$35^\circ.310 \pm 0.078$	-0.499 ± 0.012	-0.276 ± 0.039
Angle between walls	$120^\circ.0 \pm 0.0$	$23^\circ.53 \pm 0.30$	-0.296 ± 0.014	-0.255 ± 0.038

NOTES TO TABLE 4a: Four moments of characteristics of a 3-D Voronoi tessellation generated by Poissonian distributed nuclei. Each number in the table is based on four different realization of each 1000 Voronoi cells, the error estimates are based on the differences between these realizations. The second column contains the mean of the quantity, the third column contains the standard deviation, the fourth column the skewness and the fifth column the kurtosis of the characteristic involved. The dimensional quantities, such as volume, area and length, are normalized such that there is exactly one Voronoi cell, or nucleus, per unit volume.

TABLE 4b. 3-D Voronoi Tessellation properties; Anticorrelated nuclei

Quantity x	$\bar{x}$	$\sigma(x)$	$\gamma_1(x)$	$\gamma_2(x)$
Number density of vertices	6.548 ± 0.009			
Number density of edges	13.096 ± 0.018			
Number density of walls	7.548 ± 0.009			
Number density of cells	1.000 ± 0.000			
Number of vertices per cell	26.191 ± 0.037	3.801 ± 0.039	0.128 ± 0.073	-0.04 ± 0.12
Number of edges per cell	39.287 ± 0.055	5.701 ± 0.059	0.128 ± 0.073	-0.04 ± 0.12
Number of walls per cell	15.096 ± 0.018	1.900 ± 0.020	0.128 ± 0.073	-0.04 ± 0.12
Volume of cell	1.000 ± 0.000	0.144 ± 0.005	0.492 ± 0.061	0.34 ± 0.19
Surface area of cell	5.593 ± 0.002	0.492 ± 0.018	0.237 ± 0.034	-0.015 ± 0.083
Perimeter of cell	16.884 ± 0.008	1.560 ± 0.031	0.255 ± 0.099	0.08 ± 0.14
Form factor of cell	0.642 ± 0.001	0.036 ± 0.001	-0.127 ± 0.066	-0.028 ± 0.082
Number of vertices per wall	5.2051 ± 0.0010	1.385 ± 0.011	0.372 ± 0.034	-0.17 ± 0.12
Area of wall	0.3705 ± 0.0005	0.2943 ± 0.0007	0.523 ± 0.006	-0.714 ± 0.017
Perimeter of wall	2.2370 ± 0.0024	1.0281 ± 0.0028	-0.352 ± 0.010	-0.865 ± 0.019
Form factor of wall	0.6944 ± 0.0001	0.1497 ± 0.0011	-1.166 ± 0.029	1.19 ± 0.11
Distance nucleus-wall	0.6204 ± 0.0003	0.1250 ± 0.0007	0.090 ± 0.029	-0.878 ± 0.037
Volume nucleus-wall	0.0662 ± 0.0001	0.0457 ± 0.0002	0.213 ± 0.013	-0.961 ± 0.020
Length of edge	0.4298 ± 0.0005	0.2803 ± 0.0005	0.434 ± 0.015	-0.612 ± 0.021
Angle between edges	$110^\circ.837 \pm 0.013$	$29^\circ.52 \pm 0.14$	-0.667 ± 0.002	0.398 ± 0.046
Angle between walls	$120^\circ.0 \pm 0.0$	$17^\circ.159 \pm 0.078$	-0.491 ± 0.007	-0.326 ± 0.014

NOTES TO TABLE 4b: Four moments of characteristics of a 3-D Voronoi tessellation generated by anticorrelated distributed nuclei. Each number in the table is based on four different realization of each 1000 Voronoi cells, the error estimates are based on the differences between these realizations. The second column contains the mean of the quantity, the third column contains the standard deviation, the fourth column the skewness and the fifth column the kurtosis of the characteristic involved. The dimensional quantities, such as volume, area and length, are normalized such that there is exactly one Voronoi cell, or nucleus, per unit volume.

'ABLE 4c. 3-D Voronoi Tessellation properties; Correlated nuclei

Quantity x	$\bar{x}$	$\sigma(x)$	$\gamma_1(x)$	$\gamma_2(x)$
Number density of vertices	6.712 ± 0.027			
Number density of edges	13.423 ± 0.054			
Number density of walls	7.712 ± 0.027			
Number density of cells	1.000 ± 0.000			
Number of vertices per cell	26.85 ± 0.11	8.45 ± 0.11	0.485 ± 0.031	0.19 ± 0.28
Number of edges per cell	40.27 ± 0.14	12.67 ± 0.16	0.485 ± 0.031	0.19 ± 0.28
Number of walls per cell	15.423 ± 0.054	4.222 ± 0.055	0.485 ± 0.031	0.19 ± 0.28
Volume of cell	1.000 ± 0.000	0.684 ± 0.034	1.31 ± 0.22	2.34 ± 1.16
Surface area of cell	5.826 ± 0.024	2.48 ± 0.10	0.61 ± 0.12	0.26 ± 0.37
Perimeter of cell	17.54 ± 0.10	5.56 ± 0.11	0.478 ± 0.069	0.11 ± 0.23
Form factor of cell	0.477 ± 0.003	0.097 ± 0.001	-0.457 ± 0.076	0.03 ± 0.15
Number of vertices per wall	5.2219 ± 0.0027	1.6196 ± 0.0074	0.690 ± 0.027	0.297 ± 0.075
Area of wall	0.3783 ± 0.0015	0.4190 ± 0.0049	1.74 ± 0.11	3.76 ± 0.72
Perimeter of wall	2.275 ± 0.010	1.295 ± 0.011	0.318 ± 0.031	-0.507 ± 0.083
Form factor of wall	0.6145 ± 0.0039	0.1627 ± 0.0016	-0.7374 ± 0.018	0.175 ± 0.069
Distance nucleus-wall	0.6407 ± 0.0035	0.3143 ± 0.0020	0.508 ± 0.035	-0.32 ± 0.13
Volume nucleus-wall	0.0648 ± 0.0002	0.0749 ± 0.0022	2.40 ± 0.24	9.0 ± 2.4
Length of edge	0.4357 ± 0.0019	0.3430 ± 0.0043	1.022 ± 0.030	0.81 ± 0.11
Angle between edges	$111^\circ.060 \pm 0.036$	$37^\circ.94 \pm 0.28$	-0.417 ± 0.005	-0.533 ± 0.009
Angle between walls	$120^\circ.0 \pm 0.0$	$27^\circ.82 \pm 0.13$	-0.260 ± 0.008	-0.485 ± 0.008

NOTES TO TABLE 4c: Four moments of characteristics of a 3-D Voronoi tessellation generated by correlated distributed nuclei. Each number in the table is based on four different realization of each 1000 Voronoi cells, the errorestimates are based on the differences between these realizations. The second column contains the mean of the quantity, the third column contains the standard deviation, the fourth column the skewness and the fifth column the kurtosis of the characteristic involved. The dimensional quantities, such as volume, area and length, are normalized such that there is exactly one Voronoi cell, or nucleus, per unit volume.

TABLE 5a. 3-D Voronoi Tessellation Planar section (Slice) properties; Poissonian nuclei

Quantity x	$\bar{x}$	$\sigma(x)$	$\gamma_1(x)$	$\gamma_2(x)$
Number density of cells	1.4530	0.0592	0.2871	-1.0099
Number density of vertices	2.9060	0.1184	0.2871	-1.0099
Number density of edges	4.3590	0.1776	0.2871	-1.0099
Number of vertices per cell	6.0000	1.6895	0.3311	-0.1142
Area of cell	0.6882	0.4741	0.4573	-0.3902
Perimeter of cell	3.1418	1.2212	-0.5819	-0.2879
Form factor of cell	0.7050	0.1433	-1.3425	2.0875
Length of edge	0.5221	0.3631	0.6223	-0.2321
Angle between edges	$120^\circ.0000$	$31^\circ.6039$	-0.6351	0.1321
Angle between walls-section plane	$63^\circ.1812$	$18^\circ.5232$	-0.6351	-0.3520

TABLE 5b. 3-D Voronoi Tessellation Planar section (Slice) properties; Anticorrelated nuclei

Quantity x	$\bar{x}$	$\sigma(x)$	$\gamma_1(x)$	$\gamma_2(x)$
Number density of cells	1.3925	0.0468	0.1355	0.0024
Number density of vertices	2.7850	0.0936	0.1355	0.0024
Number density of edges	4.1775	0.1403	0.1355	0.0024
Number of vertices per cell	6.0000	1.5599	0.0682	-0.2408
Area of cell	0.7181	0.4181	-0.1884	-1.0937
Perimeter of cell	3.1392	1.0946	-0.9637	0.0783
Form factor of cell	0.7615	0.1357	-1.6614	2.7221
Length of edge	0.5293	0.3107	0.1988	-0.8705
Angle between edges	$120^\circ.0000$	$26^\circ.5652$	-0.8056	1.1078
Angle between walls-section plane	$63^\circ.4754$	$18^\circ.3374$	-0.6136	-0.3666

TABLE 5c. 3-D Voronoi Tessellation Planar section (Slice) properties; Correlated nuclei

Quantity x	$\bar{x}$	$\sigma(x)$	$\gamma_1(x)$	$\gamma_2(x)$
Number density of cells	1.4770	0.1925	0.5294	-0.8974
Number density of vertices	2.9540	0.3850	0.5294	-0.8974
Number density of edges	4.4310	0.5776	0.5294	-0.8974
Number of vertices per cell	6.0000	1.7607	0.3939	-0.0951
Area of cell	0.6770	0.5712	1.1890	2.1076
Perimeter of cell	3.1025	1.3964	-0.0701	-0.4989
Form factor of cell	0.6773	0.1508	-1.1117	1.2120
Length of edge	0.5170	0.3838	0.8957	0.5170
Angle between edges	120°0000	34°6159	-0.5893	-0.1774
Angle between walls-section plane	63°0346	18°6088	-0.6074	-0.3715

NOTES TO TABLE 5: Moments of characteristics of the planar sections of 3-D Voronoi tessellations. The dimensional quantities, as length, area and volume, are normalized in such a way that the number density of Voronoi cells, and nuclei, is exactly equal to one per unit volume. The second column is the mean of the quantity, the third column the standard deviation, the fourth column the skewness, and the fifth column the kurtosis. The numbers in this table were determined from 20 planar sections through 1 realization of a Voronoi tessellation of 1000 cells. Table 5a corresponds to planar sections through a 3-D Voronoi tessellation generated by Poissonian distributed nuclei, Table 5b to a tessellation generated by anticorrelated distributed nuclei, and Table 5c to a tessellation generated by correlated distributed nuclei.

TABLE 6a. 3-D Voronoi Tessellation Linear section properties; Poissonian nuclei

Quantity x	$\bar{x}$	$\sigma(x)$	$\gamma_1(x)$	$\gamma_2(x)$
Length of edge	0.6703	0.3942	0.2600	-0.6923
Dispersion length of edge	0.6123	0.1159	0.0643	0.0204
Angle between wall-line of sight	44°6988	19°5325	0.0067	-0.8080
Angle between opposite walls	75°4123	30°9389	-0.0185	-0.5829

TABLE 6b. 3-D Voronoi Tessellation Linear section properties; Anticorrelated nuclei

Quantity x	$\bar{x}$	$\sigma(x)$	$\gamma_1(x)$	$\gamma_2(x)$
Length of edge	0.7003	0.3725	-0.1100	-1.0168
Dispersion length of edge	0.5551	0.1117	-0.0433	-0.0088
Angle between wall-line of sight	44°6436	19°6246	0.0194	-0.8090
Angle between opposite walls	79°9995	31°4217	-0.2500	-0.7174

TABLE 6c. 3-D Voronoi Tessellation Linear section properties; Correlated nuclei

Quantity x	$\bar{x}$	$\sigma(x)$	$\gamma_1(x)$	$\gamma_2(x)$
Length of edge	0.6641	0.4314	0.5946	-0.0896
Dispersion length of edge	0.6677	0.1270	0.1347	0.0492
Angle between wall-line of sight	44°8522	19°7981	0.0070	-0.8235
Angle between opposite walls	72°2277	31°0546	0.1714	-0.5057

NOTES TO TABLE 6: Moments of characteristics of the linear sections of 3-D Voronoi tessellations. The dimensional quantities, as length, area and volume, are normalized in such a way that the number density of Voronoi cells, and nuclei, is exactly equal to one per unit volume. The second column is the mean of the quantity, the third column the standard deviation, the fourth column the skewness, and the fifth column the kurtosis. The numbers in this table were determined from 2500 linear sections through 1 realization of a Voronoi tessellation of 1000 cells, except for the dispersion of a linear section, which is based on 10000 linear sections. Table 6a corresponds to linear sections through a 3-D Voronoi tessellation generated by Poissonian distributed nuclei, Table 6b to a tessellation generated by anticorrelated distributed nuclei, and Table 6c to a tessellation generated by correlated distributed nuclei.

TABLE E1. Ordering of the vertices in a Delaunay tetrahedron

	α	β	γ	δ
α		(γ,δ)	(δ,β)	(β,γ)
β	(δ,γ)		(α,δ)	(γ,α)
γ	(β,δ)	(δ,α)		(α,β)
δ	(γ,β)	(α,γ)	(β,α)	

References

Aggarwal, A., Guibas, L.J., Saxe, J., and Shor, P., 1987, in Proc. 19th Ann. ACM Symp. Theory Comput., p. 39

Aurenhammer, F., and Edelsbrunner, H., 1984, Pattern Recognition, 17, 251

Bentley, J.L., 1986, Programming Pearls. Addison-Wesley

Bentley, J.L., and Friedmann, J.H., 1978, IEEE Trans. Comput., C-27, 97

Bertschinger, E., 1985, ApJS, 58, 1

Boots, B.N., 1974, in Proc. Association of American Geographers, 6, 26

Boots, B.N., 1980, Economic Geography, 56, 248

Boots, B.N., 1984, Metallography, 17, 411

Bowyer, A., 1981, The Computer Jnl., 24, 162

Broadhurst, T.J., Ellis, R.S., Koo, D.C., and Szalay, A.S., 1990, Nat, 343, 726

Brostow, W., Dussault, J.P., and Fox, B.L., 1978, J. Comp. Phys., 29, 81

Brown, K.Q., 1979, Inform. Process. Lett., 9, 223

Coles, P., 1990, Nat, 346, 446

Crain, I.K., 1976, in Merriam, D.F., ed, Random Processes in Geology, Springer-Verlag, p. 3

Delesse, M.A., 1847, C. R. Acad. Sci., 25, 544

Delone, B.V., 1934, Bull. Acad. Sci. (VII) Classe Sci. Mat., 793

Dirichlet, G.L., 1850, J. reine angew. Math., 40, 209

Dubinski, J.L., da Costa, L.N., Goldwirth, D.S., Lecar, M., and Piran, T., 1992, ApJ, in press

Finney, J.L., 1979, J. Comput. Phys., 32, 137

Fischer, R.A., and Miles, R.E., 1973, Math. Biosciences, 18, 335

Friedman, J., Bentley, J.L., and Finkel, R.A., 1977, ACM Trans. Math. Softw., 3, 209

Fujimoto, M., 1983, PASJ, 35, 159

Gilbert, E.N., 1962, Ann. Math. Stat., 33, 958

Green, P.J., and Sibson, R., 1978, Comp. J., 21, 168

Guibas, L.J., and Stolfi, J., 1985, ACM Trans. Graph., 4, 74

Hamilton, W.D., 1971, J. Teor. Biol., 31, 295

Honda, H., 1983, Int. Rev. Cytology, 81, 191

Icke, V., 1984, MNRAS, 206, 1P

Icke, V., and Van de Weygaert, R., 1987, A&A, 184, 16 (IW)

Ikeuchi, S., 1981, PASJ, 33, 211

Ikeuchi, S., and Turner, E.L., 1991, MNRAS, 250, 519

Jensen, E.B., 1984, Journ. Math., 136, 345

Johnson, W.A., and Mehl, R.F., 1939, Trans. Am. Inst. Min. Metal Eng., 135, 416

Kiang, T., 1966, Zeitschr. f. Astrophys., 64, 433

Ling, E.N., 1987, New Statistical Approaches to Galaxy Clustering, Ph.D. Thesis Univ. Sussex

Mardia, K.V., Edwards, R., and Puri, M.L., 1977, Bull. I.S.I., 47, 93

Matsuda, T., and Shima, E., 1984, Prog. Theor. Phys., 71, 855

Melott, A.L., 1983, MNRAS, 205, 637

Meyering, J.L., 1953, Philips Res. Rept., 8, 270

Miles, R.E., 1970, Math. Biosci., 6, 85

Miles, R.E., 1972, Suppl. Adv. Appl. Prob., 243

Miles, R.E., 1978, in Miles, R.E., Serra, J., eds., Proc. of the Buffon Bicentenary Symposium on Geometrical Probability, Image Analysis, Mathematical Stereology, and Their Relevance to the Determination of Biological Structures, Paris 1977, Geometrical Probability and Biological Structures: Buffon's 200th Anniversery, Springer Lecture Notes in Biomathematics, p. 115

Miles, R.E., 1984, Revista Unfon Matemática Argentina, 29, 310

Miles, R.E., and Davy, P.J., 1977, Journ. Math., 113, 45

Miles, R.E., and Maillardet, R.J., 1982, J. Appl. Prob., 19A, 97

Møller, J., 1989, Adv. Appl. Prob., 21, 37

Moran, P.A.P., 1983, Kotz, S., Johnson, N.L., eds., Encyclopedia of Statistical Sciences, Vol. 3, p. 404

Moscardini, L., Matarrese, S., Lucchin, F., and Messina, A., 1991, MNRAS 248, 424

Ogawa, T., and Tanemura, M., 1974, Progress Theor. Phys., 51, 399

Ostriker, J.P., and Cowie, L.L., 1981, ApJ, 243, L127

Rosiwal, A., 1898, Verh. K. K. Geol. Reichsanst., 5/6, 143

Serra, J.P., 1982, Image Analysis and Mathematical Morphology. Academic Press, London

Shannon, C.E., 1949, Proc. I.R.E., 37, 10

Sibson, R., 1980, Scand. J. Statist., 7, 14

Sibson, R., 1981, in Barnett, V., eds, Interpreting Multivariate Data, J. Wiley and Sons, p. 21

Stoyan, D., Kendall, W.S., and Mecke, J., 1987, Stochastic Geometry and Its Applications. Akademie-Verlag, Berlin

Stoyan, D., and Stoyan, H., 1980, Z. Geol. Wiss., 8, 1529

SubbaRao, M.U., and Szalay, A.S., 1992, ApJ, 391, 483

Tanemura, M., Ogawa, T., and Ogita, N., 1983, J. Comp. Phys., 51, 191

Thiessen, A.H., 1911, Monthly Weather Review, 39, 1082

Van de Weygaert, R., 1987, The Multidimensional Binary Tree and its Use in Astronomy, report M.Sc. research project

Van de Weygaert, R., 1991a, MNRAS, 249, 159

Van de Weygaert, R., 1991b, Voids and the Geometry of Large Scale Structure, Ph.D. thesis Leiden Univ.

Van de Weygaert, R., and Icke, V., 1989, A&A, 213, 1 (WI)

Voronoi, G., 1908, J. reine angew. Math., 134, 198

Watson, D.F., 1981, The Computer Jnl., 24, 167

Weibel, E., 1980, Stereological Methods, Vol. 2. Academic Press, London/New York

Weinberg, D.H., 1989, Reconstructing Primordial Density Fluctuations, Ph.D. thesis Princeton Univ.

Wicksell, S.D., 1925, Biometrika, 17, 84

Wicksell, S.D., 1926, Biometrika, 18, 152

Williams, B.G., 1992, Hierarchical and Cellular Structures in Cosmology, Ph.D. thesis Univ. Edinburgh
Williams, B.G., Peacock, J.A., and Heavens, A.F., 1991, MNRAS 252, 43
Yoshioka, S., and Ikeuchi, S., 1989, ApJ, 341, 16

Figure Captions

FIGURE 1. An illustration of a distribution of nuclei (stars) in a square (centre) and its corresponding Delaunay triangulation (left) and Voronoi tessellation (right), assuming periodic boundary conditions.

FIGURE 2. Topological illustration of a portion of Π_i. The nucleus j which is contiguous to the central nucleus i is represented by a filled circle. The circle also represents the contiguous pair $\{i, j\}$. The polygon in the central part indicates the face which is produced by the pair $\{i, j\}$. Open circles are the nuclei which are contiguous to both nuclei i and j. Dotted triangles reperesent Delaunay Tetrahedrons. (After Tanemura, Ogawa, and Ogita, 1983). See text for details.

FIGURE 3. Illustration of how the geometrical elements of a tessellation are linked with the generating nuclei. A nucleus defines a complete Voronoi cell (top left); two nuclei define one wall (top right), their bisecting plane, which is one of the faces of their cells; three nuclei define an edge, which forms a part of the boundary of the three walls which intersect at that edge; four nuclei define one vertex, the centre of their circumscribing sphere, which is one of the two vertices between which the edge is stretched. The four nuclei form a Delaunay tetrahedron.

FIGURE 4. Six examples of Voronoi cells, taken from a 3-D Voronoi tessellation generated by 1000 anticorrelated nuclei distributed in a box.

FIGURE 5. Stereoscopic pair of three Voronoi cells sharing a common edge. The nuclei are indicated by stars. In a stereo viewer, the dashed lines will appear at the rear of the picture. When attempting stereo fusion with crossed eyes, the pictures must be reversed to obtain the correct depth perception.

FIGURE 6. Two-dimensional point distributions equivalent in clustering properties to the three-dimensional nuclei distributions used in the presented statistical analysis. Instead of 1000 points in a box of size $100 \times 100 \times 100$ here 100 points are distributed in a square of size 100×100 in such a way that the relative distances of the points are the same in the 3-D point process as in the 2-D point process. One should therefore consider these pictures as projections of a slice taken out of the 3-D box with a width of 1/10th of the boxsize. In this way we hope to give a better idea of the point process than with a full 3-D illustration. Left: correlated distribution, $\lambda = 0.4$; Middle: Poissonian distribution, $\delta = 0.0$; Right: anticorrelated distribution, $\delta = 0.8$.

FIGURE 7. Histograms of six Voronoi cell properties. Top left: volume of cell; top right: surface area of cell; middle left: perimeter of cell; middle right: form factor of cell; bottom left: number of walls of cell; bottom right: number of vertices of cell. All dimensional properties (volume, area, length) are normalized such that the number density of Voronoi cells (or, equivalently, nuclei) is 1 per unit volume. (a) The six histograms for a Voronoi tessellation generated by 1000

Poissonian distributed nuclei, (b) for a tessellation generated by 1000 anticorrelated distributed nuclei ($\delta = 0.8$), (c) for a tessellation generated by 1000 correlated distributed nuclei ($\lambda = 0.4$).

FIGURE 8. Four scatter plots illustrating the correlations between some cell properties. Top left: volume of cell against its form factor; top right: volume of cell against number of walls of that cell; bottom left: volume of cell against number of vertices of that cell; bottom right: form factor of cell against number of walls of that cell. All dimensional properties (volume, area, length) are normalized such that the number density of Voronoi cells (or, equivalently, nuclei) is 1 per unit volume. (a) The four scatter plots for a Voronoi tessellation generated by 1000 Poissonian distributed nuclei, (b) for a tessellation generated by 1000 anticorrelated distributed nuclei ($\delta = 0.8$), (c) for a tessellation generated by 1000 correlated distributed nuclei ($\lambda = 0.4$).

FIGURE 9. Histograms of six Voronoi wall properties. Top left: area of wall; top right: perimeter of wall; middle left: distance between nucleus and wall; middle right: volume of pyramid with nucleus as tip and wall as base; bottom left: form factor of wall; bottom right: number of vertices of wall. All dimensional properties (volume, area, length) are normalized such that the number density of Voronoi cells (or, equivalently, nuclei) is 1 per unit volume. (a) The six histograms for a Voronoi tessellation generated by 1000 Poissonian distributed nuclei, (b) for a tessellation generated by 1000 anticorrelated distributed nuclei ($\delta = 0.8$), (c) for a tessellation generated by 1000 correlated distributed nuclei ($\lambda = 0.4$).

FIGURE 10. Histograms of three Voronoi tessellation properties. Top left: length of Voronoi edge, bottom left: angle between two edges in tessellation; bottom right: angle between two walls in tessellation. All dimensional properties (volume, area, length) are normalized such that the number density of Voronoi cells (or, equivalently, nuclei) is 1 per unit volume. (a) The three histograms for a Voronoi tessellation generated by 1000 Poissonian distributed nuclei, (b) for a tessellation generated by 1000 anticorrelated distributed nuclei ($\delta = 0.8$), (c) for a tessellation generated by 1000 correlated distributed nuclei ($\lambda = 0.4$).

FIGURE 11. Planar sections through 3-D Voronoi tessellations. (a) Six planar sections through a Voronoi tessellation of 1000 cells in a box of size $100 \times 100 \times 100$ (i.e. in unnormalized units), generated by 1000 Poissonian distributed nuclei. The section planes are taken parallel to the $x - y$ plane, the number below each square denotes the z-coordinate of the section plane: 25.0, 30.0, 35.0, 40.0, 45.0, and 50.0. (b) The same, but then for a tessellation generated by 1000 anticorrelated distributed nuclei ($\delta = 0.8$), while the section planes have z-coordinate 30.0, 35.0, 40.0, 45.0, 50.0, and 55.0. (c) The same, but then for a tessellation generated by 1000 correlated distributed nuclei ($\lambda = 0.4$), while the section planes have z-coordinate 60.0, 65.0, 70.0, 75.0, 80.0, and 85.0.

FIGURE 12. Histograms of four properties of cells of the planar section through a Voronoi tessellation Top left: area of cell; top right: perimeter of cell; bottom left: form factor of cell; bottom right: number of vertices of cell. All dimensional properties (volume, area, length) are normalized such that the number density of the 3-D Voronoi cells (or, equivalently, nuclei) is 1

per unit volume. (a) The four histograms for a Voronoi tessellation generated by 1000 Poissonian distributed nuclei, (b) for a tessellation generated by 1000 anticorrelated distributed nuclei ($\delta = 0.8$), (c) for a tessellation generated by 1000 correlated distributed nuclei ($\lambda = 0.4$).

FIGURE 13. Histograms of three planar section tessellation properties plus scatter plot of planar section cell properties. Top left: histogram of length of edges in planar section; bottom left: histogram of angle that each 3-D wall cut by section plane (producing a section edge) makes with section plane; bottom right: histogram of angle between section edges. Top right: scatter plot of area of sectioned cell against the volume of its 'parent' 3-D Voronoi cell. All dimensional properties (volume, area, length) are normalized such that the number density of Voronoi cells (or, equivalently, nuclei) is 1 per unit volume. (a) The four diagrams for a Voronoi tessellation generated by 1000 Poissonian distributed nuclei, (b) for a tessellation generated by 1000 anticorrelated distributed nuclei ($\delta = 0.8$), (c) for a tessellation generated by 1000 correlated distributed nuclei ($\lambda = 0.4$).

FIGURE 14. Histograms of four properties of edges of the linear section through a Voronoi tessellation. Top left: length of section edge; top right: dispersion of edge lengths in a linear section of length equal to the box edge length in which a tessellation of 1000 cells is situated; bottom left: angle that wall crossed by linear section makes with wall; bottom right: angle between two walls on opposite side of a linear section edge. All dimensional properties (volume, area, length) are normalized such that the number density of the 3-D Voronoi cells is one per unit volume. (a) The four histograms for a Voronoi tessellation generated by 1000 Poissonian distributed nuclei, (b) for a tessellation generated by 1000 anticorrelated distributed nuclei ($\delta = 0.8$), (c) for a tessellation generated by 1000 correlated distributed nuclei ($\lambda = 0.4$).

FIGURE 15. Four scatter plots illustrating the correlations between some linear section properties. Top left: section edge length against length of next section edge; top right: section edge length against volume of 'parent' 3-D Voronoi cell; bottom left: section edge length against angle that wall on one side of edge makes with the line of sight (section line); bottom right: section edge length against angle that walls on both sides of the edge make with each other. All dimensional properties (volume, area, length) are normalized such that the number density of Voronoi cells is one per unit volume. (a) The four scatter plots for a Voronoi tessellation generated by 1000 Poissonian distributed nuclei, (b) for a tessellation generated by 1000 anticorrelated distributed nuclei ($\delta = 0.8$), (c) for a tessellation generated by 1000 correlated distributed nuclei ($\lambda = 0.4$).

FIGURE A1. Illustration of the detection of a triangle with a minimum circumradius.

FIGURE C1. Two Delaunay tetrahedra $\{i, i_\alpha, i_\beta, i_\gamma\}$ and $\{i, i_\alpha, i_\beta, i_\delta\}$ that have the triangular face $\{i, i_\alpha, i_\beta\}$ in common.

FIGURE C2. Schematic diagram to show the elementary process of detecting a new Delaunay tetrahedron. The horizontal line in the figure represents the XY plane. Two black dots on the

line represents nuclei i_α and i_β. One of them should be thought to indicate the nucleus i itself. The black dot below the horizontal line is the nucleus i_γ. The dashed circle corresponds to the circumsphere of Delaunay tetrahedron $\{i, i_\alpha, i_\beta, i_\gamma\}$. The open half-plane above the horizontal line corresponds to $H_i(\alpha\beta|\gamma)$. The open dots are the nuclei belonging to $S_i(\alpha\beta|\gamma)$. Solid circles correspond to spheres which are attached to these nuclei. In the figure, nucleus i_δ is a vertex of the new Delaunay tetrahedron (after Tanemura, Ogawa, and Ogita, 1983).

FIGURE D1. Schematic diagram of successive construction of Delaunay tetrahedrons. The black dot represents the contiguous pair $\{i, i_\alpha\}$. This figure represents the intermediate stage of closing Delaunay tetrahedrons around the pair $\{i, i_\alpha\}$. For details, see text (after Tanemura, Ogawa, and Ogita, 1983).

FIGURE E1. Ordering of the vertices in a Delaunay tetrahedron. Figure corresponding to Table E1.

FIGURE F1. Illustration of the structure of a k-d tree. The top 6 frames show the division of two-dimensional space according to the rules discussed in appendix F. The first frame shows the 32 randomly distributed particles in the square, the four consecutive frames are k-d tree divisions at the 2nd until 4th level of the tree, with the 4th one corresponding to 2 particles per cell. The corresponding tree is shown below the 6 frames. The letters at the nodes correspond to the cells with the corresponding letters in the frames. The 6th frame contains a dashed rectangle, defining a search region. The black boxes in the tree correspond to the cells overlapped by this region. Links in the tree with a bar through them need not be investigated for the search.

Rien van de Weygaert
Canadian Institute for Theoretical Astrophysics
McLennan Labs,
University of Toronto,
60 St. George St.,
Toronto Ontario M5S 1A7, Canada

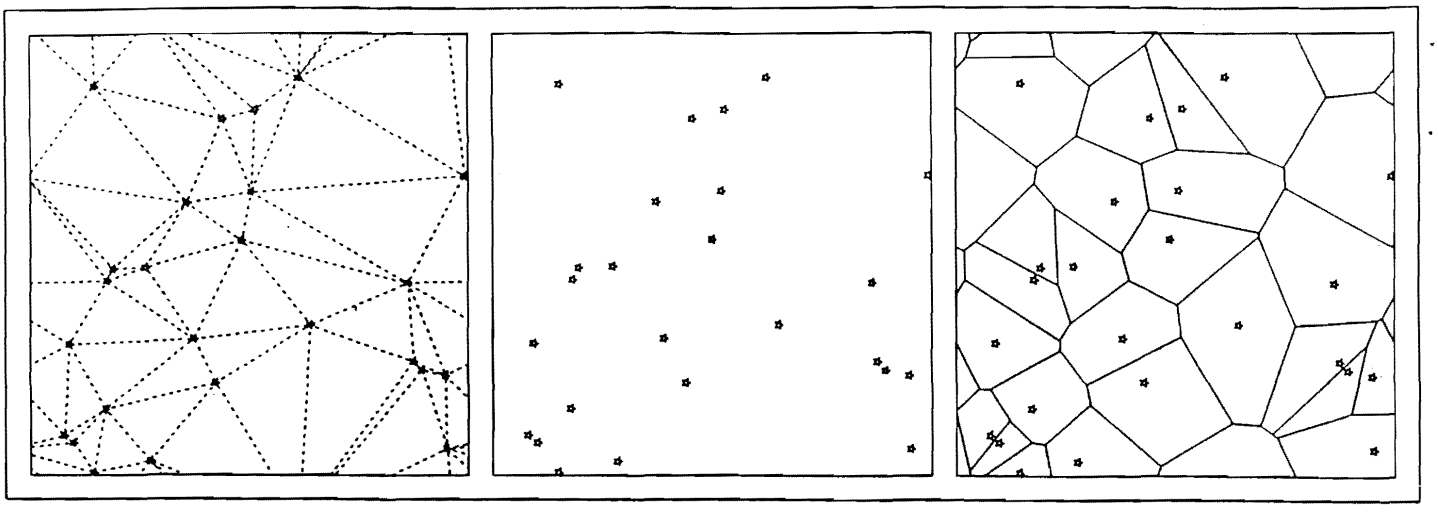

FIGURE 1.

FIGURE 2.

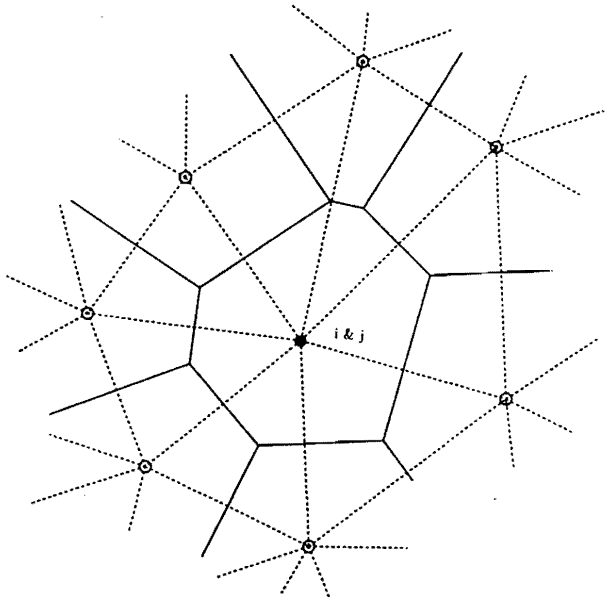

FIGURE 6.

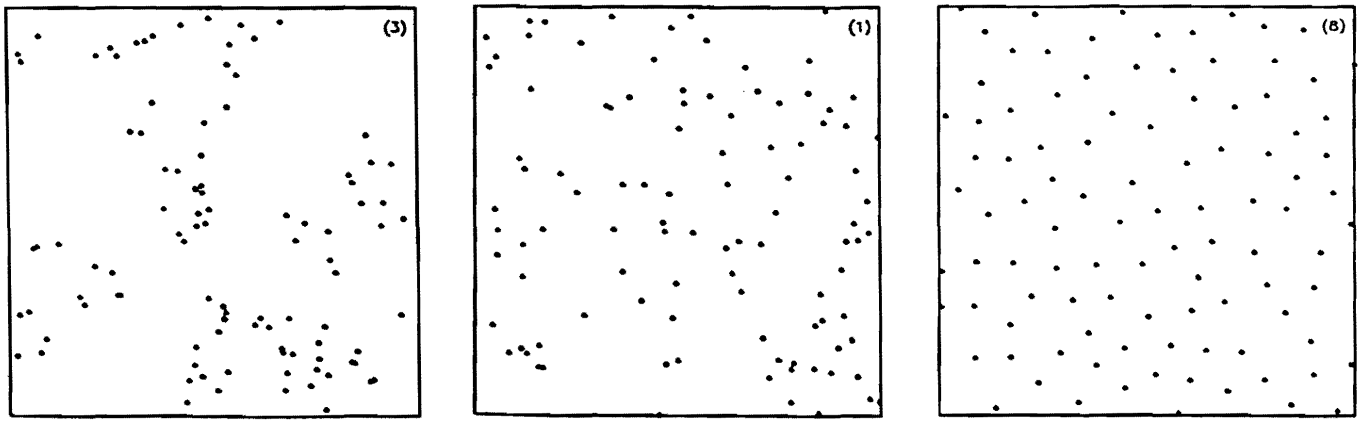

FIGURE 3.

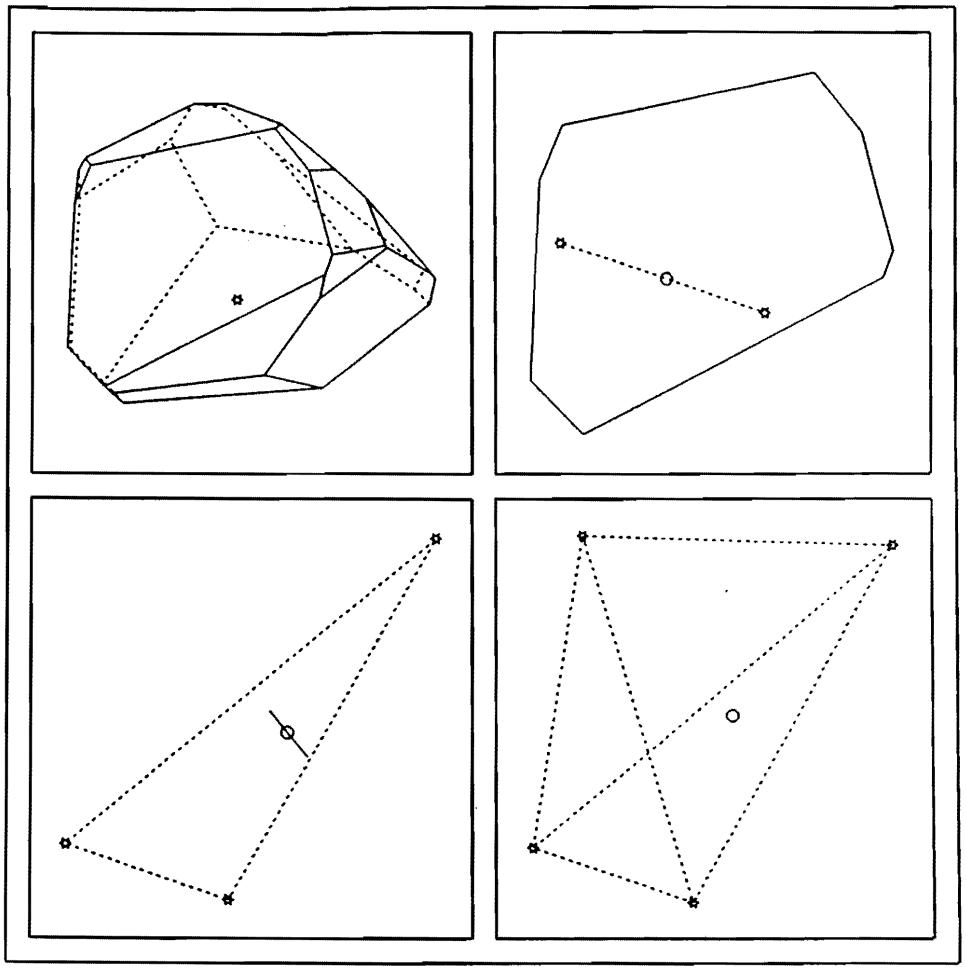

FIGURE 5.

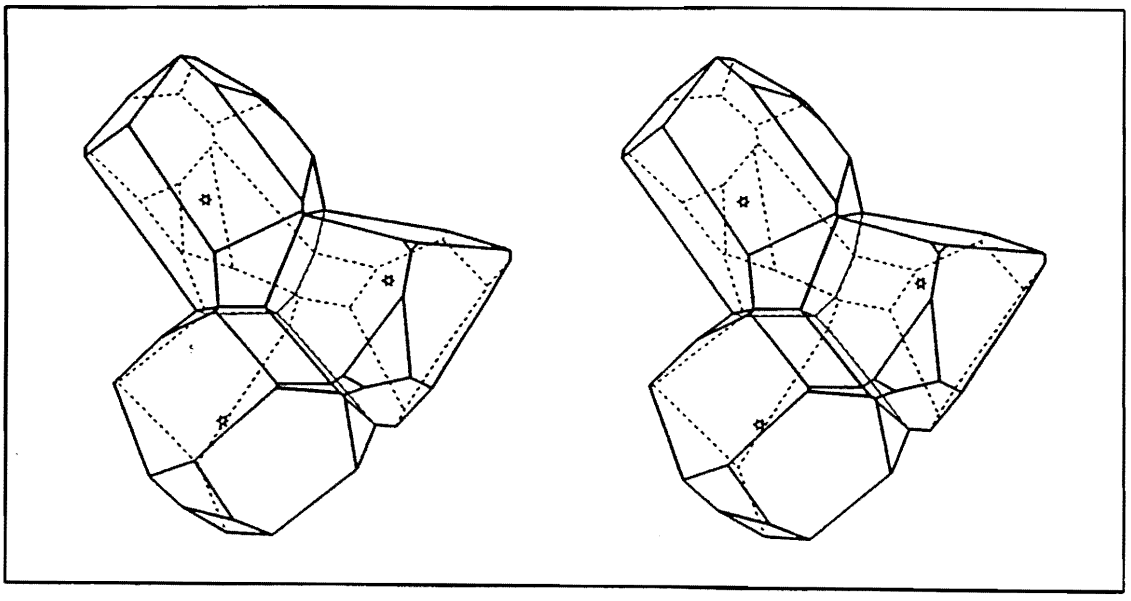

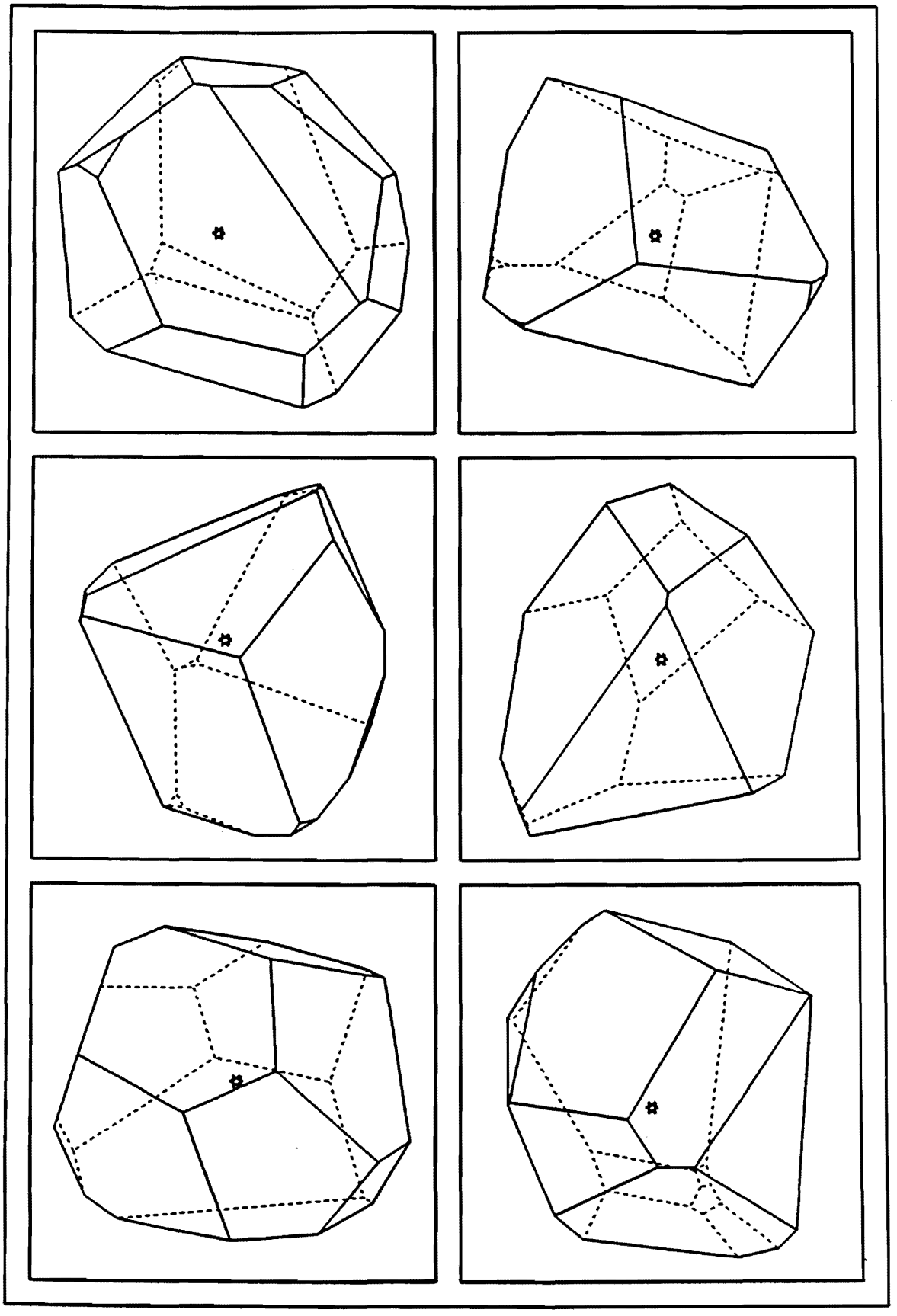

FIGURE 4.

CLASS: P

FIGURE 7a.

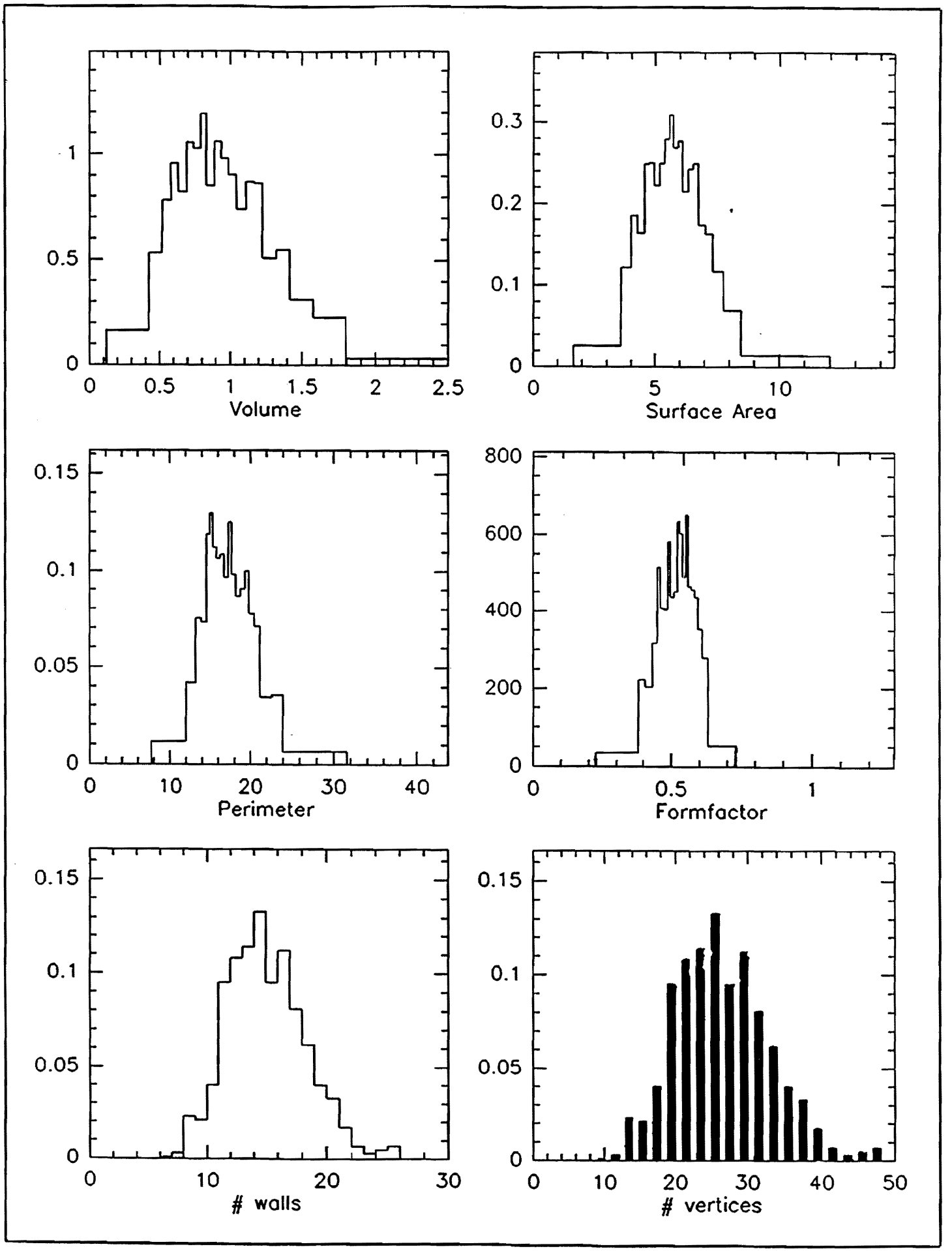

CLASS: A Parameter: 0.80

FIGURE 7b.

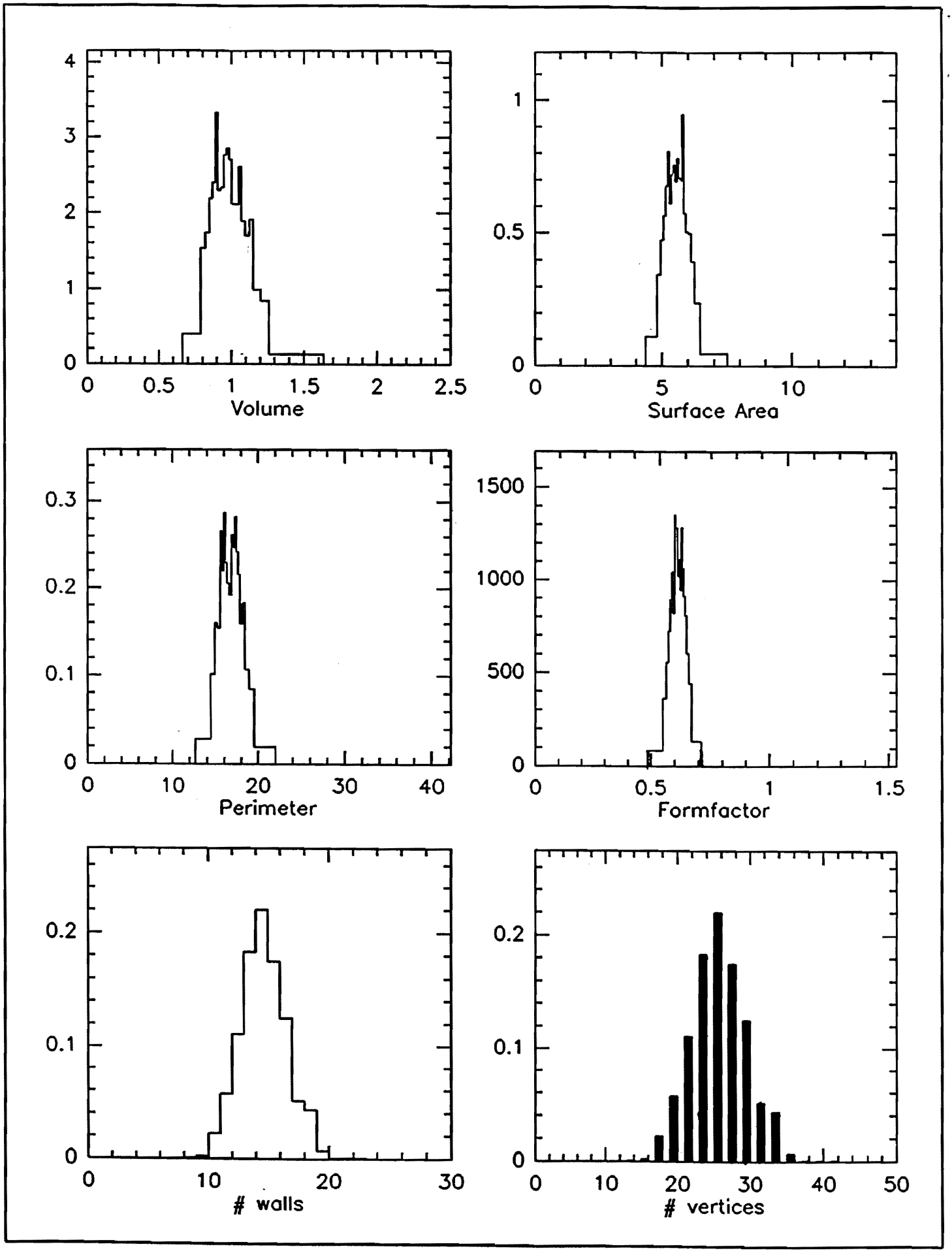

CLASS: C Parameter: 0.40

FIGURE 7c.

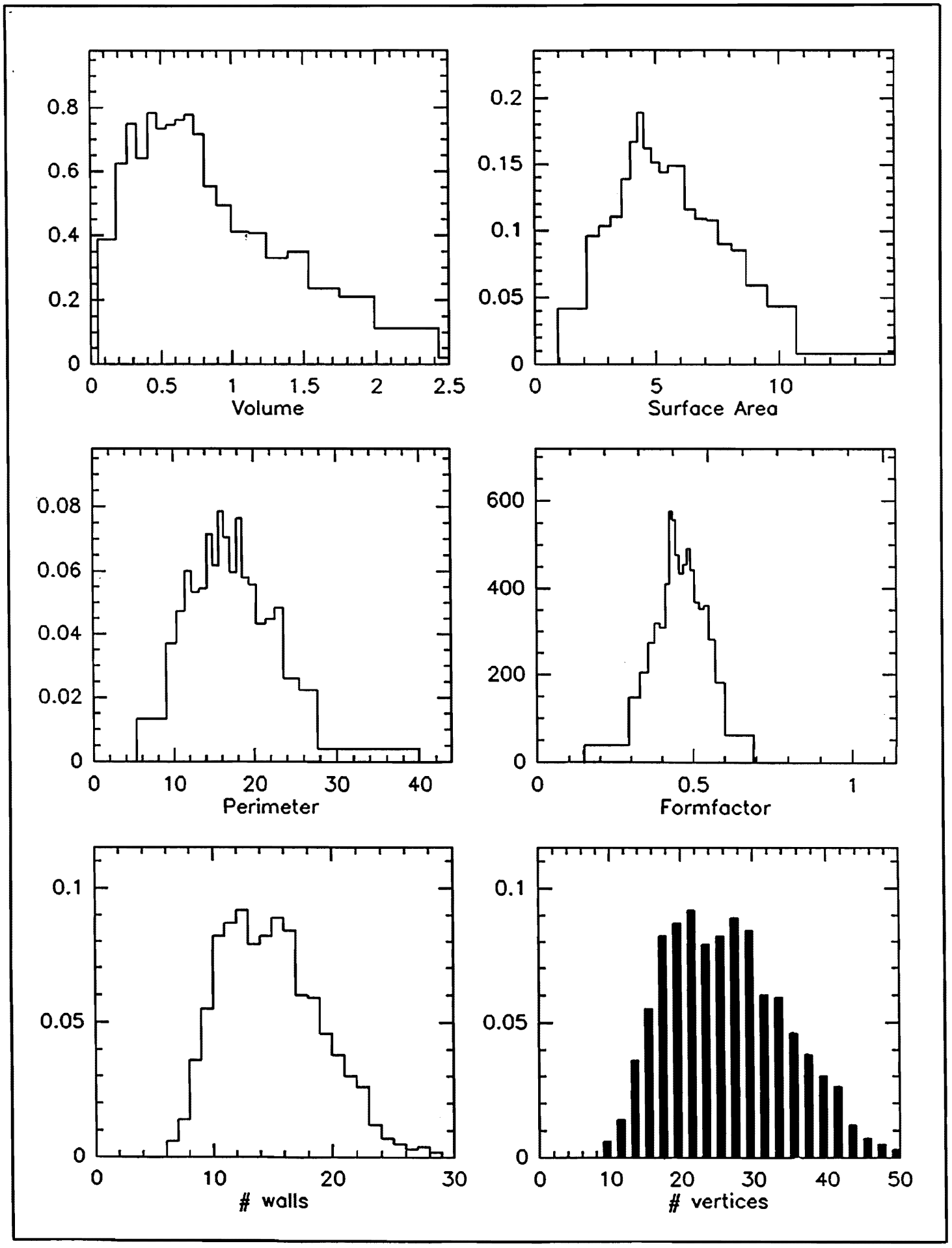

FIGURE 8a.

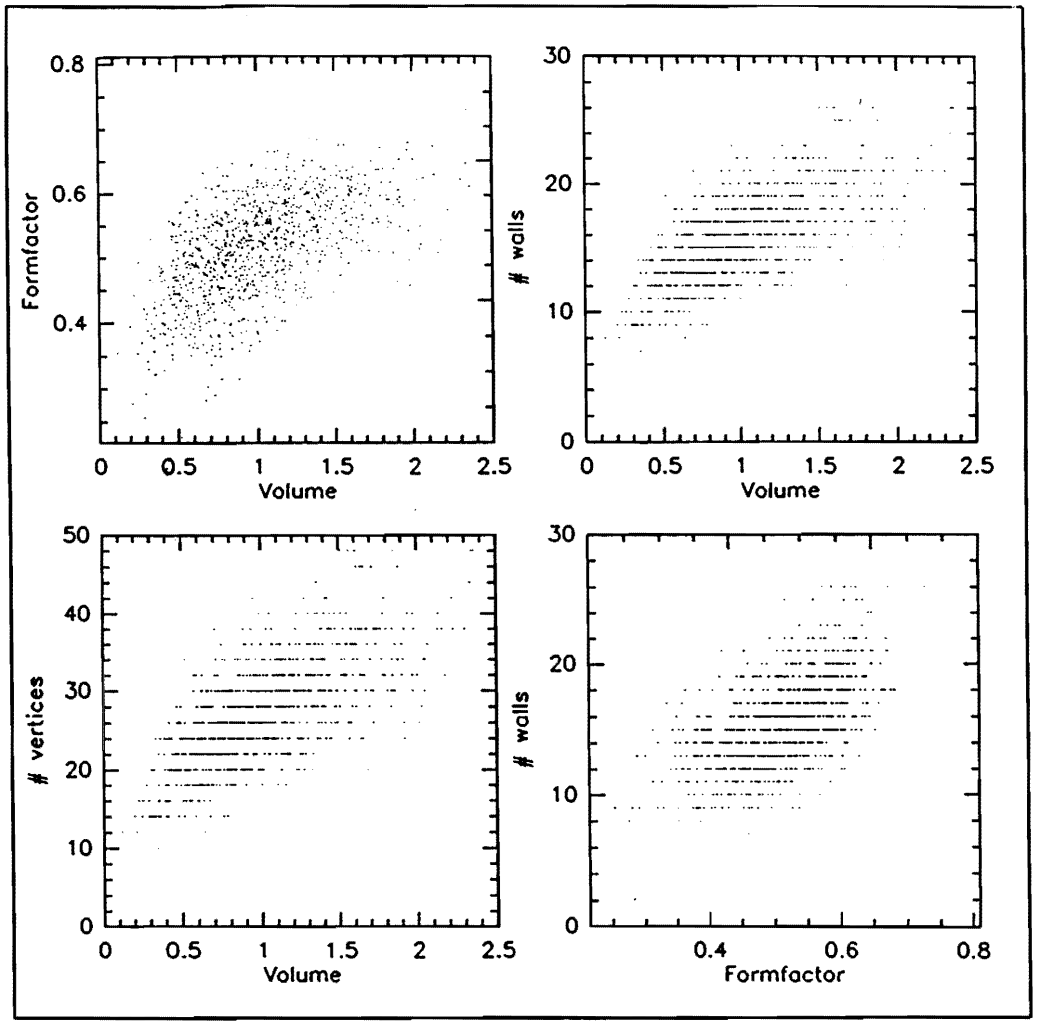

FIGURE 8b.

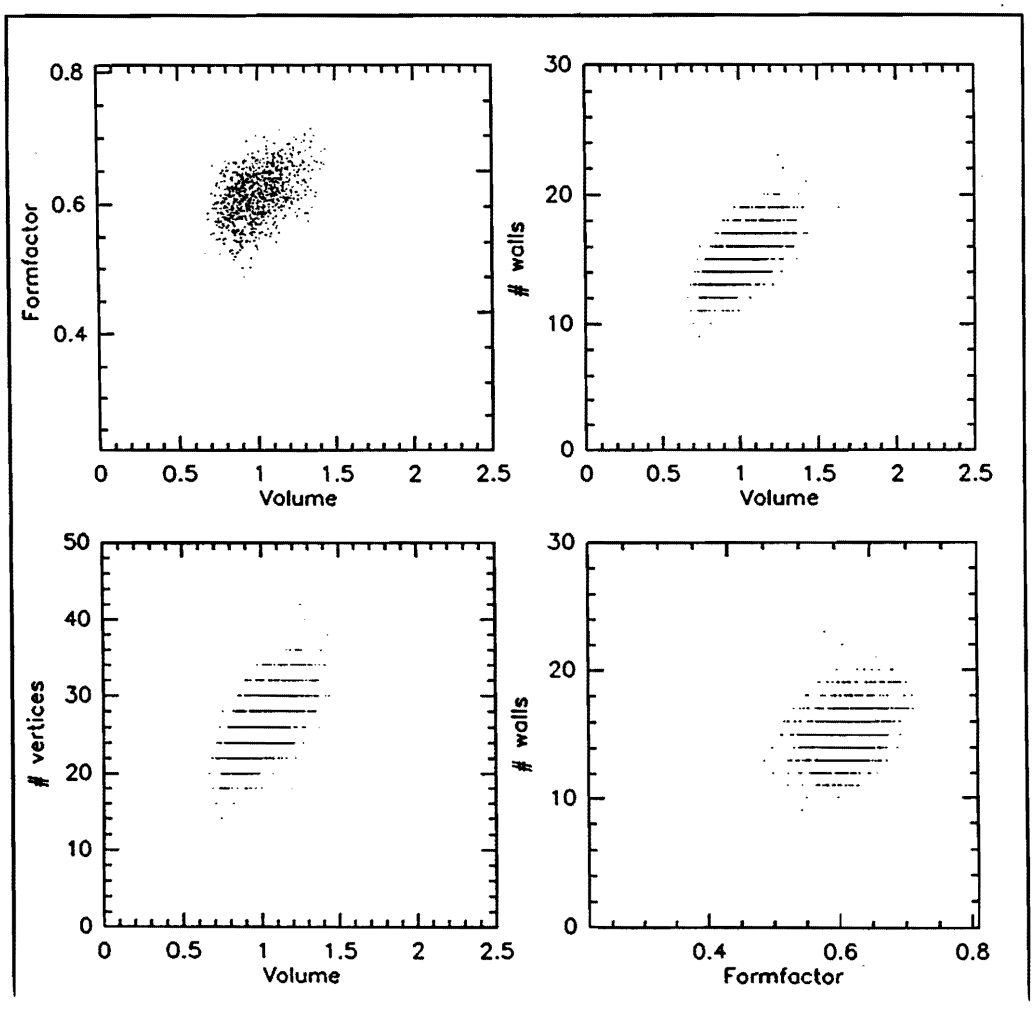

FIGURE 8c.

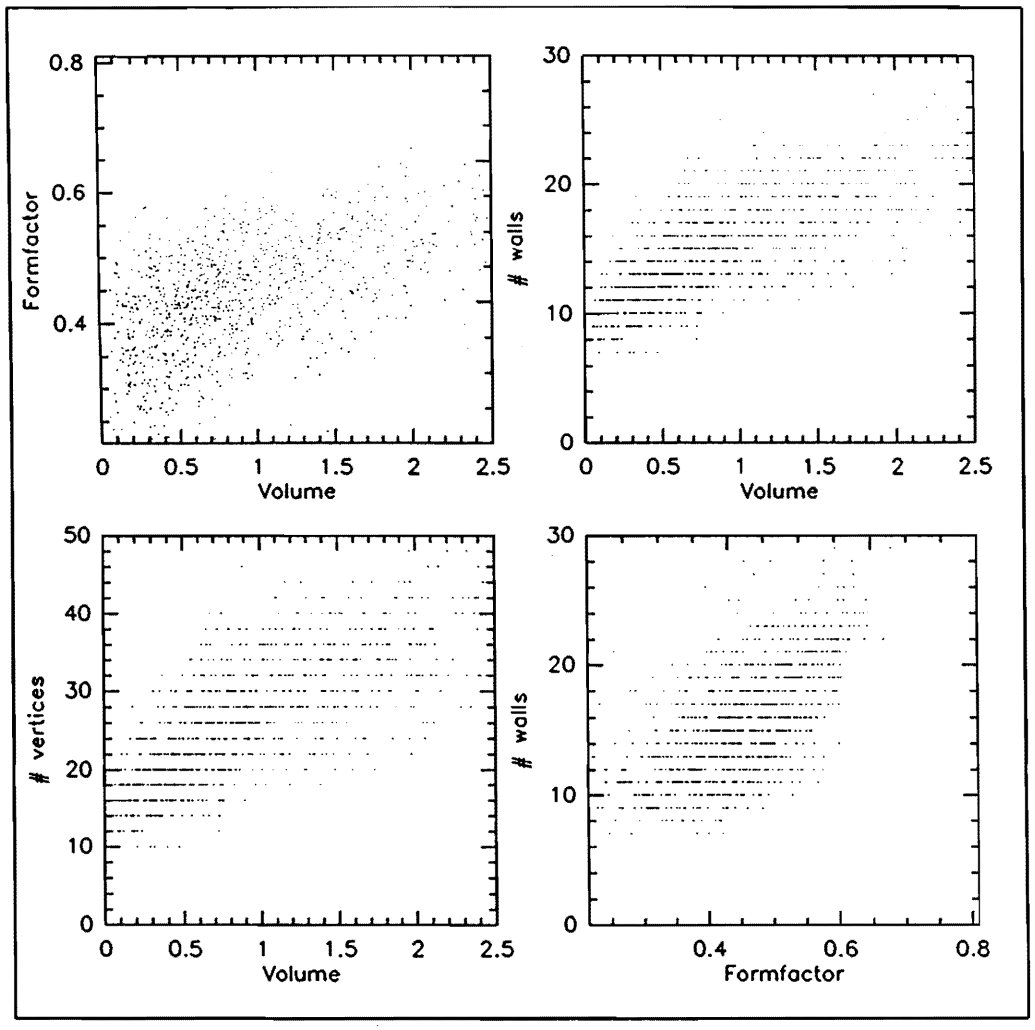

CLASS: P

FIGURE 10a.

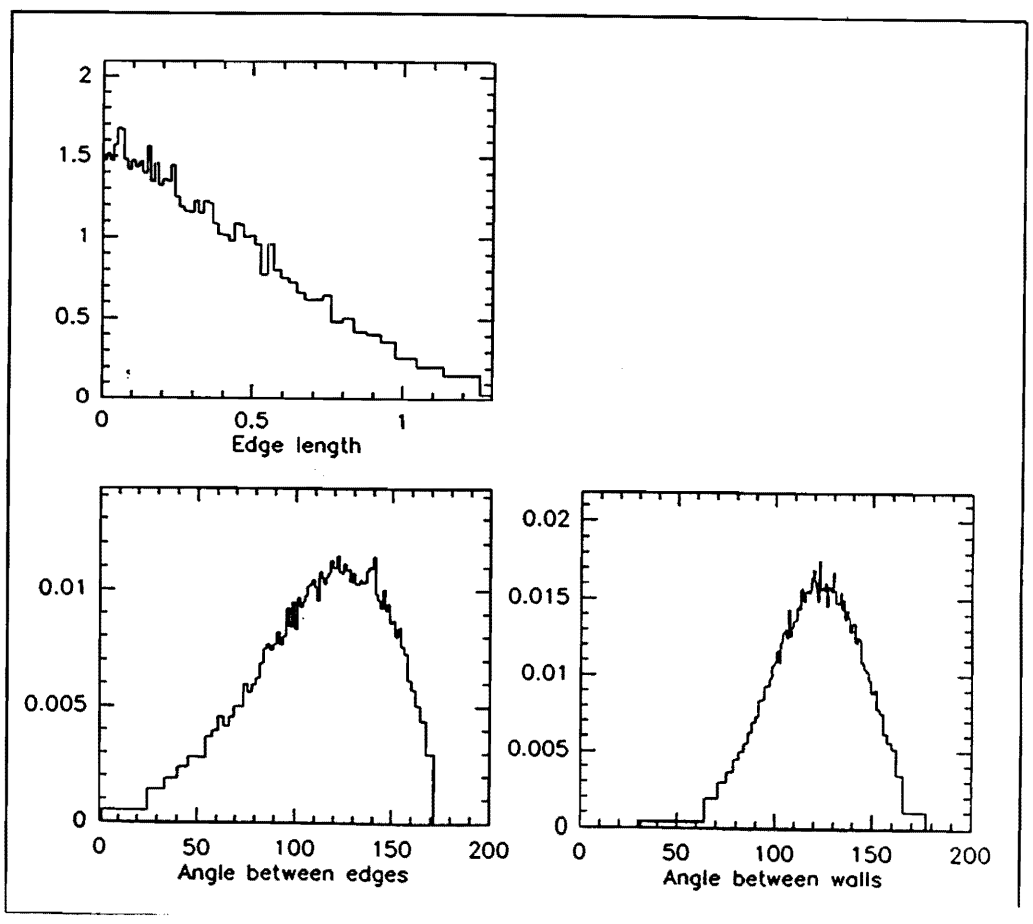

CLASS: A Parameter: 0.80

FIGURE 10b.

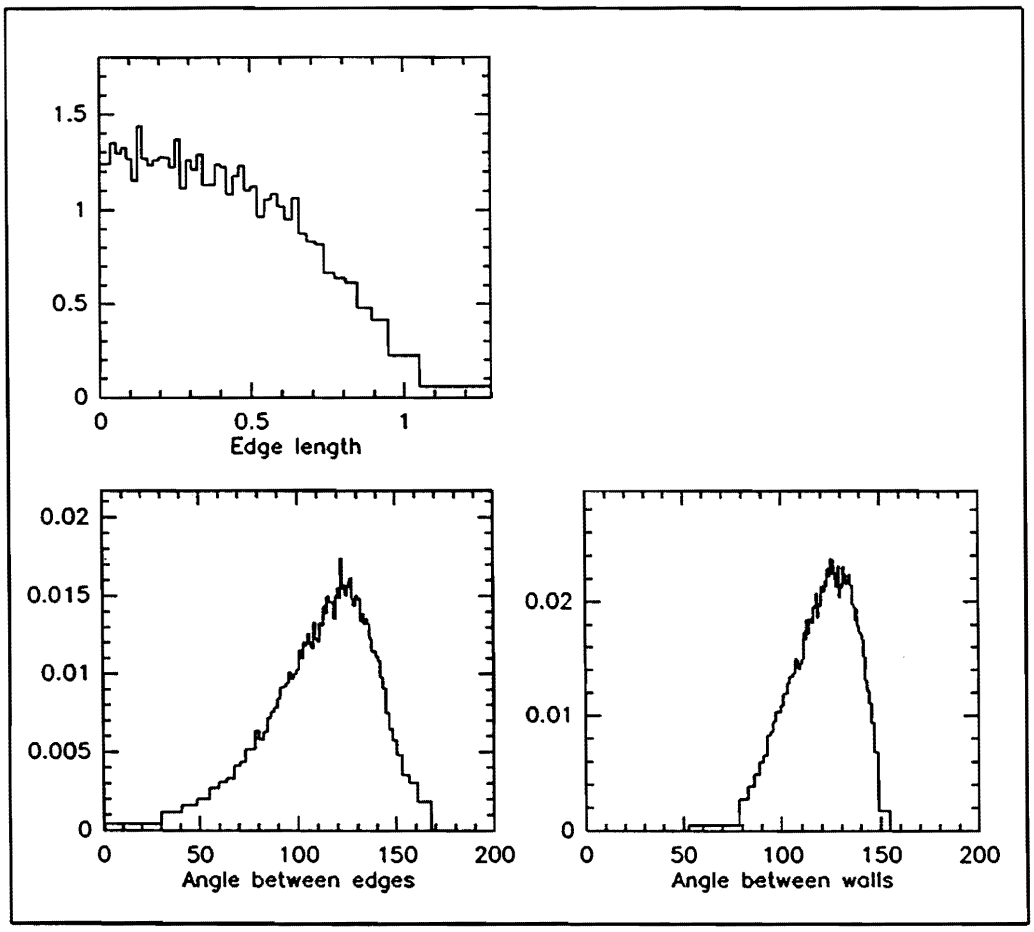

CLASS: C Parameter: 0.40

FIGURE 10c.

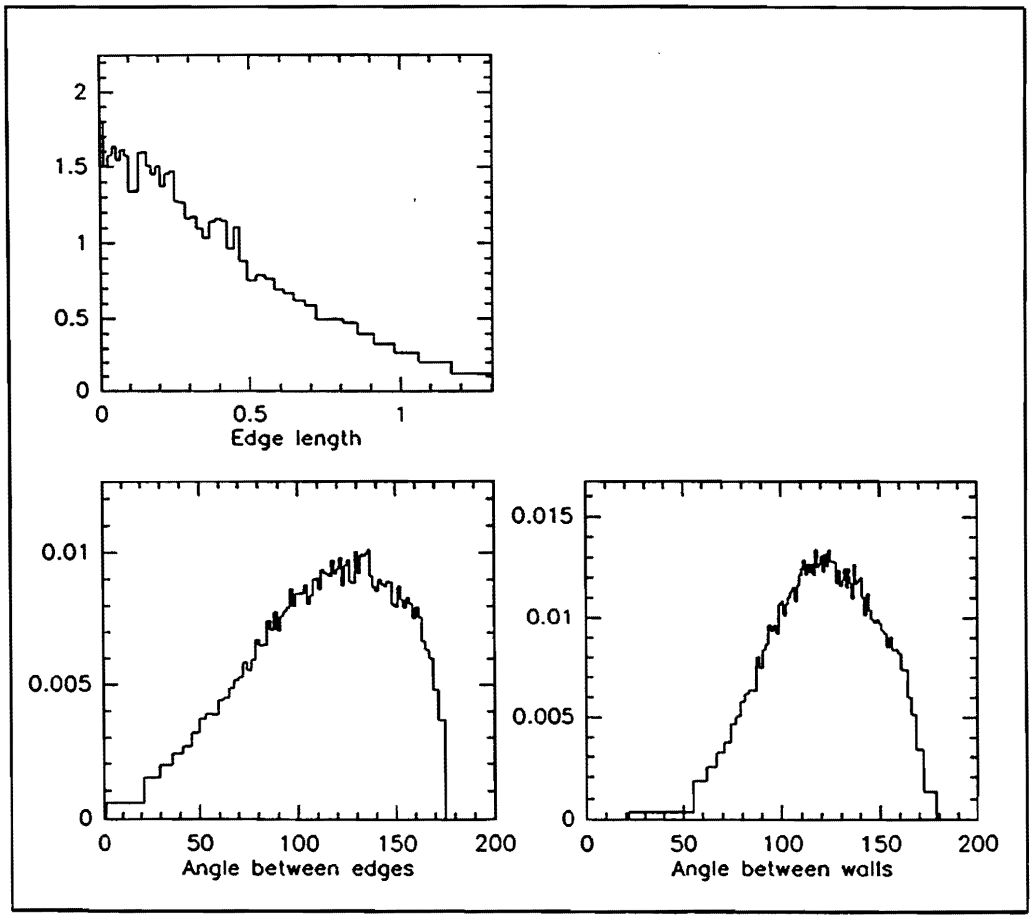

CLASS: P

FIGURE 9a.

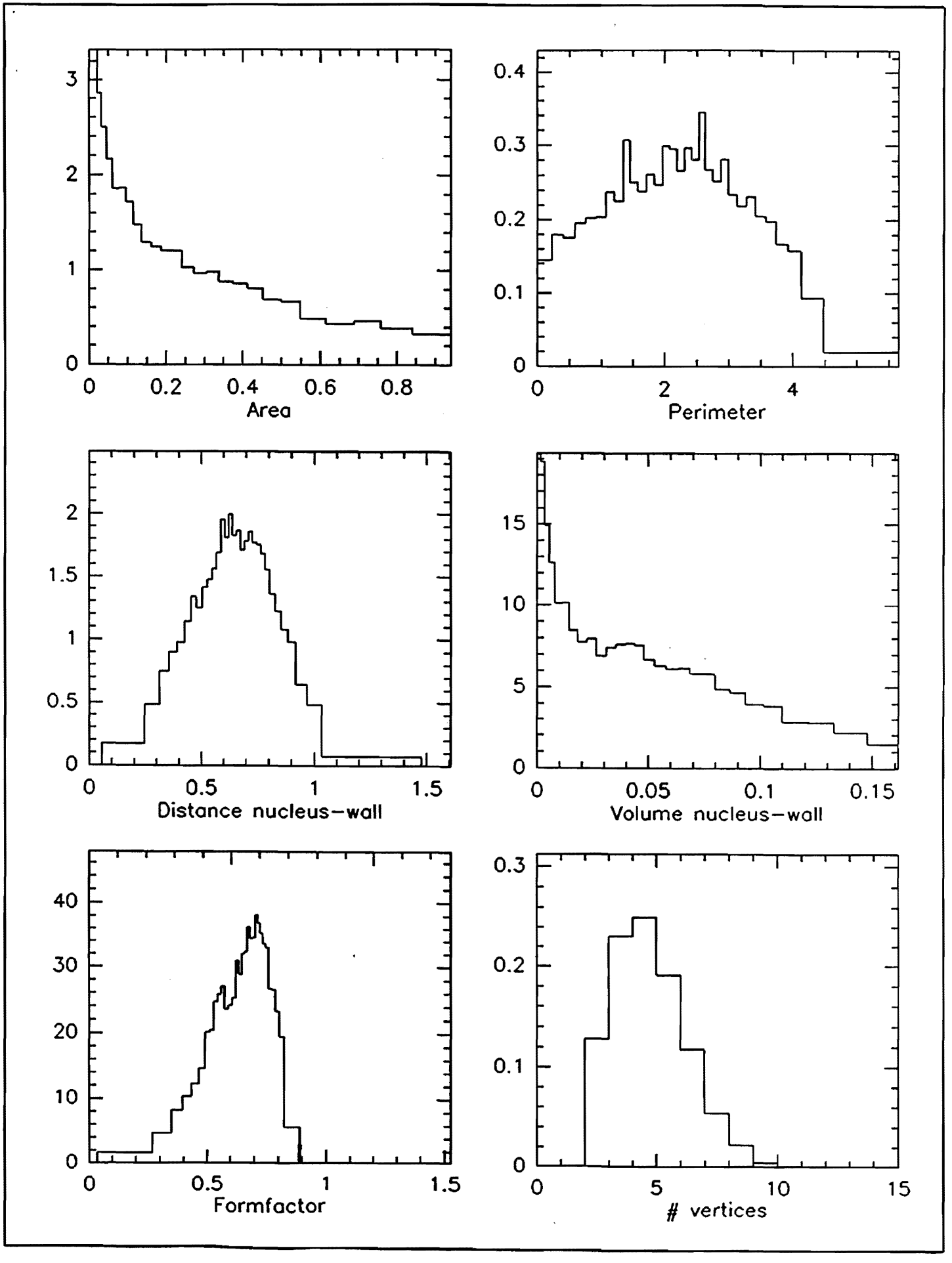

CLASS: A Parameter: 0.80 FIGURE 9b.

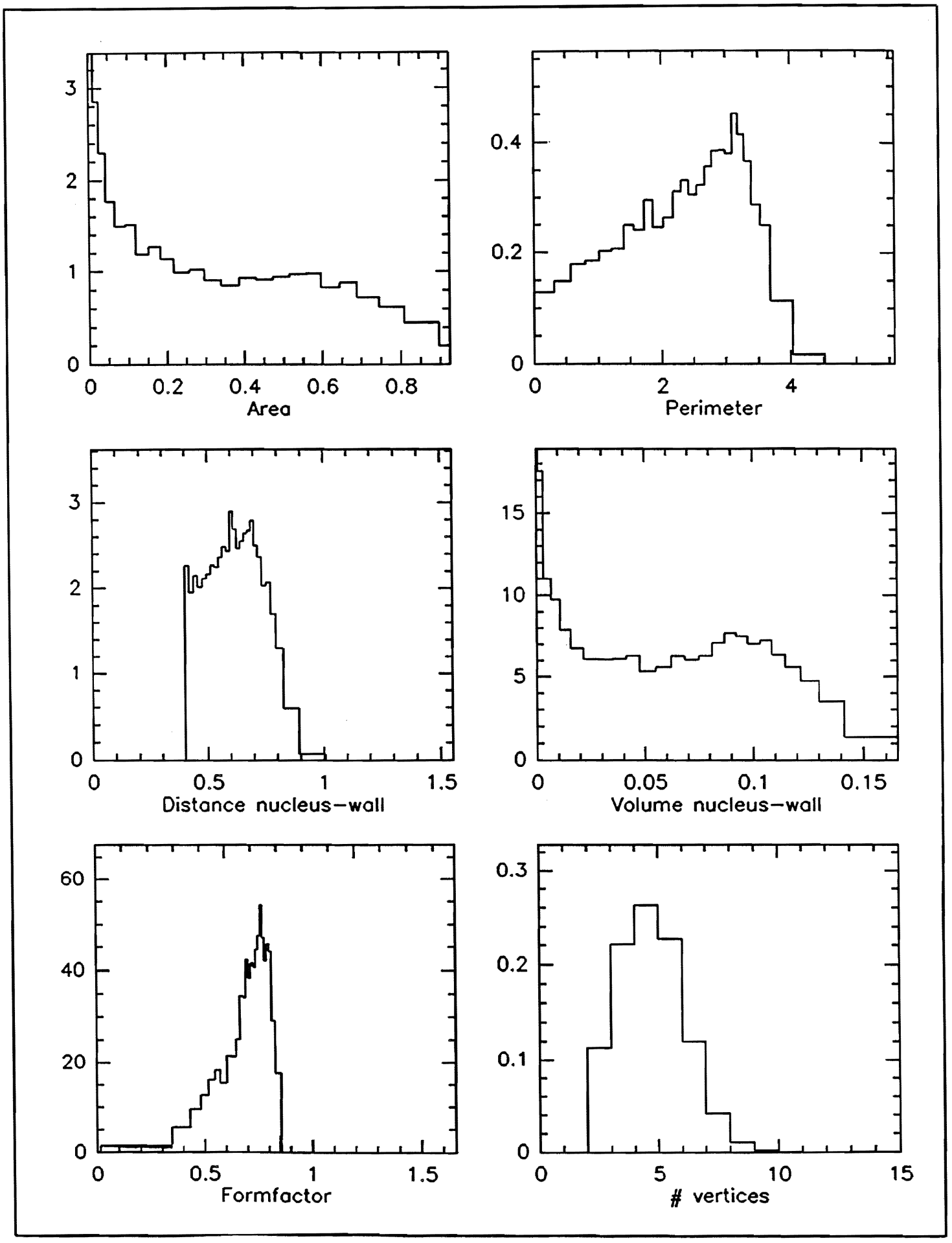

CLASS: C Parameter: 0.40

FIGURE 9c.

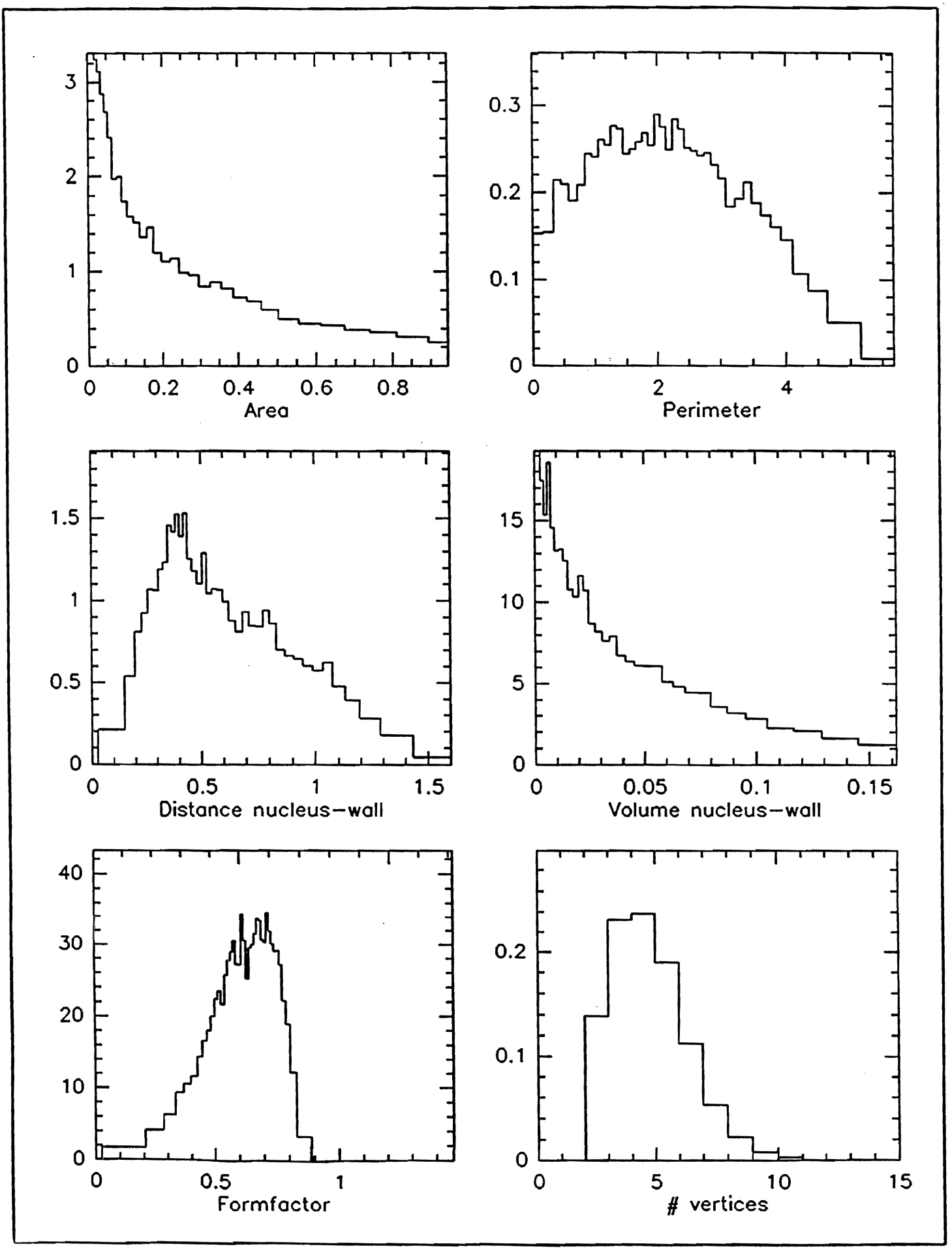

CLASS: P

# of cells in 3-D tessellation : 1000

FIGURE 11a.

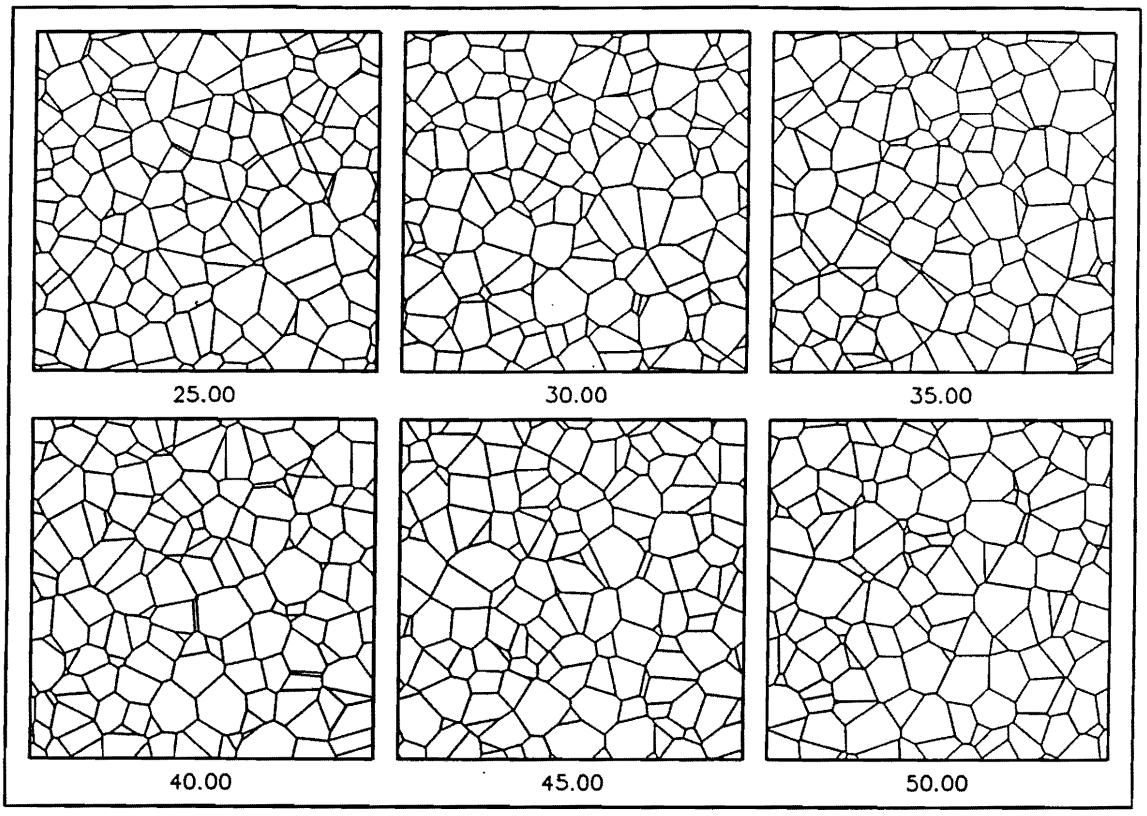

CLASS: A Parameter: 0.80

# of cells in 3-D tessellation : 1000

FIGURE 11b.

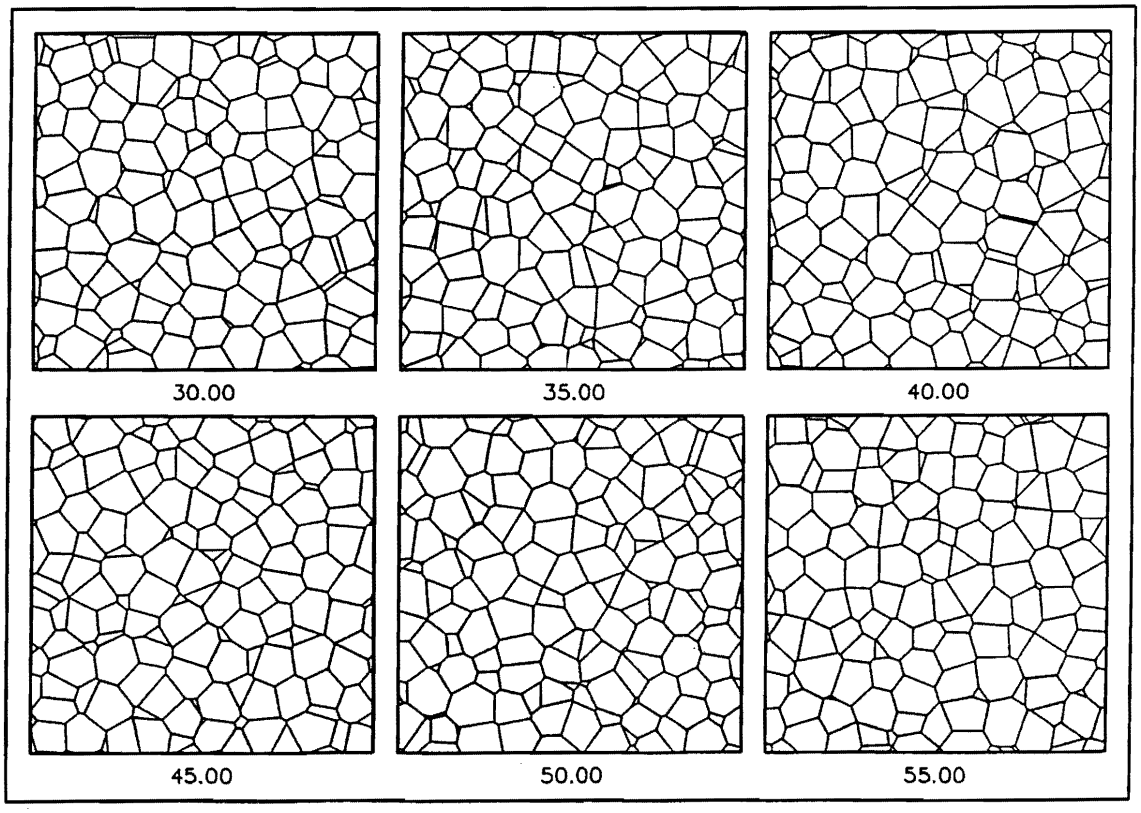

CLASS: C Parameter: 0.40

# of cells in 3-D tessellation : 1000

FIGURE 11c.

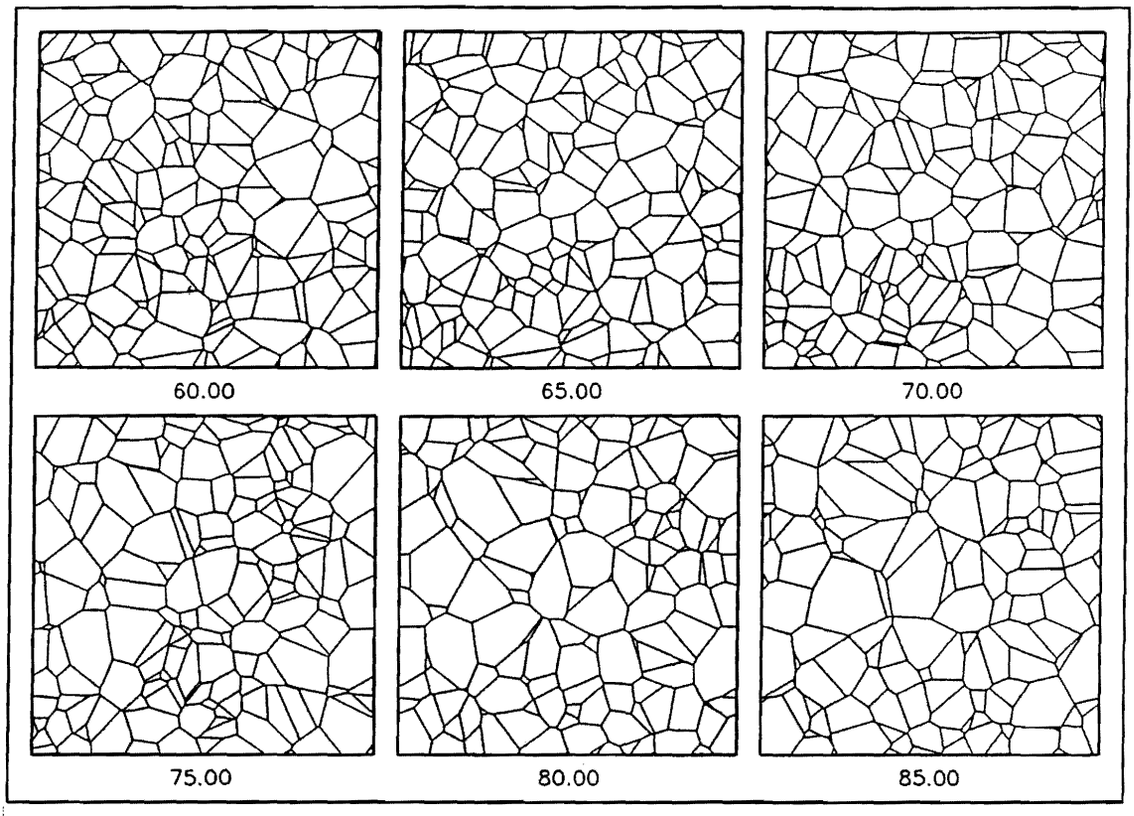

CLASS: P

FIGURE 12a.

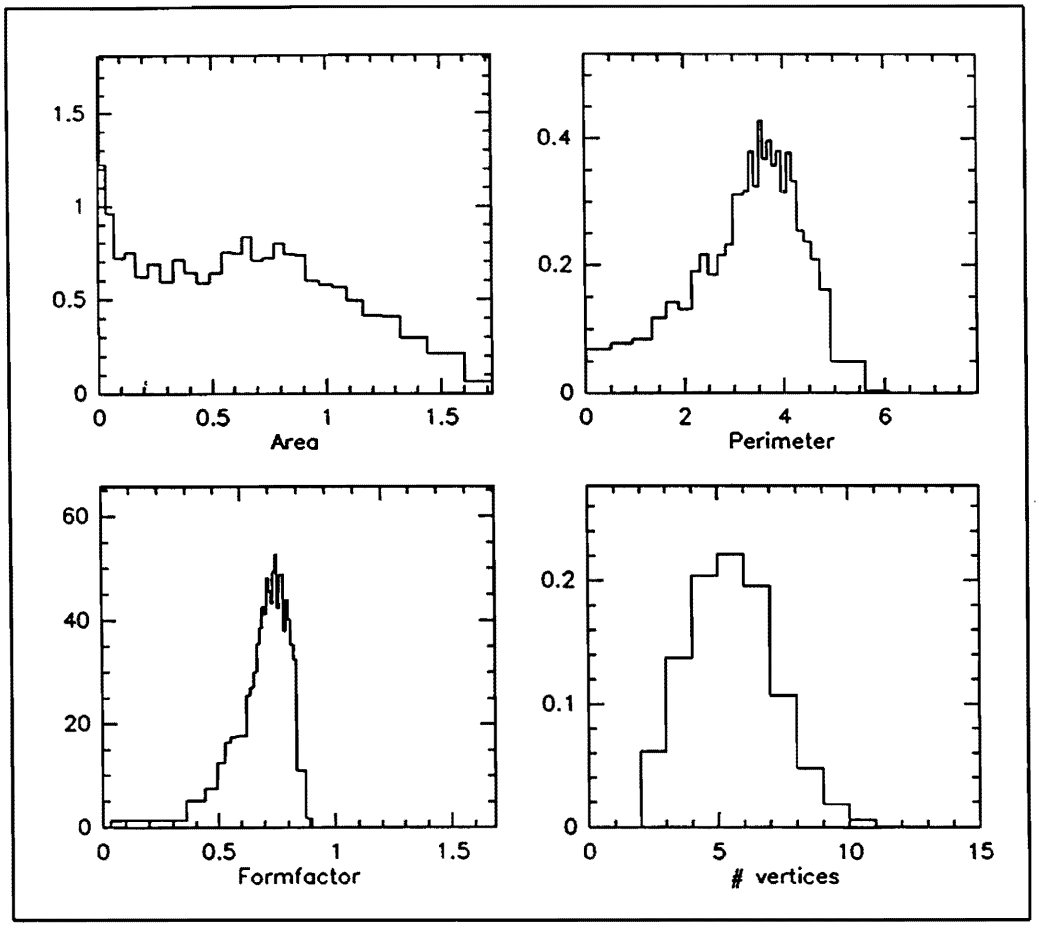

FIGURE 13a.

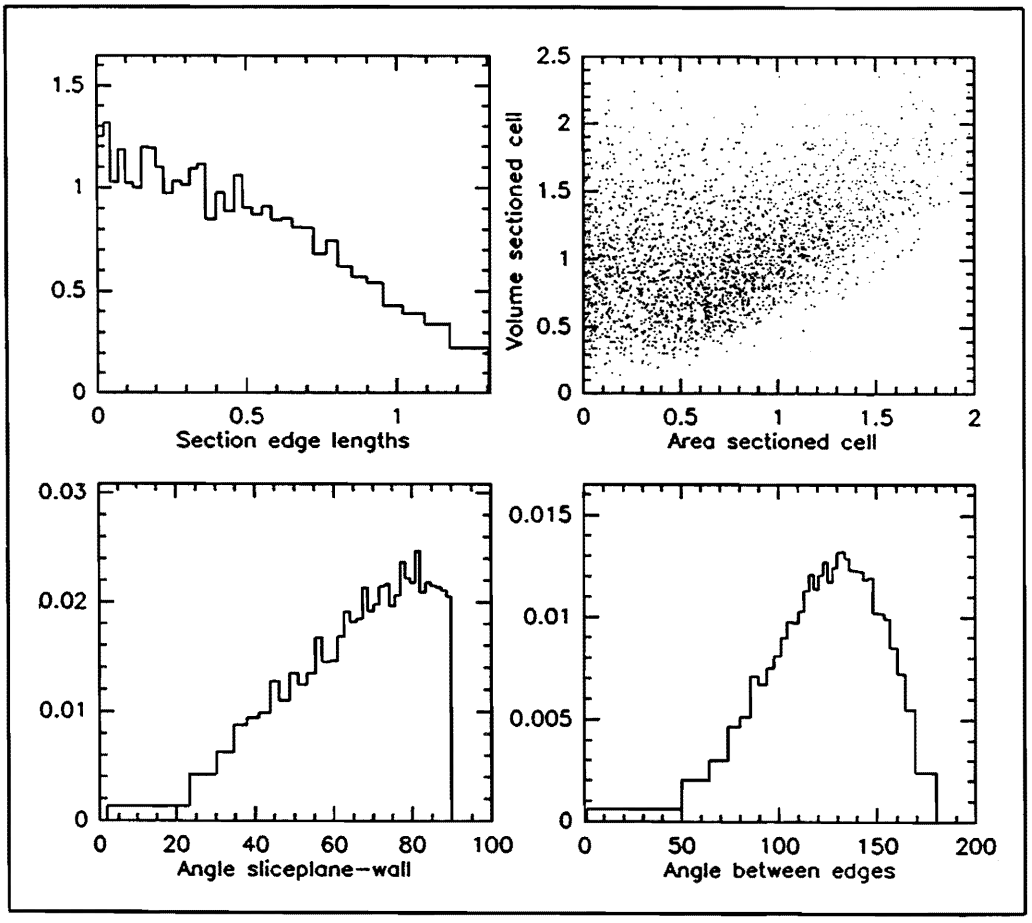

CLASS: A Parameter: 0.80

FIGURE 12b.

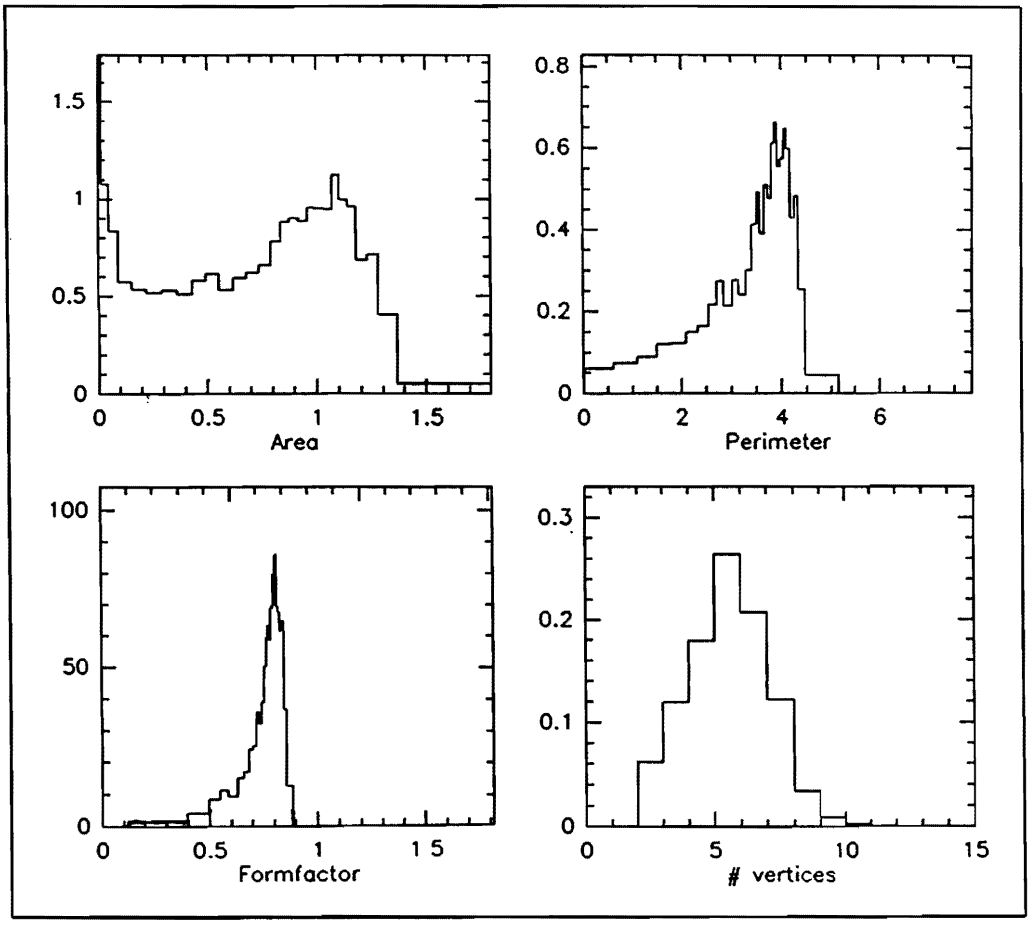

FIGURE 13b.

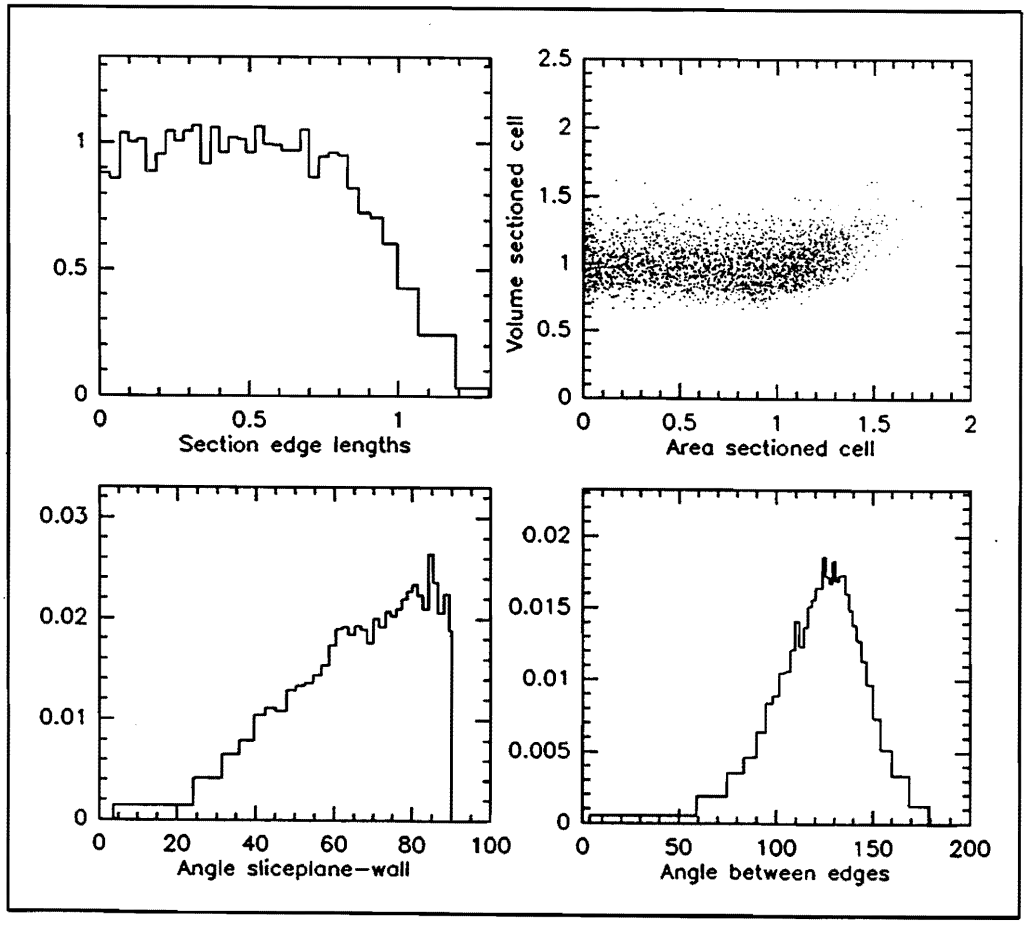

CLASS: C Parameter: 0.40

FIGURE 12c.

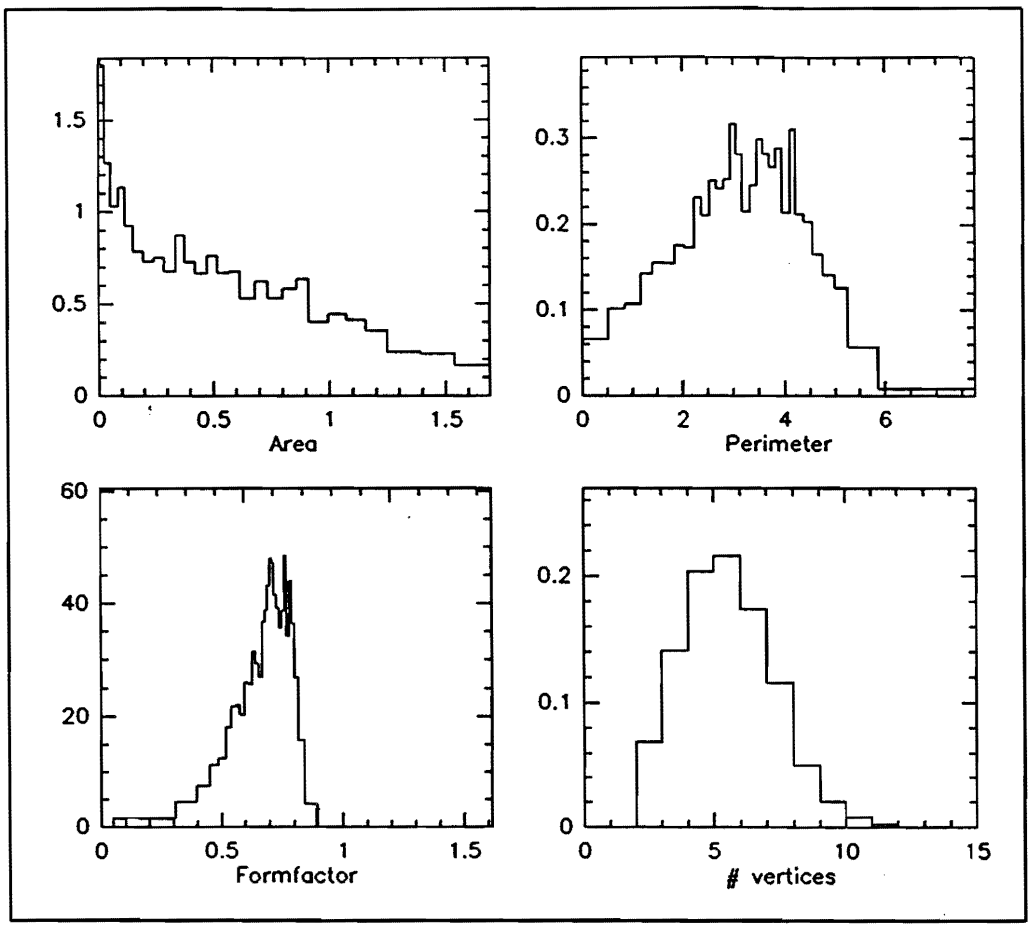

FIGURE 13c.

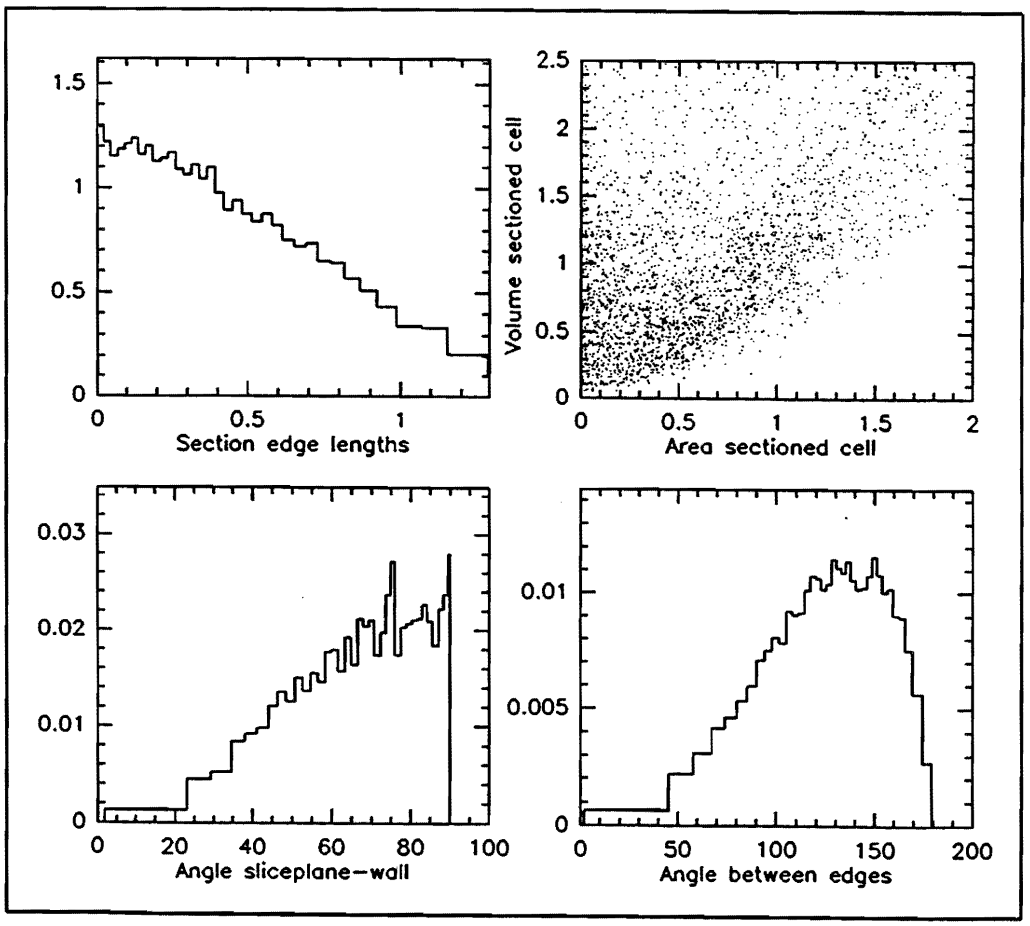

CLASS: P

FIGURE 14a.

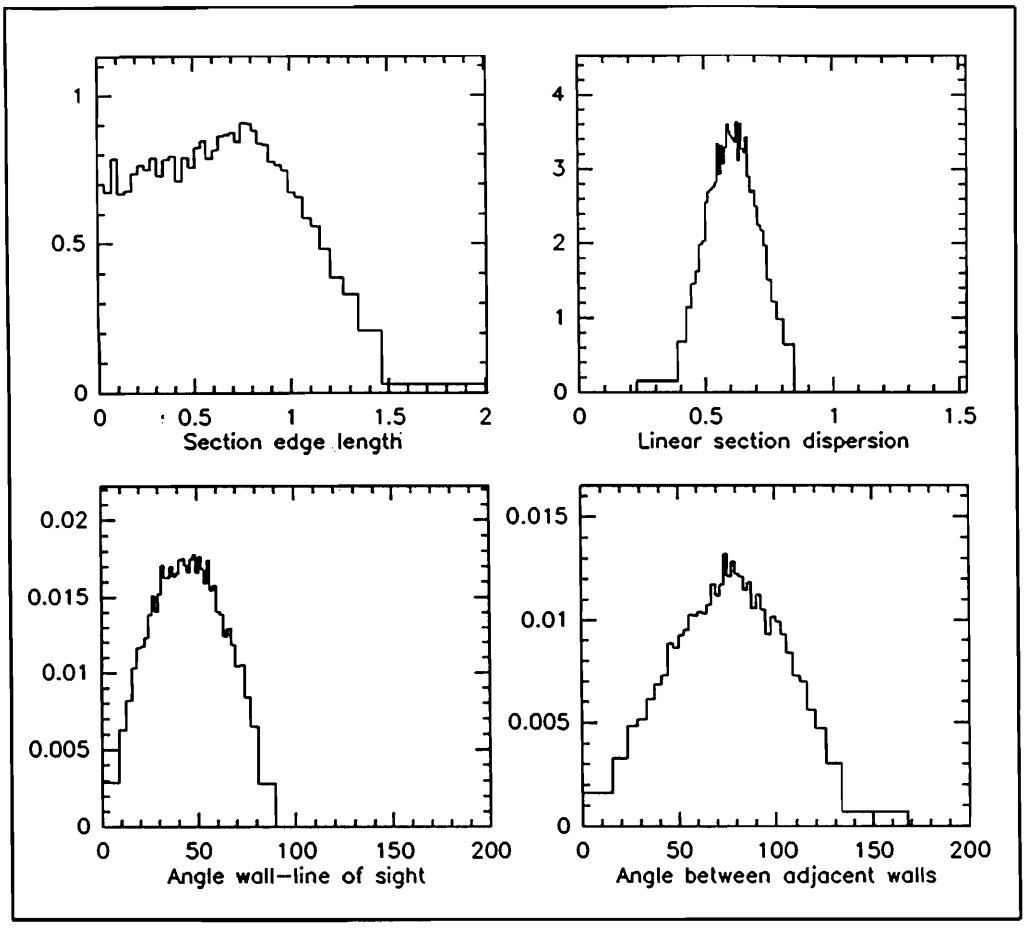

FIGURE 15a.

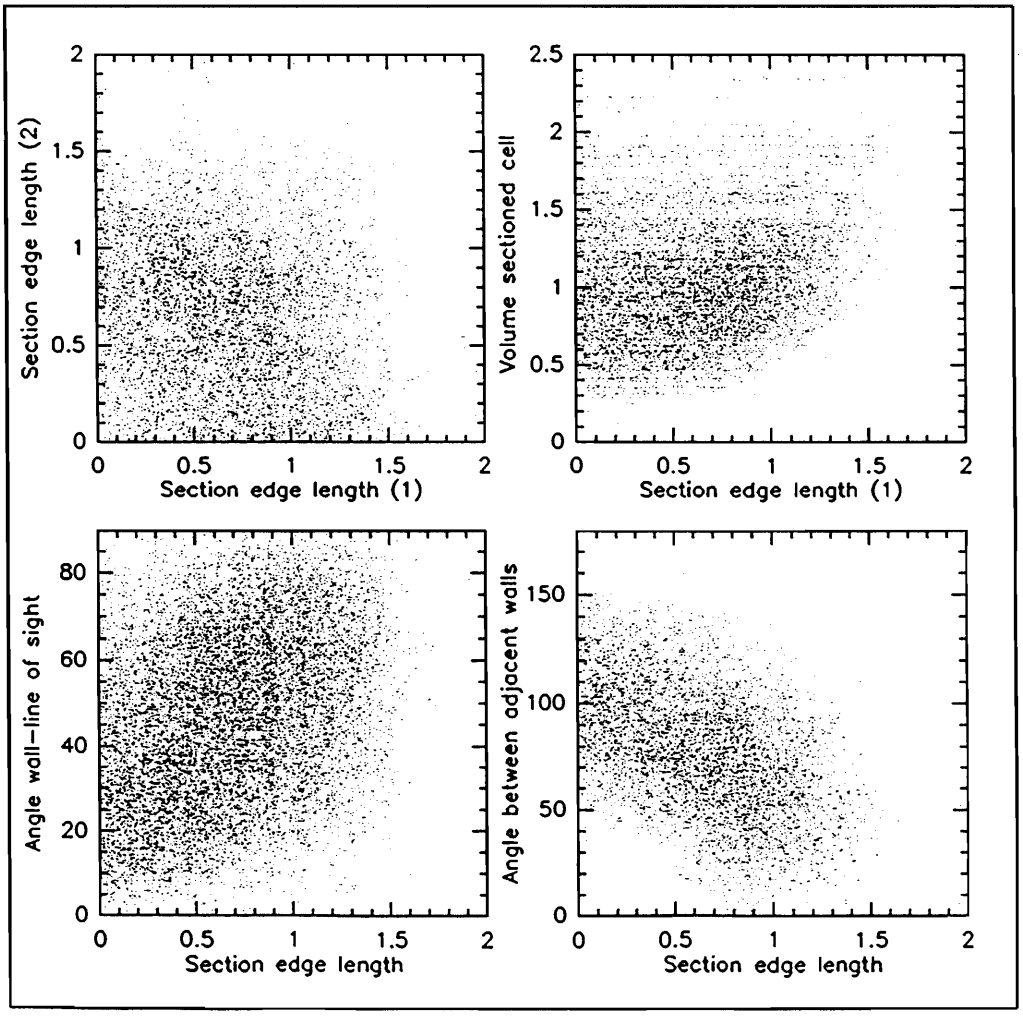

CLASS: A Parameter: 0.80

FIGURE 14b.

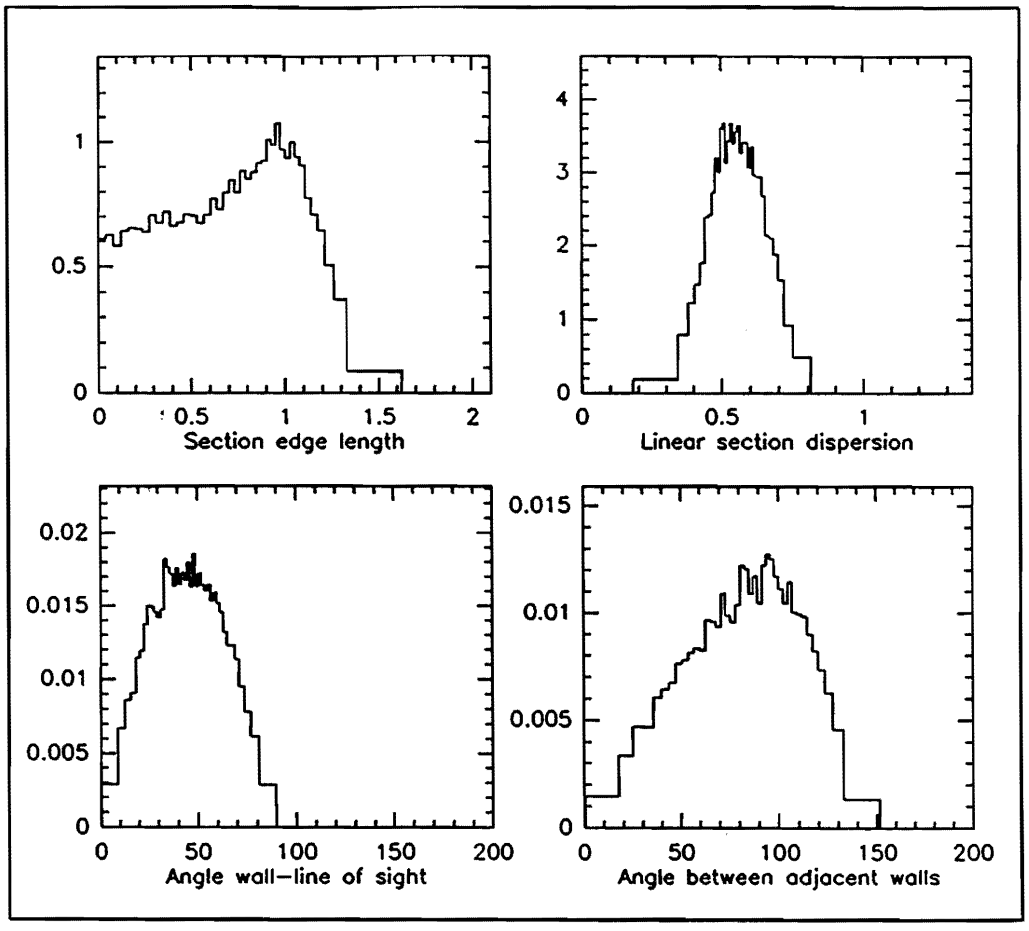

FIGURE 15b.

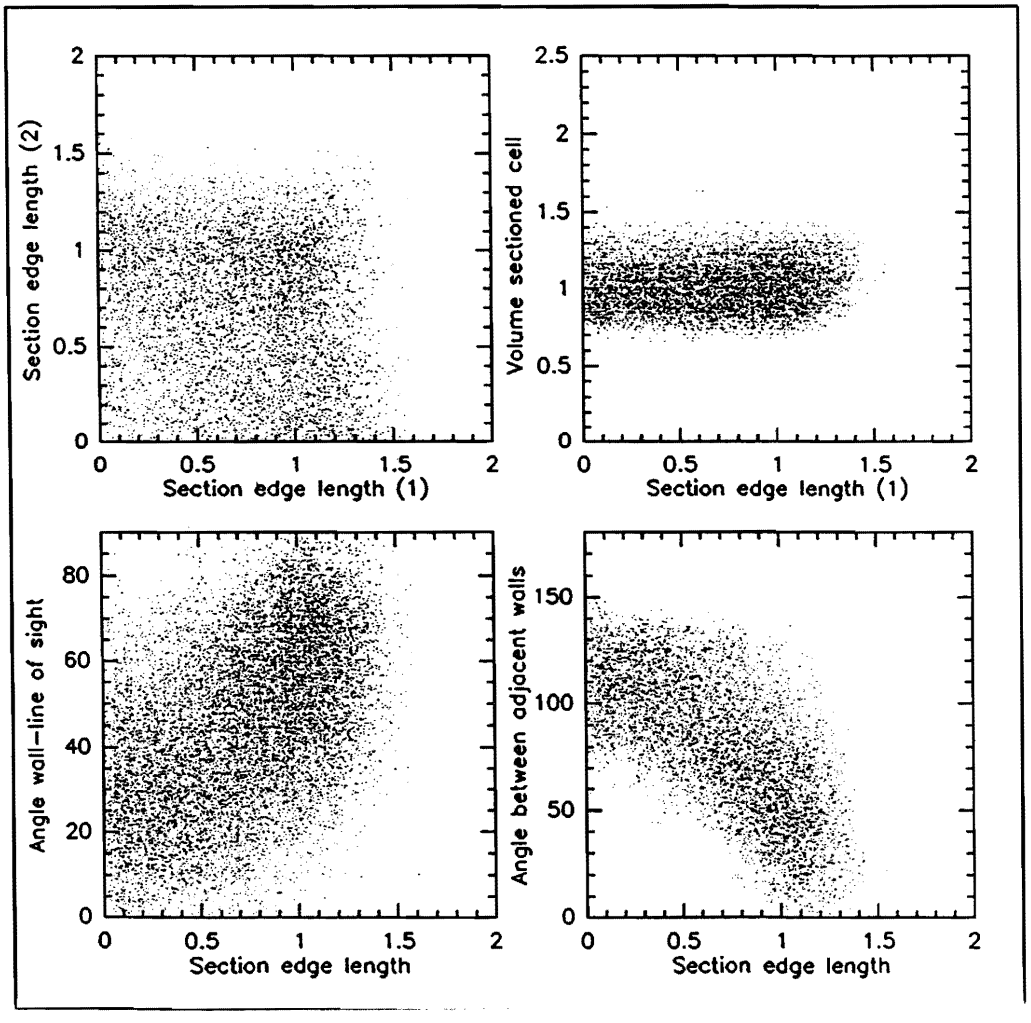

CLASS: C Parameter: 0.40

FIGURE 14c.

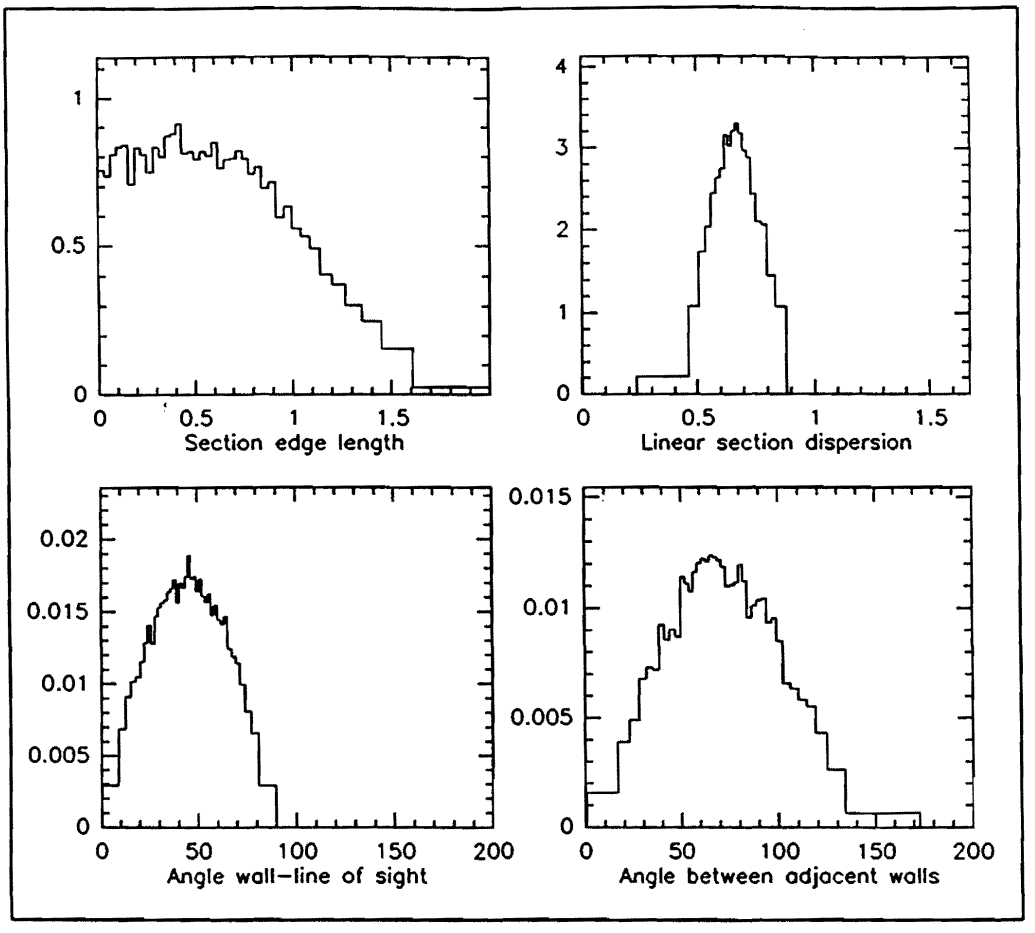

FIGURE 15c.

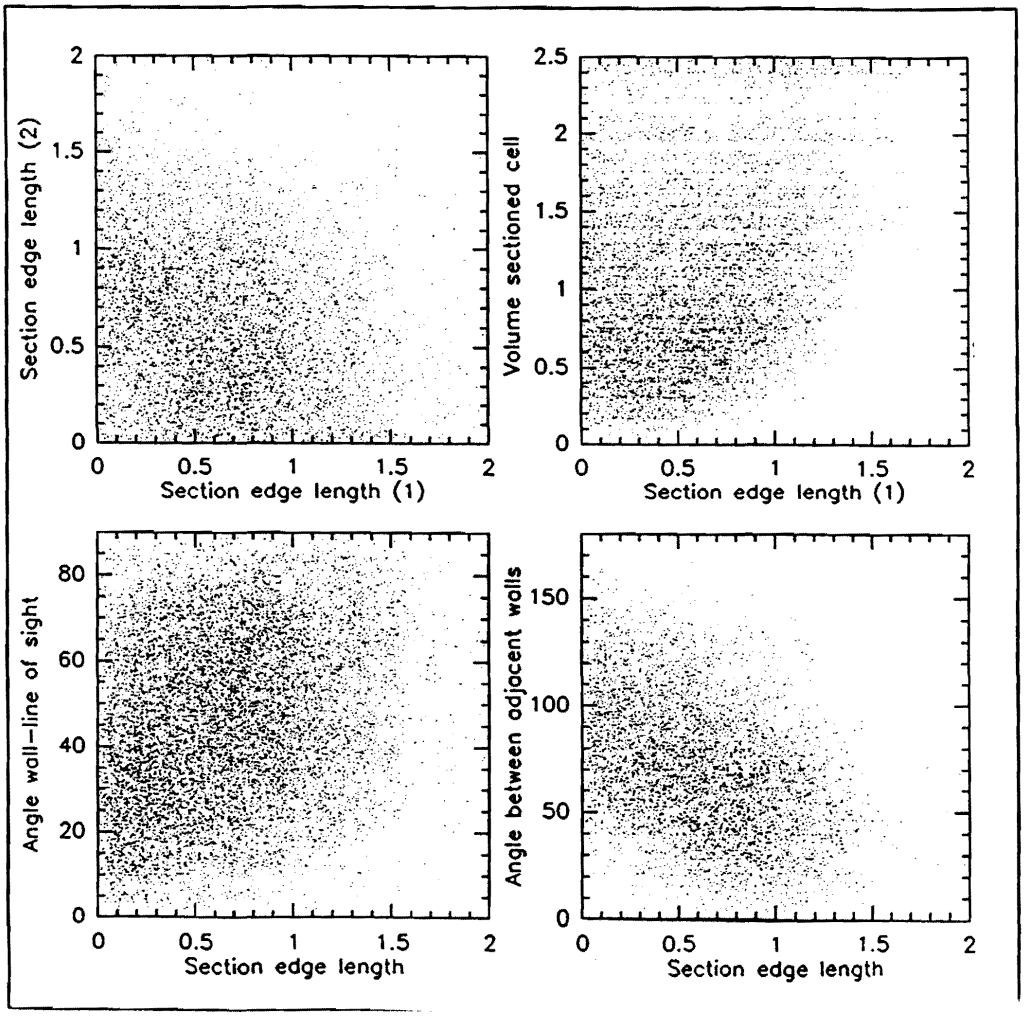

FIGURE A1.

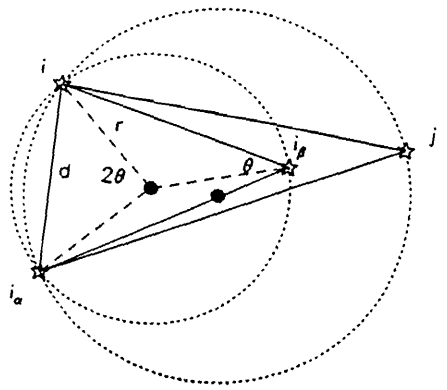

FIGURE C1.

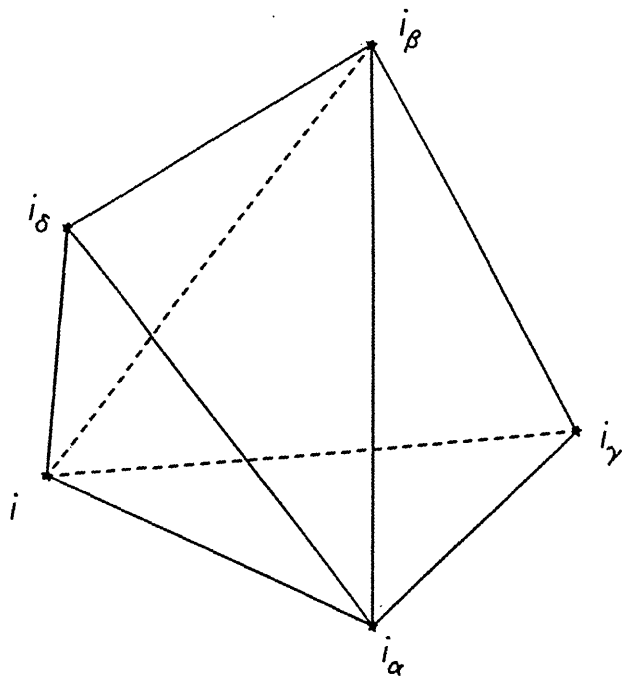

FIGURE D1.

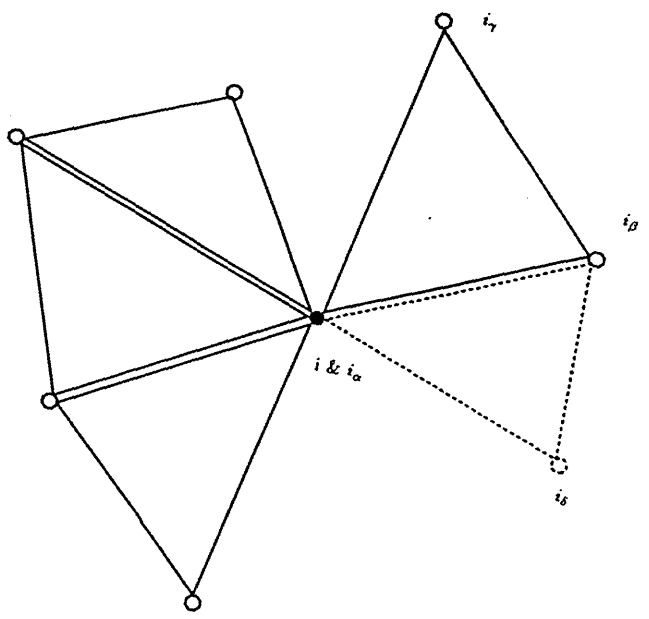

FIGURE C2.

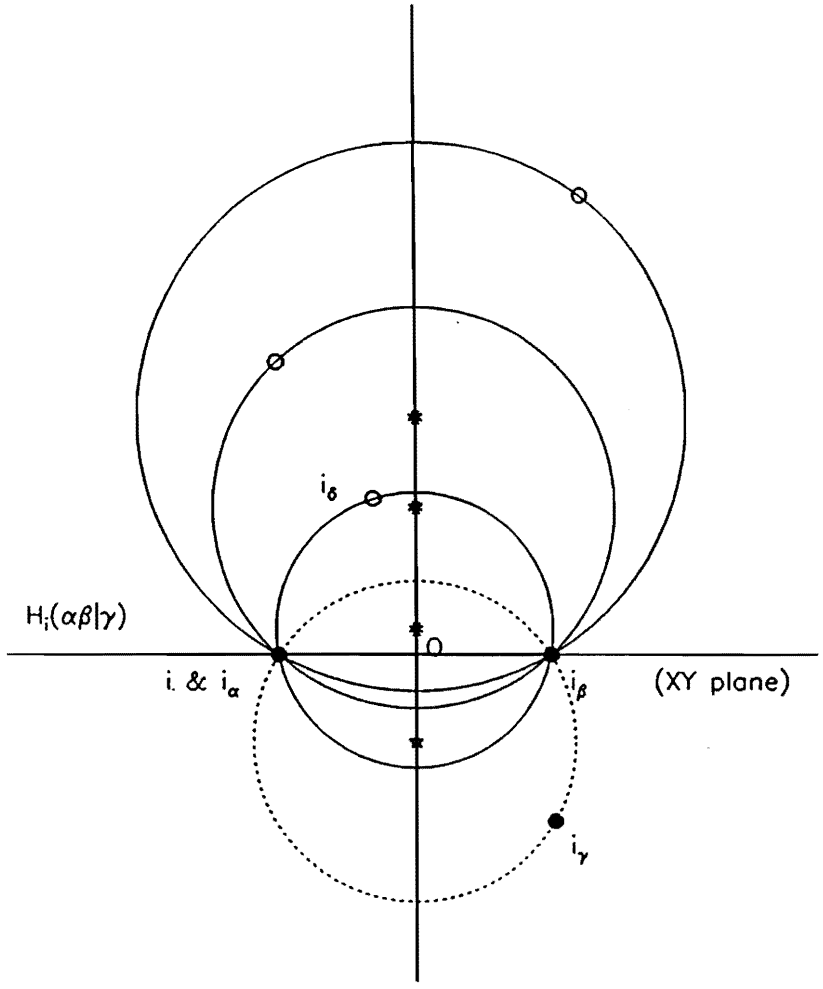

FIGURE E1.

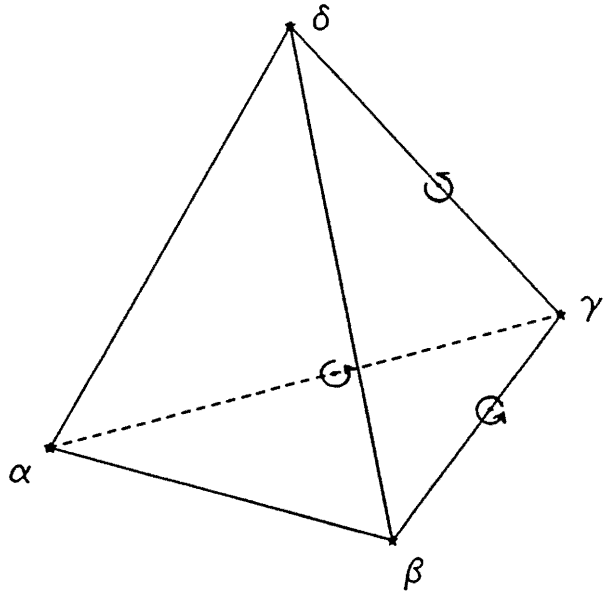

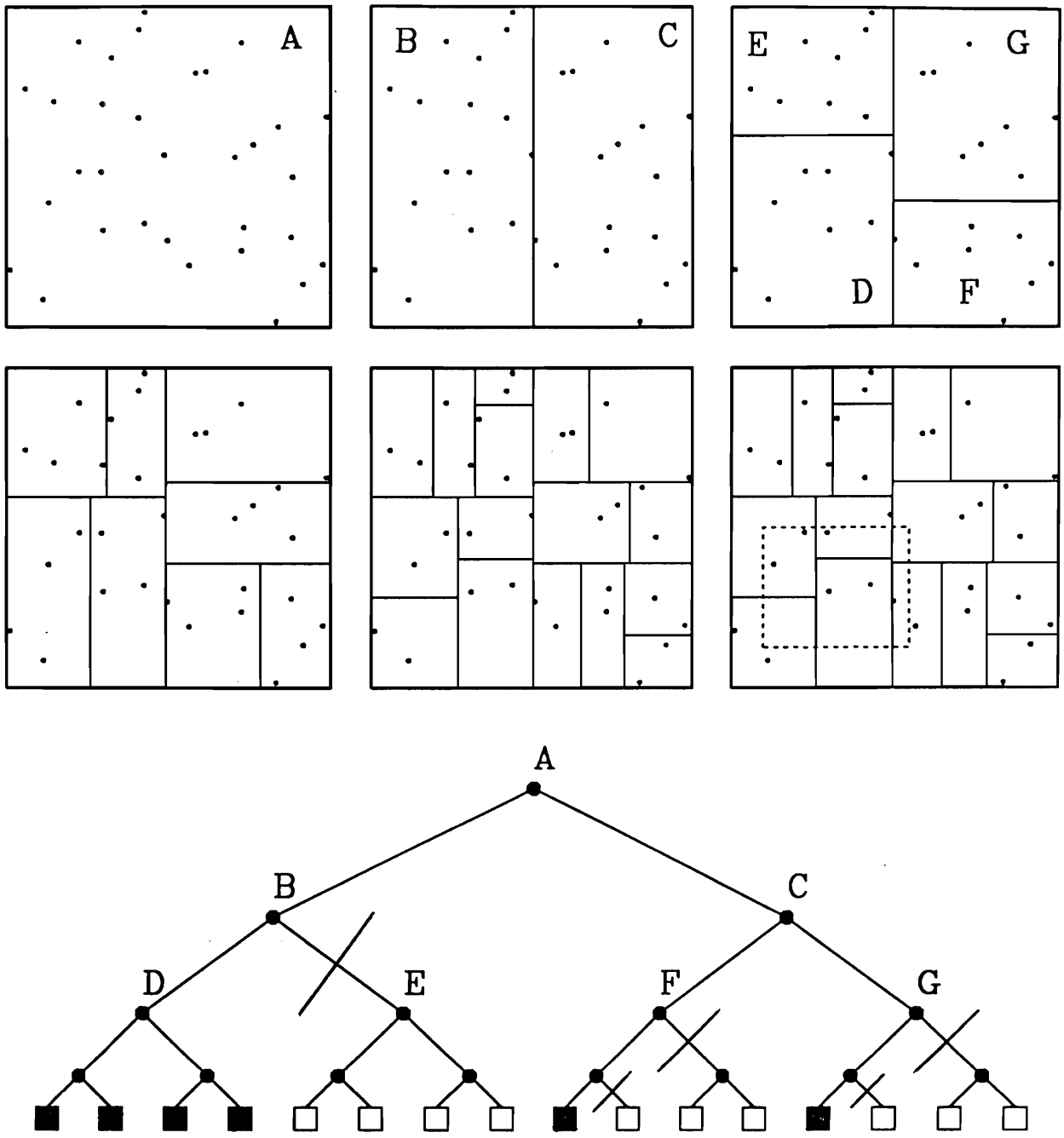

FIGURE F1.